MODELING COASTAL SHORELINE CHANGE THROUGH SATELLITE IMAGERY: A CASE STUDY DIM RIVER MOUTH, ALANYA COASTLINE

A THESIS SUBMITTED TO
THE GRADUATE SCHOOL OF NATURAL AND APPLIED SCIENCES
OF
MIDDLE EAST TECHNICAL UNIVERSITY

BY

MUSTAFA SINAN TEMIZKAYA

IN PARTIAL FULFILLMENT OF THE REQUIREMENTS
FOR
THE DEGREE OF MASTER OF SCIENCE
IN
GEODETIC AND GEOGRAPHIC INFORMATION TECHNOLOGIES

APRIL 2024

Approval of the thesis:

MODELING COASTAL SHORELINE CHANGE THROUGH SATELLITE IMAGERY: A CASE STUDY DIM RIVER MOUTH, ALANYA COASTLINE

submitted by **MUSTAFA SINAN TEMIZKAYA** in partial fulfillment of the requirements for the degree of **Master of Science** i**n Geodetic and Geographic Informatıon Technologies, Middle East Technical University** by,

Prof. Dr. Naci Emre Altun
Dean, **Graduate School of Natural and Applied Sciences** _____

Prof. Dr. Sevda Zuhal Akyürek
Head of the Department, **Geodetic and Geographic Information Technologies** _____

Prof. Dr. Ahmet Cevdet Yalçıner
Supervisor, **Geodetic and Geographic Information Technologies, METU** _____

Prof. Dr. Sevda Zuhal Akyürek
Co-Supervisor, **Civil Engineering, METU** _____

Examining Committee Members:

Prof. Dr. Mehmet Lütfi Süzen
Geological Engineering, METU _____

Prof. Dr. Ahmet Cevdet Yalçıner
Civil Engineering, METU _____

Prof. Dr. Sevda Zuhal Akyürek
Civil Engineering, METU _____

Asst. Prof. Dr. Gülizar Özyurt Tarakcıoğlu
Civil Engineering, METU _____

Asst. Prof. Dr. Murat Durmaz
Geomatics Engineering, Hacettepe University _____

Date: 18.04.2024

I hereby declare that all information in this document has been obtained and presented in accordance with academic rules and ethical conduct. I also declare that, as required by these rules and conduct, I have fully cited and referenced all material and results that are not original to this work.

Name, Last name : Mustafa Sinan Temizkaya

Signature :

ABSTRACT

MODELING COASTAL SHORELINE CHANGE THROUGH SATELLITE IMAGERY: A CASE STUDY DIM RIVER MOUTH, ALANYA COASTLINE

Temizkaya, Mustafa Sinan
Master of Science, Geodetic and Geographic Information Technologies
Supervisor : Prof. Dr. Ahmet Cevdet Yalçıner
Co-Supervisor: Prof. Dr. Sevda Zuhal Akyürek

April 2024, 118 pages

The continuous change of shoreline boundaries due to natural or human causes has created the necessity for shoreline monitoring. Sedimentation occurs in shallow water level areas where a river or creek discharges into the sea or ocean. Continuous erosion and sediment accumulation cause shoreline changes, which may result in losing land soil or destructive accumulation of sediments. This catastrophic natural event may harm coastal lands with economic value, such as beaches, agricultural areas, residential buildings, and hotels. Traditional shoreline monitoring is done by physically collecting data over a period of time in the desired location. Standard methodology requires many things, such as workforce, funding, and, more importantly, a long duration. This study examines monitoring shoreline change in Alanya, Türkiye, with Digital Shoreline Analysis System (DSAS) by using geographical information systems and remote sensing analysis. The study area is narrowed step by step by constructing different models to compare the results. The smallest microzone is selected as Dim River mouth in Alanya, Türkiye, for being naturally dynamic and having less human activity, which may cause artificial changes in shorelines. The research consists of analyzing the satellite images from two different satellites, Landsat and Planet, and corresponding reanalysis data of the

coastline. Based on the results, seasonal and cyclical behavior is obtained in the area. As the study area decreases, the changes in shoreline changes. Throughout the study area, mostly erosion is observed. In Dim River Mouth, the seasonal change in shorelines is obtained roughly between -25 and +25 meters for Landsat-8 imagery and -8 and +4 meters for Planet imagery.

Keywords: Shoreline Monitoring, Coastal Erosion, Digital Shoreline Analysis System (DSAS), Geospatial Analysis, Remote Sensing

ÖZ

UYDU GÖRÜNTÜLERİYLE KIYI ŞERİDİNDEKİ DEĞİŞİMİN MODELLENMESİ: DİM ÇAYI AĞZI, ALANYA KIYI ŞERİDİ ÖRNEĞİ

Temizkaya, Mustafa Sinan
Yüksek Lisans, Jeodezi ve Coğrafi Bilgi Teknolojileri
Tez Yöneticisi: Prof. Dr. Ahmet Cevdet Yalçıner
Ortak Tez Yöneticisi: Prof. Dr. Sevda Zuhal Akyürek

Nisan 2024, 118 sayfa

Kıyı şeritlerinin sınırlarının sürekli olarak insan etkisi ya da doğal etkilerle değişimi kıyı şeritlerinin izlenmesinin gerekliliğini doğurmuştur. Sediment birikimi; derelerin ya da nehirlerin denizle buluştuğu noktalardaki sığ su seviyelerinde oluşur. Süregelen aşınma ve sediment akümülasyonu toprak kaybına veya yıkıcı etkili sediment birikimine sebep olabilecek kıyı şeridi değişikliklerine neden olur. Bu yıkıcı doğa olayı; sahil, zirai alanlar, yerleşim yerleri ve oteller gibi ekonomik değeri olan kıyısal yapılara zarar verebilir. Geleneksel kıyı şeridi izlenmesi fiziksel olarak belirli bir zaman diliminde istenen lokasyonda veri toplanmasıyla yapılır. Geleneksel metodoloji iş gücü, fonlama ve en önemlisi uzun bir süre gerektirir. Bu tez Alanya'daki kıyı şeridi değişminin Dijital Kıyı Şeridi Analiz Sistemi (DSAS) kullanılarak coğrafi bilgi sistemleri ve uzaktan algılama ile incelenmesini amaçlamaktadır. Çalışma alanı adım adım küçültülmüştür ve her bir çalışma alanı için ayrı modeller oluşturularak bu modellerin sonuçları birbirleriyle karşılaştırılmıştır. En mikrobölge, doğal olarak dinamik olması ve kıyı şeritlerinde yapay değişikliklere neden olabilecek insan faaliyetinin daha az olması nedeniyle Türkiye'nin Alanya ilçesindeki Dim Çayı ağzı olarak seçilmiştir. Araştırma, Landsat ve Planet olmak üzere iki farklı uydudan alınan uydu görüntülerinin ve buna karşılık

gelen kıyı şeridinin yeniden analiz verilerinin analizinden oluşmaktadır. Analiz sonuçlarına göre çalışma alanında hem mevsimsel hem de periyodik değişim trendleri gözlenmiştir. Çalışma alanı küçüldükçe gözlemlenen kıyı şeridi değişim değerleri de değiştirmiştir. Çalışma alanı boyunca çoğunlukla kıyı erozyonu gözlemlenmiştir. Dim Çayı ağzı bölgesindeki mevsimsel değişim Landsat-8 görüntülerinden kabaca -25 ile +25 m arasında saptanmıştır. Bununla birlikte bu değişim Planet görüntülerinde -8 ile +4 m arasında gözlenmiştir.

Anahtar Kelimeler: Kıyı Şeridi İzlenmesi, Kıyısal Erozyon, Dijital Kıyı Şeridi Analiz Sistemi (DSAS), Uzamsal Analiz, Uzaktan Algılama

To my family for their continuous love and support,

and to my country for her generosity and wisdom…

ACKNOWLEDGEMENTS

I would like to express my deepest gratitude to my supervisors, Prof. Dr. Ahmet Cevdet Yalçıner and Prof. Dr. Sevda Zuhal Akyürek, for their perpetual support and guidance throughout my MSc. study.

I also want to thank Prof. Dr. Uğur Murat Leloğlu, Prof. Dr. Kemal Önder Çetin, Prof. Dr. Adnan Yazıcı, Prof. Dr. Erdal Çokça, Prof. Dr. İsmail Yücel, Dr. Murat Durmaz, Dr. Ceyhan Temürcü, Dr. Huzur Keskin and Dr. Alparslan Bayraktar for bringing me another perspective thorough their courses and guidance in my MSc. education.

I owe many thanks to my friend Berkay Akpınar for providing me with his knowledge. I need to thank my MBA friend, Tiffany Anning, for proofreading this study and making the text more fluent and grammatically correct.

Moreover, I would like to thank Planet Labs PBC for their permission to use their data free of charge, which was used to make a sensitivity analysis in this thesis.

TABLE OF CONTENTS

LIST OF TABLES

TABLES IN THE MAIN TEXT

TABLES IN APPENDICES

LIST OF FIGURES

FIGURES IN THE MAIN TEXT

FIGURES IN APPENDICES

LIST OF ABBREVIATIONS

ABBREVIATIONS

ANN	Artificial Neural Network
AOI	Area of Interest
DDWI	Direct Difference Water Index
DEM	Digital Elevation Model
DSAS	Digital Shoreline Analysis System
EPR	End Point Rate
EROS	Earth Resources Observation Satellites
ETM+	Enhanced Thematic Mapper
GIS	Geographical Information Systems
GLS	Global Land Survey
GPS	Global Positioning System
HWL	High Water Level
KNN	k-nearest Neighbor
LDII	LIDAR-Derived Intensity Image
LL	Low Water Level
LRR	Linear Regression Rate
MLC	Maximum Likelihood Classification
MNDWI	Modified Normalized Difference Water Index
MRS	Multi-Resolution Segmentation
MS	Multi-Spectral
MSS	Mean Shift Segmentation
NDWI	Normalized Difference Water Index
NIR	Near Infrared
NSM	Net Shoreline Movement
OBIA	Object-Based Image Analysis
OLI	Operational Land Imager
PBC	Public Benefit Corporation

PBIA	Pixel-Based Image Analysis
RF	Random Forest
RGB	Red Green Blue
ROI	Region of Interest
SAR	Synthetic Aperture Radar
SCE	Shoreline Change Envelope
SOM	Self-Organizing Map
SVM	Support Vector Machine
SWIR	Short Wave Infrared
TIRS	Temporal Infrared Sensor
TM	Thematic Mapper
UAV	Unmanned Aerial Vehicle
USGS	United States Geological Survey
WLR	Weighted Linear Regression

CHAPTER 1

INTRODUCTION

The natural environment of coastal areas provides habitats for complex ecosystems and is crucial for supporting socio-economic activities (Demir et al., 2017). A variety of species that contribute to the health of these areas and support human activities exist in these ecosystems. A shoreline exists where sea, ocean, and land meet (Parthasarathy et al., 2021). They are dynamic environments and can change rapidly due to the effects of both natural and human causes. Coastal shoreline changes result from several dynamic inductions, such as waves, currents, tides, and movements of sediments (Ergin et al., 2006). The change should be monitored continuously to prevent potential threats to coastal areas close to the sea or ocean, such as beaches, agricultural lands, residential buildings, and seaside tourist facilities. One of the most crucial coastal zone management issues is monitoring coastal erosion and accretion (Ari et al., 2007). The primary issue in seaside areas is presenting the dynamics of the location and estimating the future behavior of these dynamics (Hoffmann et al., 2007).

Shoreline changes are investigated by several methods, including numerical modeling of sediment transportation, optical remote sensing applications, unmanned aerial vehicles (UAV), synthetic aperture radar (SAR) imagery usage with remote sensing applications, and physical maps and their digitizations. Numerical modeling processes require enormous data collection over time in the desired location, which requires adequate manpower, funding, and special devices. Processing of this data necessitates modeling with intricate mathematical equations that take into account the influences of waves, currents, and winds. Additionally, coastal morphology evolution includes multifactoral physical characteristics, which makes it difficult to

represent all these characteristics in a mathematical model (Ari et al., 2007). Further, numerical modeling is a deterministic approach to the phenomena founded on the results of the collected data and laboratory tests that may not suit the real case scenarios completely.

Extraction of changes in different features on large-scale surfaces can be granted using remote sensing data. Satellite imagery, unmanned aerial vehicles (UAV), and synthetic aperture radar (SAR) are data to obtain top-view displays of the desired locations. Satellite imagery is a beneficial data source for shoreline extraction and is freely available to some extent of resolution both in multispectral and radar sensors (Demir et al., 2017). Remote sensing techniques are essential for identifying, monitoring, and mapping coastal zones by evaluating temporal changes and commenting on their environmental importance (Kennedy et al., 2009). These techniques allow for the use of different methodologies while assessing data and create an option to index the data that may be further used to generate different analyses after detecting shoreline changes. Considering the effects of coastal erosion and accretion could lead to further analyses that include risk mapping, disaster management, and coastal zone management. Moreover, satellite imagery may reduce the investigation cost of creating a mathematical model by detecting the potential zones open for dynamic forces and assisting investigators with the collection of data in narrower zones.

1.1 Scope and Objectives

The scope of this study is to obtain the shoreline change in the Mediterranean Region's coastal zone in Türkiye over time by employing remote sensing and GIS using Landsat-8 imagery. The reason for using Landsat imagery is that it has a 30 by 30-meter pixel resolution, and it is provided freely and open-source by the United States Geological Survey (USGS) agency; it can be accessed easily. Additionally, the aim is to confirm the accuracy of Landsat-8 derived shorelines by comparing it with the shoreline retrieved from Planet Public Benefit Corporation (PBC) data

having a 3-meter resolution. There are three primary objectives within the scope of this thesis, seeking answers to the following questions. These are:

1. Can Landsat-8 imagery be used for shoreline monitoring?

2. What is the relative sensitivity of the shorelines extracted from Landsat-8 imagery?

3. Can a Digital Shoreline Analysis System (DSAS) be used in modeling the shoreline changes?

1.2 Contributions of the Study

a. The study proves the use of Landsat-8 images for shoreline monitoring purposes as well as their reliability for use in real-world applications. Data has been available since the launch of the Landsat satellite in 1985. An image from 1987 is the earliest included in this study and is the starting point of the analysis.
b. The study utilizes different USGS data and tools such as DSAS. These free and open-source data and tools contribute to the literature. The study area is examined for the first time using the Landsat-8 and GIS tools. Further, this study proposes a procedure to analyze large-scale areas affected by shoreline changes.
c. The study proposes a procedure to extract the shorelines. Since the DSAS tool uses the given data, it is essential to have minimal error to overcome potentially wrong results. The rates that DSAS calculates are as correct as the accuracy of the shorelines (Himmelstoss et al., 2021).

1.3 Outline of the Thesis

This thesis includes seven chapters: Introduction, Literature Review, Study Area, Methodology and Data Characteristics, Analysis and Results, Discussion, and

Conclusion. The Introduction discusses the necessity of this study, its aim, and its contributions to literature. This section also presents an outline of the thesis. The Literature Review section summarizes the historical development and methodology based on the previous articles, theses, and conference papers for shoreline extraction and monitoring. Further, a conceptual framework behind the primary concepts this thesis explores is included in this chapter. The Study Area Chapter includes location characteristics, boundaries, and factual information. The procedure followed throughout the study is presented in the Methodology Chapter. Different data sources are used in this study. The required explanations for the data sources and their characteristics and the procession of these data are also explained in the Methodology and Data Characteristics Chapter. The fifth chapter follows with the analysis submission, and results based on the study are presented. This procedural study requires extensive discussions and highlights key points of the study. This requirement is fulfilled in the sixth chapter. Finally, the overall process is summarized in the seventh and final chapter.

CHAPTER 2

LITERATURE REVIEW

Shoreline change monitoring contributes to many disciplines because of the high number of interdisciplinary studies in the coastal zones, such as geology, biology, engineering, and geospatial sciences. In this chapter, the theoretical and empirical literature relevant to shoreline extraction and shoreline change monitoring is reviewed. The literature examines both numerical and geospatial analysis methods. In the first part, shoreline extraction studies are discussed and presented. In the second part, shoreline change determination procedures are studied both numerically and geospatially. In the literature, many studies have been proposed to monitor shoreline change and extract shoreline data. Differentiation occurs in the methodology and the source of data.

2.1 Shoreline Extraction

Optical and Synthetic Aperture Radar (SAR) data are both widely used to extract coastlines (Acar et al., 2012). Acar et al. (2012) developed an algorithm to extract shorelines from SAR images. They used histogram equalization to separate land and sea. As a result of the histogram equalization process, two main types are generated as an output: “too noisy” and “less noisy.” If the imagery is classified as “too noisy” after histogram equalization, further algorithms were applied to reduce the noise and normalize the image. It is noticed that the noise is caused by the same grey value of a pixel that has a particular value. Mathematical morphology is used to eliminate pixels that have random noise values. After mathematical operations, a fit-coast algorithm is used for the resulting image.

Global positioning system (GPS) devices are efficient for getting real-time data and measurements from desired locations. Gokceoglu et al. (2015) obtained their data

using real-time kinematic measurements via GPS on the Antalya coast in Türkiye. The researchers utilized high water level (HWL) and low water level (LL) measurements to determine the shoreline in the desired location. To classify the boundary of the coastal zone, normalized difference vegetation index (NDVI) is applied to their study. As a result, a coastal zone is obtained based on the measured and collected land data.

Different research areas are developed using different data sources to get better results in shoreline extraction processes. Demir et al. (2017) used Rasat Multi-Spectral (MS) pan-sharpened image and Sentinel-1A imagery as the primary data sources. Initially, a random forest classifier is applied to the Rasat image, and fuzzy parameters are determined from this classification. Then, these parameters are used to extract the shoreline from the Sentinel image. Their proposed methodology includes four steps. These steps are pre-processing, classification, post-processing, and quality assessment.

The use of programming allows the implementation of different approaches together to get better results in the studies. Using the Matlab platform, Bayram et al. (2017) extracted shorelines using the Random Forest algorithm on Landsat-8 and Gokturk-2 images. The Random Forest classification algorithm is a pixel-based machine-learning method relevant to decision trees (Bayram et al., 2017). Near-infrared (NIR) bands of Landsat-8 and Gokturk-2 images are analyzed. The analysis results are compared with the manually digitized shorelines using the Digital Shoreline Analysis System (DSAS). The average distances between manually digitized and extracted shorelines for Landsat-8 and Gokturk-2 imageries are reported as 11 m and 3 m, respectively.

Light detection and ranging (LIDAR) is one of the devices that creates detailed images while scanning over surfaces. Incekara et al. (2018) presented a study that normalized difference water index (NDWI)-based shoreline extraction. They used a LIDAR-derived intensity image (LDII) as an infrared band and compared the results with an orthophoto from Pléiades Satellite. The LDII image was added to the red-

green-blue (RGB) image as an infrared image to obtain a layer-stacked image. Their methodology includes pre-processing to reduce the noise in the images. Then, an NDWI calculation is conducted to separate the data into land and water. After separation, the shoreline is extracted. Results are compared with manually digitized vectors. Distance values range from 0 to 72 m and 0 to 114 m, which indicates that the dataset was heterogeneous. As a result, the use of LDII imagery as an infrared band needs to be evaluated more in detail for further studies based on their findings.

Moreover, Demir et al. (2019a) also used LIDAR and synthetic aperture radar (SAR) datasets in their study. They preprocessed and analyzed the data from the LIDAR dataset to estimate parameters used in SAR image analysis. Sentinel-1 Level 1 grade is used as a synthetic aperture radar (SAR) source. SAR images are also pre-processed before the analysis using external digital elevation model (DEM) data. Additionally, they employed a similar procedure in another study conducted in the same year using Sentinel-1A and Rasat pan-sharpened imagery. The use of optical and radar images together is exceptionally more effective for the correct extraction of shorelines (Demir et al., 2019b). The mean difference between the reference data was reported as 18.53 m in their study, while the k-means approach has a mean value of 23.69 m.

The effectiveness of Artificial Neural Network (ANN) added Self-Organizing Map (SOM) by the use of random forest (RF) methods to extract the shorelines from Landsat-8 imagery is investigated by Bayram et al. (2019). SOM, ANN, and RF are implemented in the Matlab environment to carry out the necessary calculations. The results are compared with the manually digitized shorelines. Further, Bayram et al. (2019) investigated the effectiveness of different machine-learning methods for shoreline extraction from UAV Images.

Image processing is another tool for shoreline extraction in the literature. Bamdadinejad et al. (2021) used support vector machine (SVM) classification and maximum likelihood classification methods to implement image processing into shoreline extraction studies. Landsat imagery is used, and the results are checked by

having overall accuracy and kappa coefficient calculation. The minimum and maximum of the pixel values in each band were reported as in the range of (0,1), which indicates the correctness of their calculations.

Karaman (2021) examined and compared different thresholding methods for shoreline extraction using Landsat-8 and Sentinel-2 imagery. Different atmospheric correction analyses are used in his study, and results are compared with the help of statistical methods.

Machine learning is a valuable tool for eliminating human mistakes and making studies more automated. Bengoufa et al. (2021) used Pléiades imagery that has high resolution in their study. The same Pléiades image is used for shoreline extraction by four different machine-learning models. These models can be categorized as pixel-based image analysis (PBIA) and object-based image analysis (OBIA). In their machine learning model, two machine learning classifiers, random forest (RF) and support vector machine (SVM), and two segmentation algorithms, multi-resolution segmentation (MRS) and mean shift segmentation (MSS), are used. They obtained six different shorelines for the same data; further, GPS data were collected from the location based on high water level (HWL) to compare the results using DSAS. As a result, it can be seen that object-based image analysis (OBIA) is more accurate in extracting shorelines in an automated manner.

It is clear that there are many extraction methods for shorelines that use multispectral images using NDWI values and others. These methods are mainly based on the classification of pixels obtained from satellite imagery to divide the image into different features. However, object-based analyses are used in some studies to obtain shorelines that implement the use of shape, texture, and other topological features (McAllister et al., 2022). The available methods for the extraction of shorelines are categorized and presented in Figure 2.1.

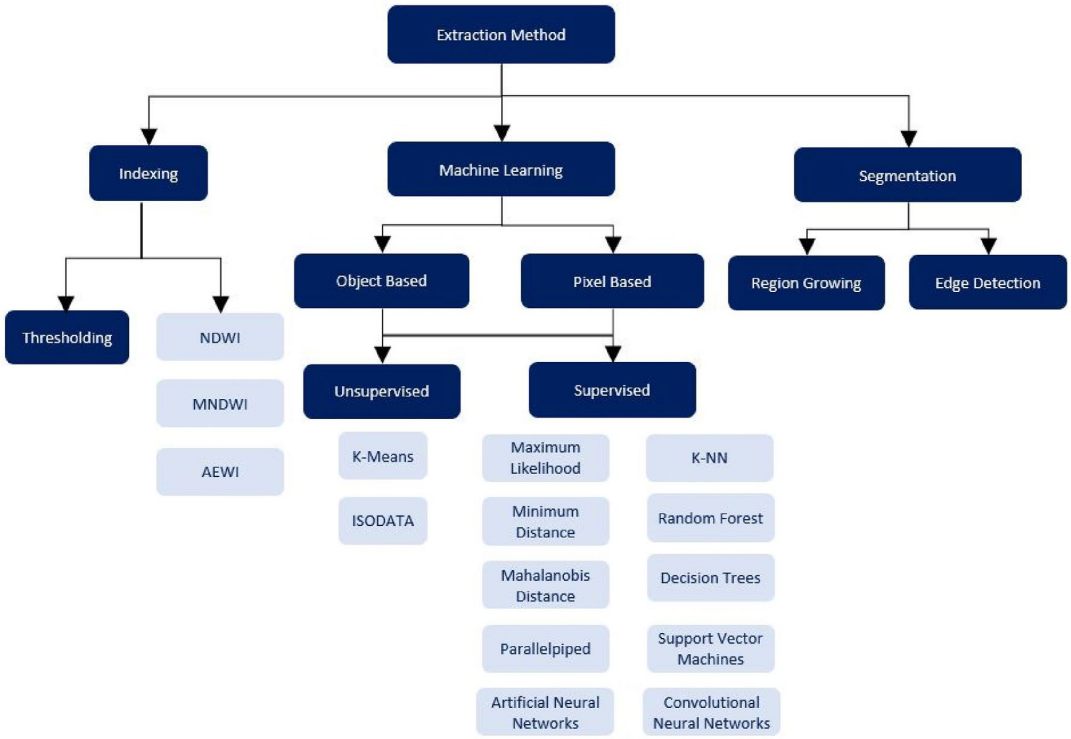

Figure 2.1. Available Shoreline Extraction Techniques (McAllister et al., 2022)

2.2 Shoreline Change Determination

There are two main approaches in the literature to obtain shoreline changes. These are numerical determination methods and geospatial determination methods. Numerical methods use data measurements from areas of interest (AOI), laboratory testing, and mathematical modeling of dynamic factors such as wind, wave, tide, and currents (Ergin et al., 2006).

On the other hand, geospatial modeling of shoreline changes uses satellite imagery, remote sensing techniques, and different algorithmic analyses. In this section, these two methods in the literature are reviewed.

2.2.1 Numerical Determination

Shoreline change models such as one-line theory are quite promising if continuous and uninterrupted, and the correct data for prediction of wave-induced longshore sediment transport is provided. Also, the data on resulting shoreline changes are necessary (Ergin et al., 2006).

All contours are assumed to have similar shapes and shift both landward and seaward together to a restraining offshore depth, with the depth of closure becoming a single contour line (Kamphuis, 2000). Based on assumptions, the sand continuity equation is derived for a given coordinate system and represented in Equation 2.1 and Figure 2.2.

$$\frac{\partial y}{\partial t} = -\frac{1}{D_C + B}\left(\frac{\partial Q}{\partial x} + q_y\right) \tag{2.1}$$

where y: along shoreline distance

t: time

D_c : depth of closure

B: beach berm height above still water level

Q: longshore sediment transport rate

x: longshore distance

q_y: sources/sinks along the coast

The depth of closure, D_C, which is used to calculate the change in time in the perpendicular direction to the shore, is formulated by Hallermeier (1978). The formula is represented in Equation 2.2.

$$D_C = 2.28 * H_s, 12 - \frac{68.5(H_s, 12)^2}{g * T^2} \quad (2.2)$$

where D_c : depth of closure

Hs,12 : non-breaking significant wave height that exceeded 12 hr per year

T : significant wave period

g : gravitational acceleration

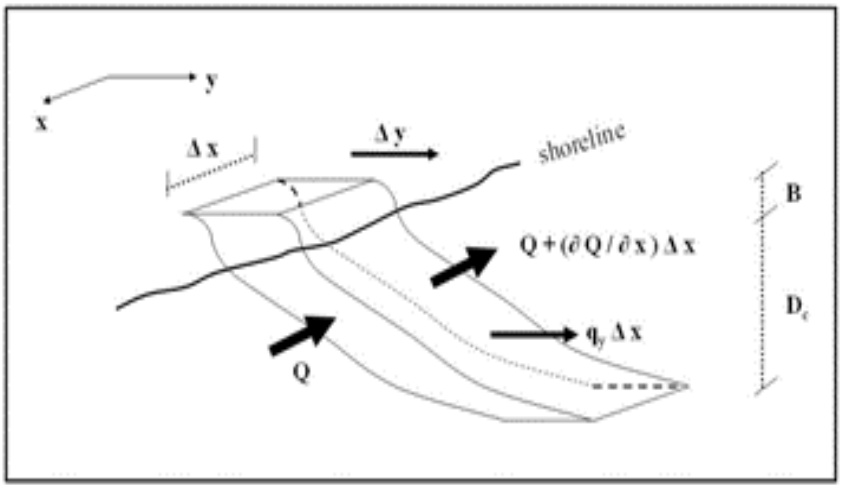

Figure 2.2. Sand Continuity Equation Sketch (Ergin et al., 2006)

Kamphuis (1991) developed experiments with three-dimensional(3-D) physical models of regular and irregular waves to define an expression for longshore sediment transport rate with a wide range of efficient parameters. Eventually, the following experimental formula, Equation 2.3, was derived with the application of non-dimensionalization.

$$Q = 7.3\, H_{sb}^{2}\, T^{1.5}\, m_b^{0.75}\, D_{50}^{-0.25}\, \sin^{0.6}(2\alpha_{bs}) \qquad (m^3/hr) \qquad (2.3)$$

where H_{sb}: significant breaker wave height (in m.)

T: significant wave period(in sec.)

m_b: beach slope at breaker location

D_{50}: median grain size diameter(in m.)

α_{bs}: efficient wave-breaking angle

Further, Ergin et al. (2006) used the one-line theory employing numerical model fundamentals in coastal engineering such as wave transformation, wave-structure interaction and sediment motion, and explicit solution of sand continuity equation to have an experimental study in the Black Sea region of Türkiye. The result of this study shows the usability of annual average wave heights in numerical models by comparing the results of the model with the field measurements.

Other applications of the one-line theory for shoreline change determination are made by Güler et al. (1998) and Ari et al. (2007). Ari et al. (2007) also used geospatial analysis in their study. The numerical model data is compared with the remote sensing techniques applied to the IKONOS data.

2.2.2 Geospatial Determination

The time, cost, availability of satellite imagery, and level of proficiency are deriving factors that direct the method and materials of the research to be used in shoreline changes (Süzen et al., 2003). Historical data is the most essential tool as it is a considerable source for disaster risk management and coastal zone management (Süzen et al., 2003). Süzen et al. (2003) used digitization of shorelines from hard copy maps and KVR-1000 images to obtain the change in shorelines in Yesilirmak

Delta. Further, 500-meter interval transects are implemented in the studied area to measure the changes in the shoreline. Transects are placed by using the “best fit” method. Moreover, Süzen et al. (2005) used aerial photographs to detect active shoreline changes in the Büyük Menderes River Delta for a period of 50 years.

Bayram et al. (2013) used object-oriented classification in their study while monitoring the shoreline and basin change of Terkos Lake. Landsat-8 and thematic mapper(TM) imagery are used as data sources. Automatic shoreline extraction techniques are used to develop shorelines. The error range of shorelines equals almost a pixel based on Landsat-8 imagery. Error estimation is made by using manually digitized maps. Ozturk et al. (2015) applied a similar methodology to their study. They investigated the shoreline and basin change in the Kizilirmak Delta. They also used the Digital Shoreline Analysis System (DSAS) tool to analyze the shoreline data.

By integrating artificial intelligence into different disciplines, machine learning methods are used and studied in different areas. Shoreline extraction and change detection have also taken advantage of these trends. Kumar et al. (2020) investigated the efficiency and capability of using machine learning for mapping shorelines on the eastern Indian coast. Artificial neural network (ANN), k-nearest neighbors (KNN), and support vector machine (SVM) algorithms were integrated into their study as a machine learning model. The integration of machine learning to shoreline change studies created a chance to combine both numerical and geospatial methods. As previously mentioned in Section 2.2.1., the numerical determination of shoreline changes has some challenges, such as implementing all deriving factors to the numerical models. Kumar et al. (2020) incorporated to reflect the wind speed and wave height data into their ANN model, which resulted in an 86.2% accuracy rate when comparing it with the KNN and SVM models. Based on the analysis of their study, the most outstanding elements of shoreline shift prediction are wind speed and wave height.

Additionally, tidal currents are the most effective shoreline change effects in Asia. Therefore, continuous detection of shoreline change is needed in Asia. Due to the nature of satellites, big storage spaces are needed to evaluate the continuous shift of shorelines. To overcome this problem, big data platforms like Google Earth Engine enable users to develop their studies on cloud computing platforms. Arjasakusuma et al. (2021) used Google Earth Engine to extract shorelines from multitemporal satellite images from Landsat-7 ETM and Landsat-8 OLI by using the normalized difference water index (NDWI) in East Java Province, Indonesia. Further, using these extracted images, the Digital Shoreline Analysis System (DSAS) calculates the rate of change of shorelines year by year. Consequently, the end point rate (EPR) was reported in their study location. Ding et al. (2021) also used the Google Earth Engine to monitor the changeable shorelines in the Malay Islands with a similar methodology.

The Digital Shoreline Analysis System (DSAS) is a valuable tool by the United States Geological Survey (USGS) to evaluate the change between shorelines from different dates for the exact location. As previously mentioned in this chapter, even though the data sources and shoreline extraction methodologies change, researchers tend to use DSAS for the calculations and results. There are many applications of DSAS all around the world. For instance, Hossain et al. (2021) used DSAS in their study to monitor the shoreline change in the southeast coast of Bangladesh. The end point rate (EPR) and linear regression rate (LRR) are reported based on their study and shoreline extraction methodology. Besides this, Elkafrawy et al. (2021) implemented DSAS in their study to evaluate the effectiveness of coastal structures along the Eastern Nile Delta in Egypt. Shorelines are extracted by using histogram band thresholding. Besides, Shenbagaraj et al. (2021) chose to use unmanned aerial vehicle (UAV) imagery to monitor the shore. Results are obtained using vector overlay techniques to evaluate the areas where shoreline change occurs and DSAS to get the rates of change of shorelines annually. Natarajan et al. (2021) used an analogous model for shoreline change in India. Following that, the Kalman filter is employed to predict the future potential shoreline change in 2040. Matin et al.

(2021), Koulibaly et al. (2021), Al Ruheili et al. (2021), Quang et al. (2021), Kumar Das et al. (2021), Yiğit et al. (2022), Xu et al. (2022) studied different parts of the world through their research by using distinct data sources but similar methodologies. DSAS is commonly used in their papers, and similar shoreline extraction techniques have been implemented.

2.3 Comprehensive Summary of the Chapter

A comprehensive summary of the literature for the determination of shoreline change is provided in this chapter. Shoreline changes are of interest to scientists globally due to the value of coastal ecosystems and the economic importance of coastal changes. Studies involve mainly two explicit approaches.

The first of these methods is the numerical modeling of sediment transportation. Numerical models are used to predict and understand the shoreline change behavior. The nature of shorelines causes the lack of these methods. Shoreline change occurs for different reasons, such as wind, wave, tide, current, and vegetation effects, excluding deliberate human effects. These effects sometimes occur individually, but generally, two or more of them are the deriving factors for the transformation. The one-line theory is introduced as a commonly used theory in numerical models of sediment transportation. However, a well-known fact for the numerical models is that the results depend on the given wave data input (Ergin et al., 2006). Therefore, generalization of results requires more experimental studies and statistical evaluation of these studies.

The second method is the use of remote sensing techniques. In literature, different shoreline extraction methods exist using physical maps, UAV scans, and satellite imagery. Moreover, different machine learning methods are used to extract shorelines automatically with the lowest error. Using programming and artificial intelligence contributes to the automatization of shoreline extraction. However, a significant amount of error is generated through these implementations. Errors are

generally checked by using manually digitized shorelines throughout the studies. While comparing the shorelines, an error is generally estimated to be close to the resolution of a pixel, which concludes to be in an acceptable range for continuing the process (Bayram et al., 2013). In addition to shoreline extraction, quantifying shoreline changes and their effects is an important part of the studies. Generally, the DSAS tool is observed throughout the literature review to determine the relative change of shorelines numerically. The deriving factor for the shoreline change varies in different parts of the world. Some studies are needed due to the effects of tides and coastal erosion. On the other hand, some studies have been developed to examine the effects of accretion by wind and wave induction.

CHAPTER 3

STUDY AREA

The Eastern Mediterranean Region of Türkiye is well-known for its attractive tourist facilities and natural surroundings. Two cities lie in the eastern part of the Mediterranean region. These cities are Antalya and Mersin. Antalya holds many counties on its territory. One of these sub-cities is Alanya, which has many rivers and streams that carry sediments from the Taurus Mountains. Dim River is a small stream that carries lots of sediments and is one of the most dynamic sections of this city in terms of shoreline change. It is located to the east of Alanya city center.

The study is conducted using different models, starting from the large-scale surface corresponding to the swath size of the Landsat satellite, which is about 250 km, to the low-scale surface covering the Dim River mouth area, which is about 10 km. The initial study area equals the swath size of the Landsat satellite, which has Antalya city center on the west side and Tekmen Harbor on the east side, as shown in Figure 3.1. Then, the focus is narrowed to the entire coastline of Alanya to eliminate potentially high errors due to the nature of shoreline change. Shoreline change may differ from point to point. Thus, large-scale studies increase the error of estimation. End point rate (EPR) and linear regression rate (LRR) are generally reported as a result of analysis of shoreline changes, and using large-scale while estimating these rates may result in the wrong outcomes.

At the last step of modeling, another area reduction is made up to the affected area of Dim River. Dim River creates a dynamic environment regarding shoreline changes and is affected by the seasonal precipitation regime. Human effects are known to be less than the average from the entire Alanya coastline. Hence, this location is selected to understand the natural behavior of shoreline change. Since it

is impossible to monitor the shoreline changes by the effect of humans, the location characteristics of the site must be naturally dynamic.

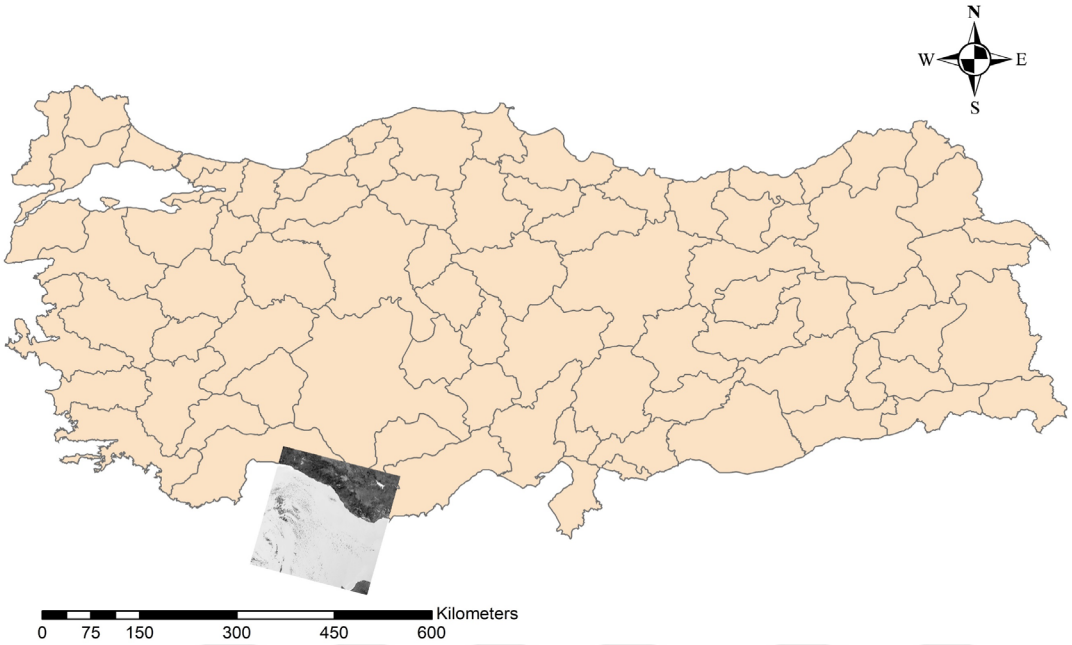

Figure 3.1. 30th of August, 2023 Landsat-8 Image on Türkiye Map

3.1 Initial Study Area

The analysis of this thesis primarily uses Landsat-8 images used to extract the shorelines. Imaging that begins in the middle of Antalya City Center and ends at the east border of Tekmen Harbor, Mersin, has been extracted from available Landsat data to show the shoreline changes. This shoreline is about 243 kilometers in length based on the calculations in ArcGIS software from the manually digitized shoreline data that belongs to the 30th of August, 2023 Landsat-8 Image, as shown in Figure 3.2.

Figure 3.2. Initial Study Area Representation

3.2 Characteristics of Alanya

Alanya is a prominent geographical entity within Antalya Province. It is strategically positioned along the Mediterranean coast of Turkiye and situated approximately 135 km eastward from the city center of Antalya. The total surface area is approximately 175,658 hectares. Thus, Alanya generates a multifaceted topographical and hydrological diversity. The boundaries of Antalya, Alanya, and generated shorelines are represented in Figure 3.3.

The northern districts of Alanya are externalized by the orogenic branching of the Taurus Mountains, conjoined at the connection of Geyik and Akçalı Mountains, whose altitudinous peaks surpass 1,000 meters. Conversely, the southern topography is restricted by the iconic Alanya peninsula. It is fortified by a continuous wall extending over 6,500 meters, which effectively segregates it from the adjacent plains and the Taurus Mountain range. Despite the formidable topographical obstacles,

traversing passages such as Koçdovat Gediği, Kuşyuvası, Yelköprü, and the valleys etymologically affiliated with the Dim and Alara rivers facilitate connectivity with Inner Anatolia.

The geostrategic significance of Alanya is further underscored by its role as a natural harbor on the eastern periphery of the peninsula. A prominent geological characteristic of Alanya is the prevalence of Permian crystalline limestones, constituting the foundational substrate of the peninsula. This geological substrate, punctuated by apparent fractures indicative of recent tectonic activities, metamorphosed into an expanse of plains through alluvial deposition, imparting a geomorphological panorama.

The northern expanse of Alanya, characterized by summits, plateaus, and peaks, serves as a seasonal habitat for the indigenous populace, who establish summer settlements amid these altitudinous locales (URL-1). The lower altitudes metamorphose into coastal plains, demarcating the Alanya peninsula from the Taurus Mountains and highlighting the region's geomorphic diversity. A labyrinthine system of rivers articulates Alanya's hydrographic network. Further, each seep provides distinctive hydrological behaviors across different times.

During the hot summers characterized by dry weather, the reduction in river flow gives way to the revival of watercourses following autumnal precipitation. In spring, there is a peak in water levels due to the thawing of the Taurus Mountain snowpack, leading to accelerated river flow and an increase in erosional tendencies due to steep topography that results in sediment transportation through rivers and streams.

The primary rivers vital for agricultural irrigation in the region are the Alara River, Kargı River, Serapsu River, Oba River, and Dim River, marking the boundary between the districts of Manavgat and Alanya. The developmental trajectory of the Dim River is further emphasized by ongoing initiatives related to the Dim Dam project (URL-1).

Land use in Alanya is divided into distinct categories, including agricultural activities, meadows, and pastures, and is predominantly dedicated to the civil and cultural domain. The climatic and soil conditions in the region grant Alanya the distinction of possessing the most fertile soil in the Mediterranean.

Efforts in afforestation, with an annual allocation of approximately 750 hectares, contribute to the expansion of the arboreal domain. Coniferous ecosystems, including pine and cedar varieties, adorn the elevated areas of the mountains, while extensive pine forests grace the coastal expanses. Notable agricultural cultivation includes citrus orchards and banana plantations, along with the growing cultivation of economically significant arboreal species such as avocado and kiwi (URL-1). Alanya's arboreal composition extends to the horticultural domain, incorporating cold-resistant fruit varieties such as apple, pear, and quince, which are visible in the mountainous and plateau regions. The introduction of ornamental eucalyptus trees, initially used for wetland reclamation, now contributes to the aesthetic enhancement of roadside environments.

Alanya has a typical Mediterranean climate, which gets hot and dry in the summers and mild and rainy in the winters (URL-1). The daytime cooling during summer happens because of the coastal breeze from the sea, which helps reduce the overall heat. All of this makes Alanya a captivating destination in the world of tourism.

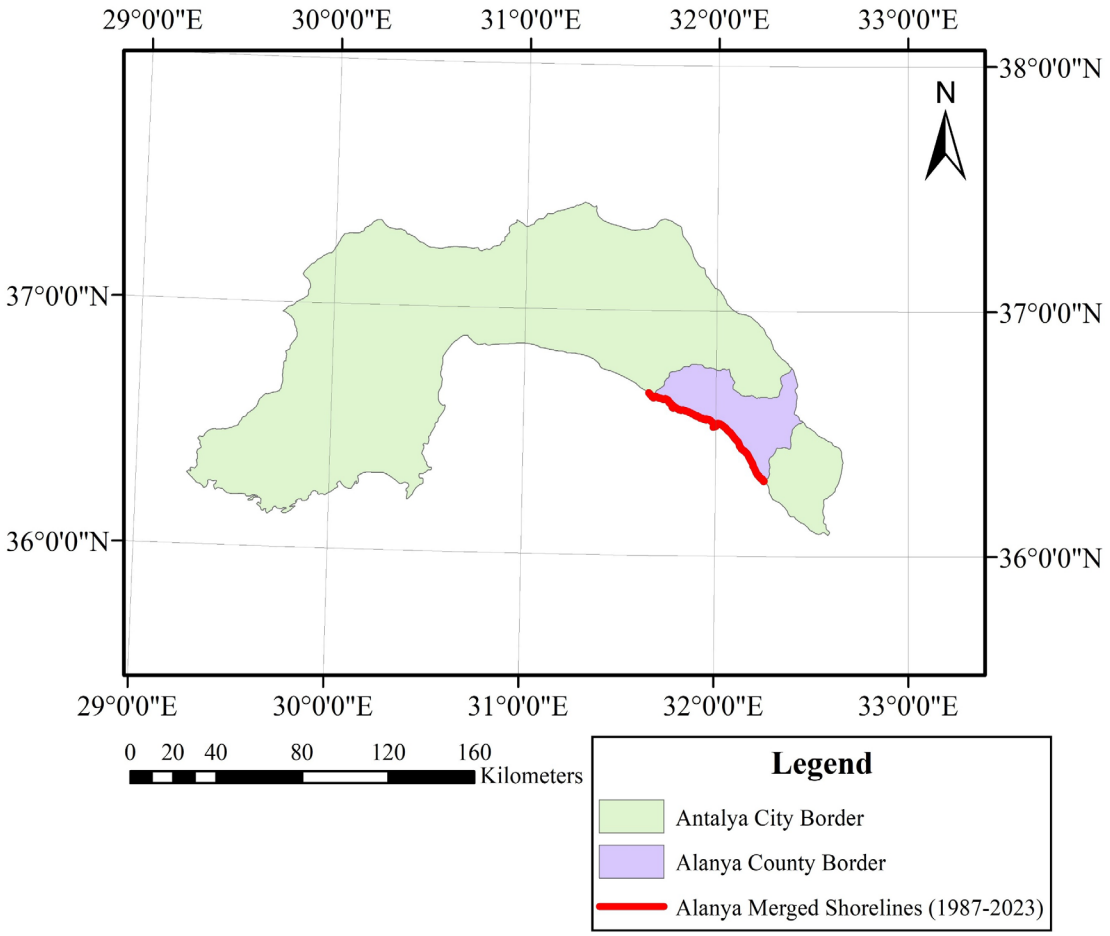

Figure 3.3. Borders of Antalya and Alanya with the Extracted Shorelines

3.3 Characteristics of Dim River

The coastal dynamics of the Dim River mouth in Alanya are regarded as essential for both environmental considerations and developmental initiatives. The river marks the administrative boundaries between the districts of Manavgat and Alanya.

The coastal dynamics of the Dim River mouth are characterized by sophisticated interactions between sedimentation, erosion, and hydrodynamic processes, necessitating scholarly attention. Factors such as tidal influences, sediment transport

mechanisms, and the impact of anthropogenic interventions are subjected to comprehensive examination within academic discourse. The location of Dim River is presented in Figure 3.4. Moreover, in Figure 3.5. three different Google Earth images of Dim River Mouth are represented in 3-month periods.

The geomorphological configuration of the Dim River mouth is inherently dynamic, reflecting complex interdependencies between fluvial and marine forces. Analyses of coastal dynamics in this context involve investigating the morphological changes induced by the river's discharge and its convergence with marine currents. Such analyses contribute to an academic understanding of the evolving coastal landscape, offering insights into potential implications for ecological integrity and sustainable land use practices. Furthermore, the bathymetric geomorphology is also considered to check whether there is a geological formation under the sea that has a formation like a submarine valley by using bathymetric maps, which are represented in Figure 3.6.

In addition to its geomorphic significance, the Dim River assumes agricultural relevance, as it is utilized as a vital water source for irrigation practices underlying local agricultural pursuits as a contribution of Dim Dam. Dim Dam is located on the Dim River in the Alanya district of Antalya, presented in Figure 3.4. constructed between 1998 and 2004. The dam serves the purposes of irrigation, energy generation, and the supply of drinking water. It has a concrete and rock-filled dam structure. The dam's height from the riverbed is 135 meters, and at the average water level, the reservoir has a volume of 265 hm^3 and an area of 4.48 km^2. The dam provides irrigation services to an area of 5,312 hectares and produces 38 MW of power, generating an annual electricity output of 123 GWh (URL-2). Additionally, the dam supplies 11 hm^3 of drinking water annually to the city of Antalya. Dim Dam's features highlight its role in water management and energy production and in providing essential resources for agriculture and the local community.

Therefore, an investigation of the coastal dynamics of the Dim River mouth transcends its geological complexity, incorporating considerations of social implications and sustainable resource utilization.

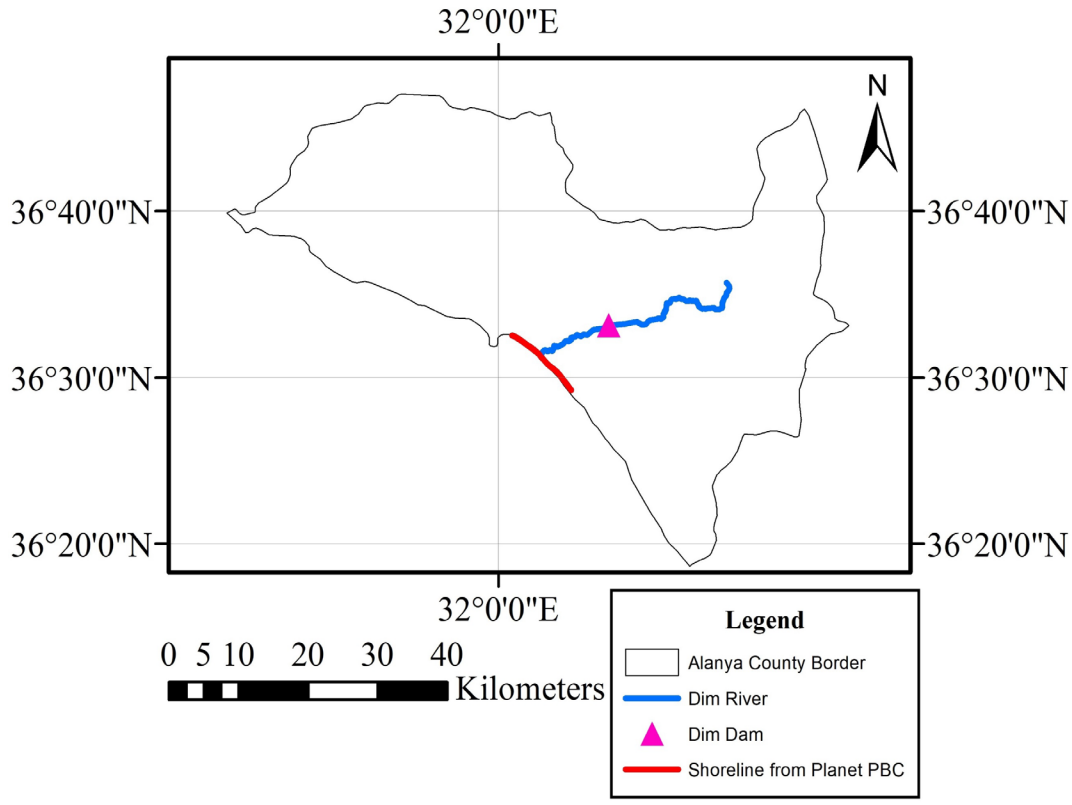

Figure 3.4. Location of Dim River

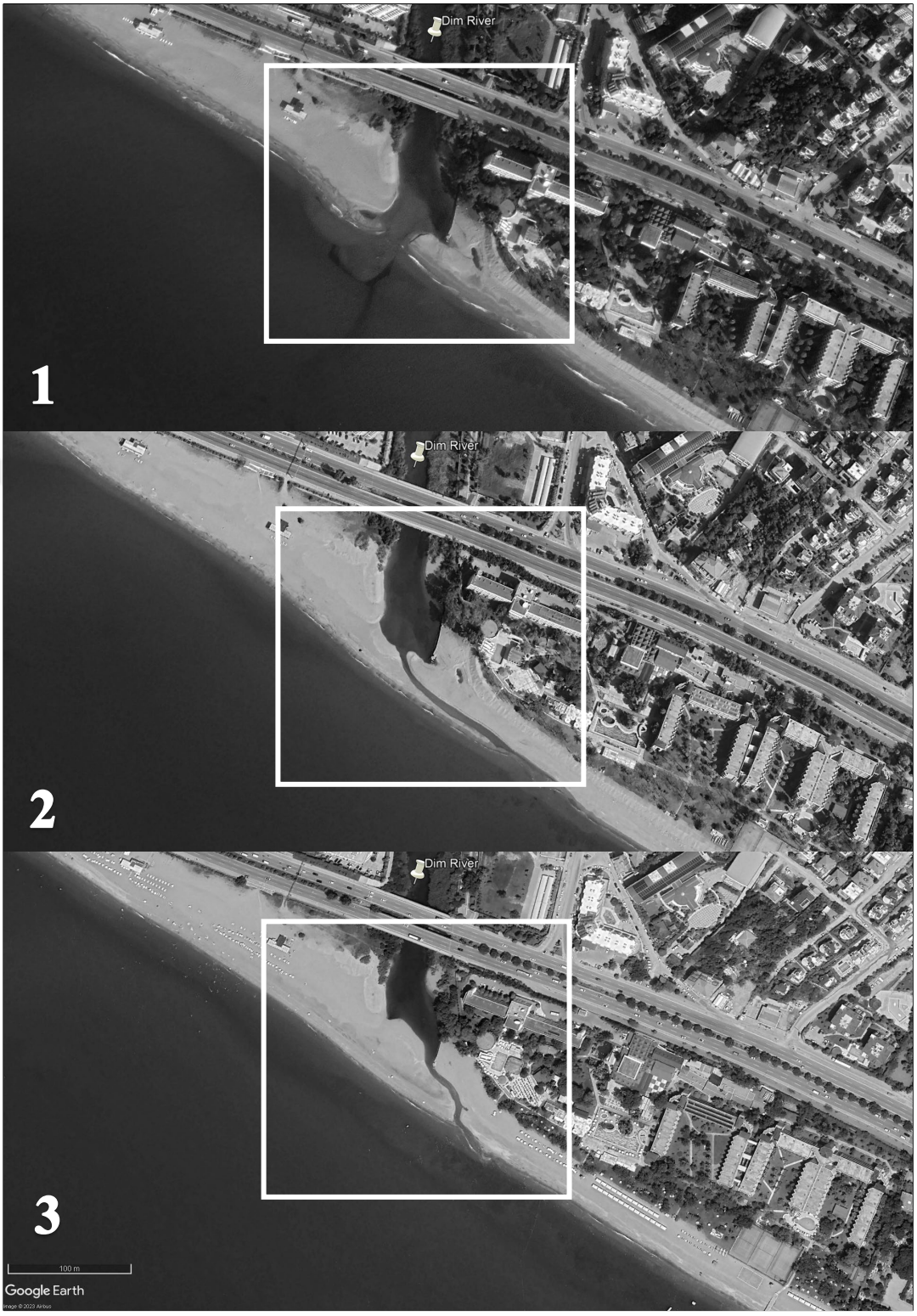

Figure 3.5. Google Earth Images of Dim River (1st Photo belongs to December, 2022, 2nd photo belongs to March, 2023, and 3rd photo belongs to June, 2023)

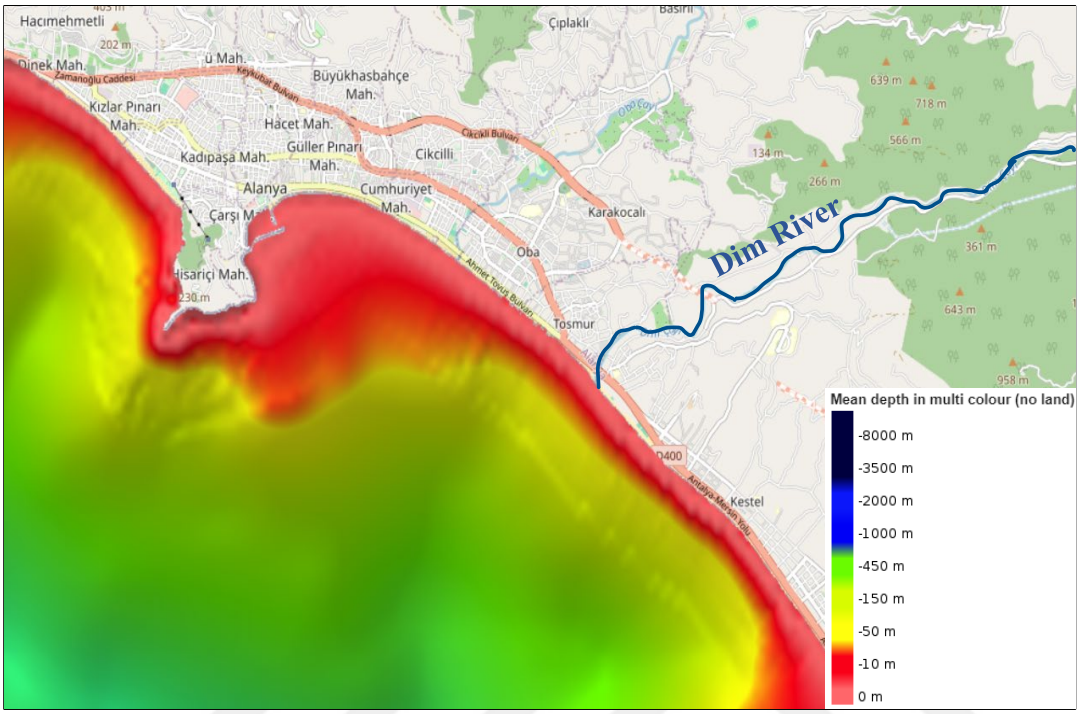

Figure 3.6. Bathymetry Map of Dim River Mouth (URL-3)

CHAPTER 4

METHODOLOGY AND DATA CHARACTERISTICS

The methodology includes several steps. These steps are data collection, shoreline extraction from the collected data, modeling of the shorelines and change by using a Digital Shoreline Analysis System (DSAS), and, ultimately, analysis of the results of the models.

This chapter provides the shoreline extraction procedure, modeling of the shorelines, and analysis methodology. These steps are tabulated in Figure 4.1. Two different types of data were used in the study. The data collection and processing differs from one dataset to another. The theoretical background and procession steps in this study are also discussed in this chapter.

This study also includes a suggested procedure for shoreline extraction. The steps of shoreline extraction include Normalized Difference Water Index (NDWI) application to the data, reclassification of the NDWI imagery, two consecutive data type conversions, and manual editing to obtain the shoreline. Additionally, after extracting a single shoreline, several attributes are provided that are needed to create the model later.

Modeling requires two layers. These layers are the baseline layer and shorelines layer. After the creation of these layers, the model is executed, and the intersections and transect layers are created automatically. The baseline and shoreline layers require several mandatory attributes for the model to function properly. These attributes and execution procedures are provided in this chapter.

After the modeling, a detailed analysis is carried out to generate meaningful results from the model. Different results are calculated based on the data provided. The tool provider notes that the results depend on the reliability of the inputs provided

(Himmelstoss et al., 2021). The shoreline change envelope (SCE), net shoreline movement (NSM), end point rate (EPR), and linear regression rate (LRR) are calculated after the creation of the model.

As the last step of this study, further analysis is made with higher-resolution data from Planet Public Benefit Corporation (PBC) Satellite. This analysis is used to assess the sensitivity of this study.

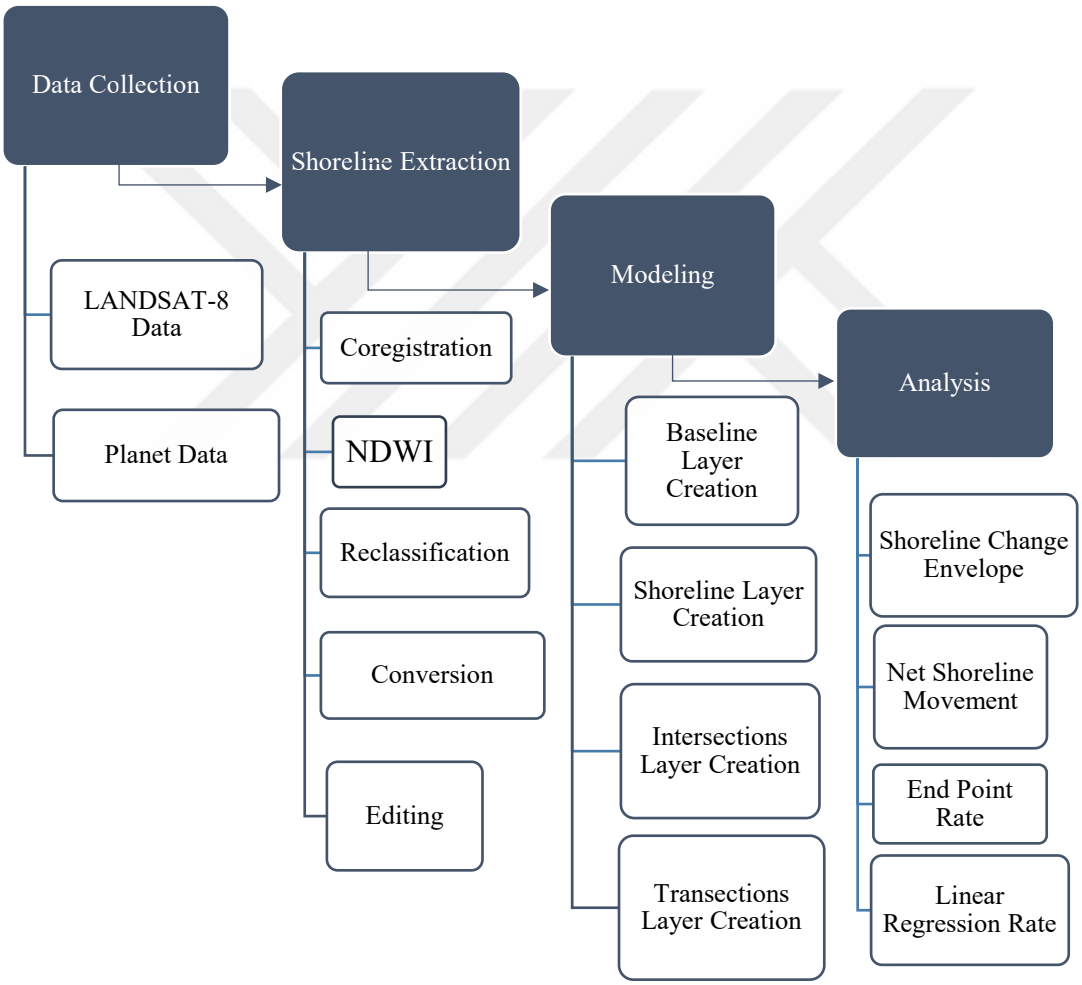

Figure 4.1. Overall Flowchart of the Study

4.1 Satellite Data Characteristics and Processing

In this study, two different data sources are used. Landsat data is considered mainly for the construction of the shoreline change model. Then, Planet data is used to validate the accuracy of the results obtained from Landsat data.

The shoreline imaging was taken between 1987 and 2023. The summer months of June, July, and August were selected to eliminate the cloud cover on the imagery. The available Landsat data was sorted using this restriction to ensure that at most 10% of cloud coverage was present. The dataset shows that the Landsat image bands correspond to an image change depending on the year. It, therefore, directly affects the calculation of the normalized difference water index (NDWI).

Landsat data holds nine different bands to evaluate the images. However, Planet data has only four bands. Due to the difference in the number of bands, different procedures are followed in the shoreline extraction process.

4.1.1 Landsat Data

The name Landsat corresponds to the name of the original mission. The Landsat mission was initiated under Project EROS (Earth Resources Observation Satellite) in the early 1960's in the United States. The main target of the mission was to develop and launch Earth observation satellites for the sake of humanity.

Over the years, different Landsat satellites have been launched. Landsat-1 was launched in 1972. The launches of Landsat-2, Landsat-3, and Landsat-4 followed in 1975, 1978, and 1982, in order. Then, Landsat-5 was launched in 1984, and it operated for about twenty-eight years by providing high-resolution continuous data. Landsat-6 failed to achieve Earth orbit. Landsat-7 in 1999, Landsat-8 in 2013, and Landsat-9 in 2021 were launched, respectively (Wulder et al., 2016). The evolution of Landsat satellites is represented in Figure 4.2.

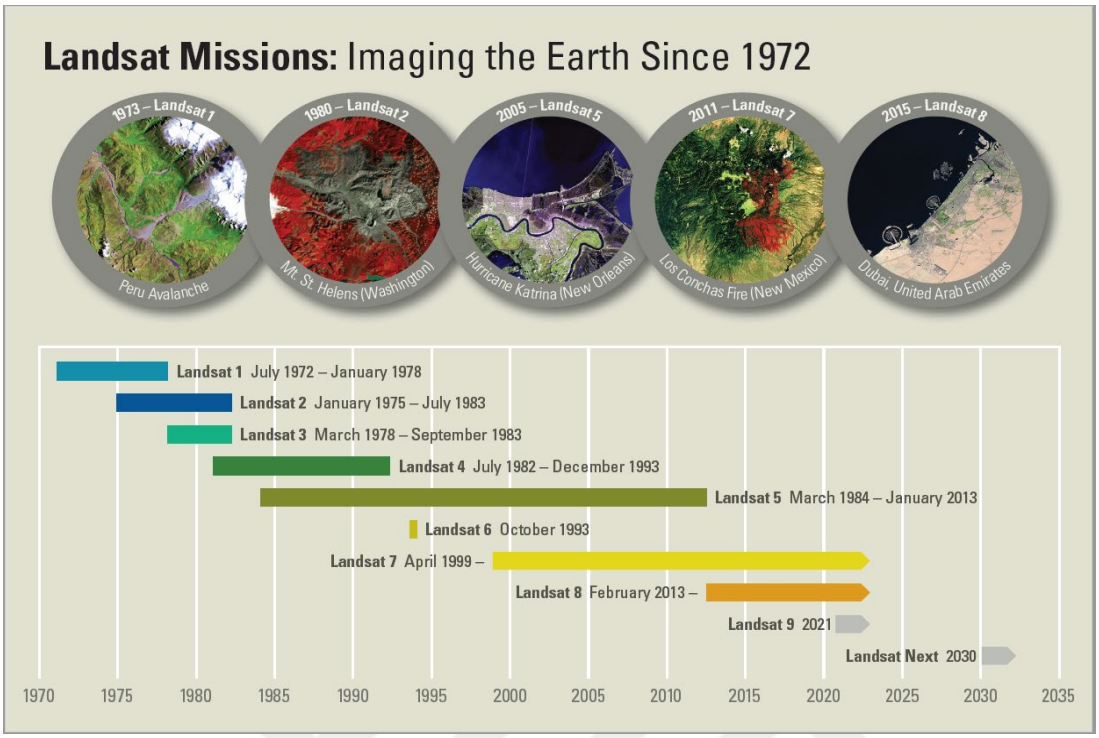

Figure 4.2. The Evolution of Landsat Satellites (Source: Public Domain)

Most of the data used in this study was obtained from Landsat-8. Landsat-8 satellite includes two sensors. These are Operational Land Imager (OLI) and Thermal Infrared Sensor (TIRS). The Landsat-8 satellite generates 30-meter resolution, 11-band images. All bands, excluding the Band 8, Band-10 and Band-11 have a 30-meter resolution. And the spectral range changes from 0.43 µm to 12.51 µm. The study data consists of imagery between the years 1987 and 2023. Before 2013 there are four shorelines used for this study. These data correspond to the Landsat-5 and Landsat-7 satellites. The Global Land Survey (GLS) datasets consist of orthorectified Landsat-type satellite images with minimized cloud cover. These images offer nearly comprehensive coverage of the world's land area approximately every decade since the early 1970s (Gutman et al., 2013). The images for the years 1987, 2005, and 2009 are taken from GLS collections. Further, the image from the year 2000 is taken from the L1G collection. All these data correspond to either

Landsat-5 or Landsat-7 satellites. The sensor type in these satellites is ETM+, which is different from the Landsat-8. Due to the usage of different sensors in these satellites, the band numbers change. Landsat-5 has seven bands, while Landsat-7 has eight bands. The corresponding bands, the spectral ranges, the resolution values of bands, and the names of the bands of Landsat-8 data are tabulated in Table 4.1.

A total of sixty-six images are used to extract shorelines from different dates. The details of these images are given in Table A.1. in Appendix A.

Table 4.1 Landsat-5-7-8 Bands

Band No.	*Name of the Band*	*Spectral Range (μm)*	*Resolution (m)*	*Landsat No.*
Band 1	Coastal Aerosol	0.43 – 0.45	30	Landsat-8
Band 2	Blue	0.45 – 0.51	30	Landsat-8
Band 3	Green	0.53 – 0.59	30	Landsat-8
Band 4	Red	0.64 – 0.67	30	Landsat-8
Band 5	Near-Infrared	0.85 – 0.88	30	Landsat-8
Band 6	Short Wave Infrared-1	1.57 – 1.65	30	Landsat-8
Band 7	Short Wave Infrared-2	2.11 – 2.29	30	Landsat-8
Band 8	Panchromatic(PAN)	0.50 – 0.68	15	Landsat-8
Band 9	Cirrus	1.36 – 1.38	30	Landsat-8
Band 10	TIRS - 1	10.6 - 11.19	100	Landsat-8
Band 11	TIRS - 2	11.5 - 12.51	100	Landsat-8
Band 1	Blue	0.45 – 0.52	30	Landsat-7
Band 2	Green	0.52 – 0.60	30	Landsat-7
Band 3	Red	0.63 – 0.69	30	Landsat-7
Band 4	Near-Infrared	0.77 – 0.90	30	Landsat-7
Band 5	Short-wave Infrared	1.55 – 1.75	30	Landsat-7
Band 6	Thermal	10.40 – 12.50	60	Landsat-7
Band 7	Mid-Infrared	2.08 – 2.35	30	Landsat-7
Band 8	Panchromatic	0.52 – 0.90	15	Landsat-7
Band 1	Visible Blue	0.45 – 0.52	30	Landsat-5
Band 2	Visible Green	0.52 – 0.60	30	Landsat-5
Band 3	Visible Red	0.63 – 0.69	30	Landsat-5
Band 4	Near-Infrared	0.76 – 0.90	30	Landsat-5
Band 5	Near-Infrared	1.55 – 1.75	30	Landsat-5
Band 6	Thermal	10.40 – 12.50	120	Landsat-5
Band 7	Mid-Infrared	2.08 – 2.35	30	Landsat-5

4.1.2 Planet Data

Planet is a leading Earth imaging company that operates the PlanetScope satellite constellation. The PlanetScope features approximately 130 satellites that capture detailed imagery of Earth's surface. Utilizing advanced sensors, these compact CubeSat satellites are designed in a 3U form factor, measuring 10 cm by 10 cm by 30 cm, enabling them to capture high-resolution data (*Planet Scope*, 2023)

The second-generation satellites are known as Dove-R or PS2.SD, use a multistripe frame with bands divided between RGB (Red, Green, Blue) and NIR (Near-Infrared), enhancing the spectral resolution of the imagery. Meanwhile, the third-generation SuperDove or PSB.SD satellites, equipped with sensors launched in early 2020, produce daily imagery with eight spectral bands. These bands include Coastal Blue, Blue, Green I, Green, Red, Yellow, Red Edge, and Near-Infrared, offering a comprehensive view of the Earth's surface. The sophisticated sensor technology enables Planet to provide valuable data for various applications, including environmental monitoring, agriculture, and land cover analysis (Planet Scope, 2023). The image processing chain of Planet consists of three categories with different applications to the raw data to enhance the number of bands, represented in Figure 4.3.

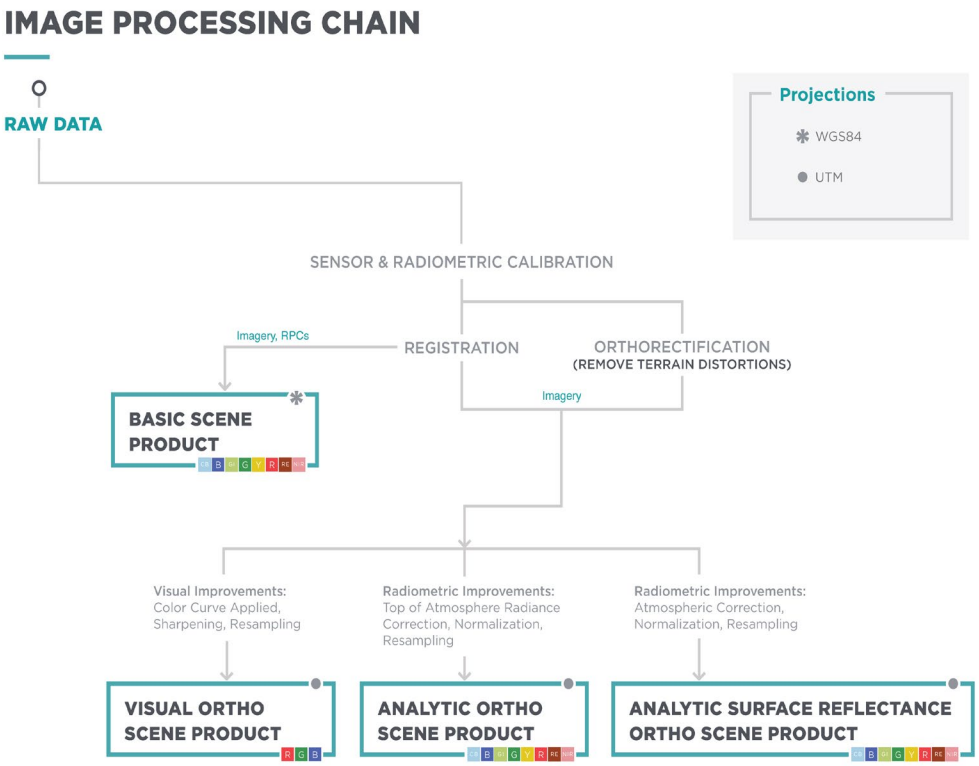

Figure 4.3. Image Processing Chain of Planet (*Planet Scope*, 2023)

Planet provides 3-band, 4-band, and 8-band datasets based on user requirements and demand. PS2 and PS2.SD sensors provide only 3-Band and 4-Band imagery. However, third-generation sensors are named as PSB.SD provides all three types of imagery: 3-band, 4-band, and 8-band. Planet has a 3-meter resolution, ten times greater than a typical Landsat image with a 30 by 30-meter resolution. The corresponding characteristics of the Planet image are represented in Table 4.2.

Table 4.2 Planet PS2 4-Band Data Characteristics

Band Number	*Name of the Band*	*Spectral Range (μm)*	*Resolution (m)*
Band 1	Red	0.59 – 0.67	3
Band 2	Green	0.50 – 0.59	3
Band 3	Blue	0.455 – 0.515	3
Band 4	Near-Infrared	0.78 – 0.86	3

This study uses only an RGB-band Planet Image to develop the sensitivity. The date of the planet image is selected by considering similar criteria used in the Landsat image selection. To overcome the cloud interruption, the most available summer image is selected. The characteristics of the data used in sensitivity in this study are represented in Table 4.3.

Table 4.3 Sensitivity Data

Year	*Image Date (MM.DD.YYYY)*	*Source*
2023	07.27.2023	Planet
2023	07.29.2023	Landsat-8

4.2 Shoreline Extraction Procedure

The accuracy of the shoreline extraction procedure is the essence of this study since the results of the study are heavily dependent on the accuracy of the provided data. The nature of satellite imagery consists of many pixels that have a resolution based on the type of the satellite. Landsat-8 images have a 30-meter resolution, which means the axis of a pixel corresponds to a 30-meter length in lateral and vertical distance. The semi-automatic shoreline extraction process consists of five sections: coregistration of the images, the separation of images as land and sea sections, reclassification of these sections, two consecutive conversions of data from raster to polygon and polygon to polyline, and elimination of unnecessary parts of the digitized images.

After extracting a single shoreline, several attributes are provided automatically by the ArcGIS software or by user creation. The flowchart of the shoreline extraction process is represented in Figure 4.4.

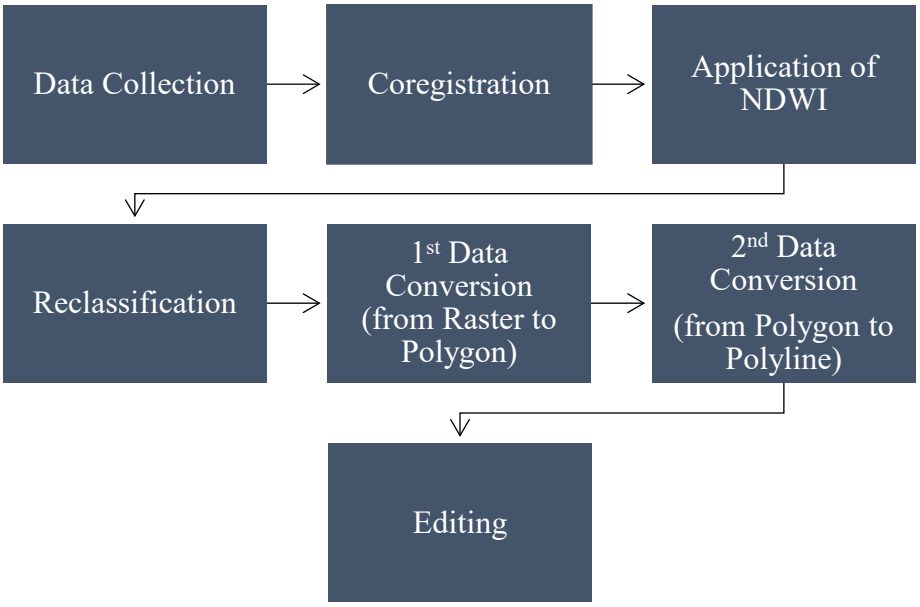

Figure 4.4. Flowchart of Shoreline Extraction

The same object from the real world from different data sources that are collected at different times is represented in geospatial studies. To overcome potential distortions in Landsat images that are collected from different years and months, co-registration is applied before making any application in the shoreline extraction process. Some certain landmarks are selected on the images, and each image is checked to determine whether there is any distortion or not in the collected imagery. A representation of the coregistration process is visualized in Figures 4.5. In these figures, the lighthouse of Alanya port is selected with a red square polygon, and different Landsat and Planet images are expressed as the visualization of the coregistration process.

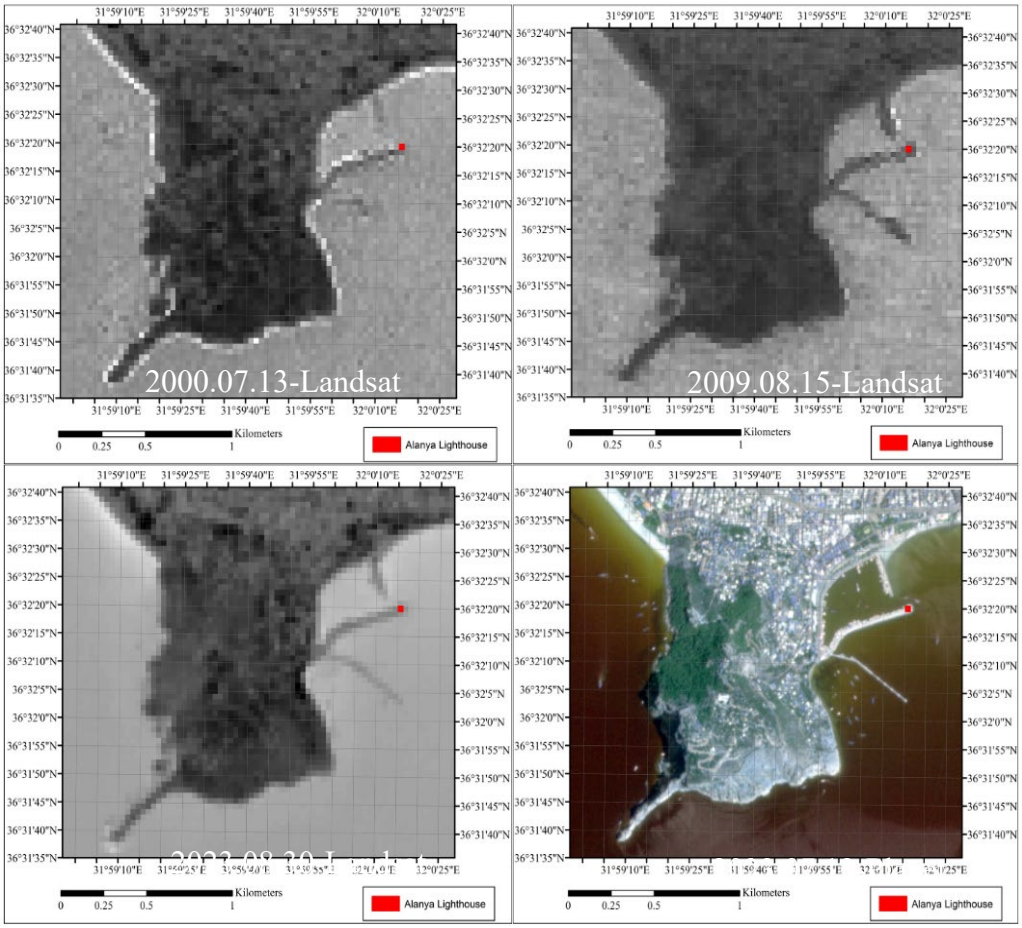

Figure 4.5. Co-registration Representation

Reclassification refers to the process of taking input cell values and changing them with new output cell values. Reclassification is frequently employed to streamline or alter the interpretation of raster data by substituting a specific value with a new one or consolidating ranges of values into a singular value. In other words, reclassification tools modify raster values, and the reclass by individual value tool facilitates a one-to-one alteration of specific values within the raster. In scenarios like habitat analysis, where distinct values in a land use raster signify different land use types, reclassification assigns a preference range to each value, providing meaning to each land use type. This process involves assigning higher values to more favored land types and lower values to less preferred ones. The reclassification is executed individually, resulting in an output range of values (*Reclass by Ranges of Values*, n.d.) Additionally, the reclassification of value ranges is a process where alternative values are assigned to specific intervals of values. This is particularly useful when dealing with continuous data, as seen in applications like habitat analyses. Instead of specifying each value and its alternative, the reclassification tools require lower and upper bounds inputs for the existing values and the corresponding alternative value for the defined range. The output then assigns the alternative value to all original raster values within the specified range. The handling of boundary breaks varies depending on the specific tool used for reclassification by ranges (Reclass by Ranges of Values, n.d.). In this study, images are reclassified after applying NDWI calculation to the raster files. Reclassification is based on two output zones with natural breaks to identify the raster files as land and sea.

The Normalized Difference Water Index (NDWI) calculation and reclassification are applied to raster files from the satellite imagery. Two conversions are applied to the raster files after the NDWI application and reclassification. Firstly, a reclassified raster file is converted to a vector file to form polygons. This conversion allows the potential polygons from the raster file to be obtained for further analysis. Then, the sea polygon is converted to the polyline file to extract the shoreline. Additionally, some fluctuations occur on the shoreline at the end of the semi-automatic process. These fluctuations are manually edited to eliminate potential errors in the analysis.

In Figure 4.6, the elimination of fluctuations is represented. The red-colored line is the corresponding shoreline of the image. The top picture is an ill-conditioned shoreline, and the bottom picture is a corrected shoreline.

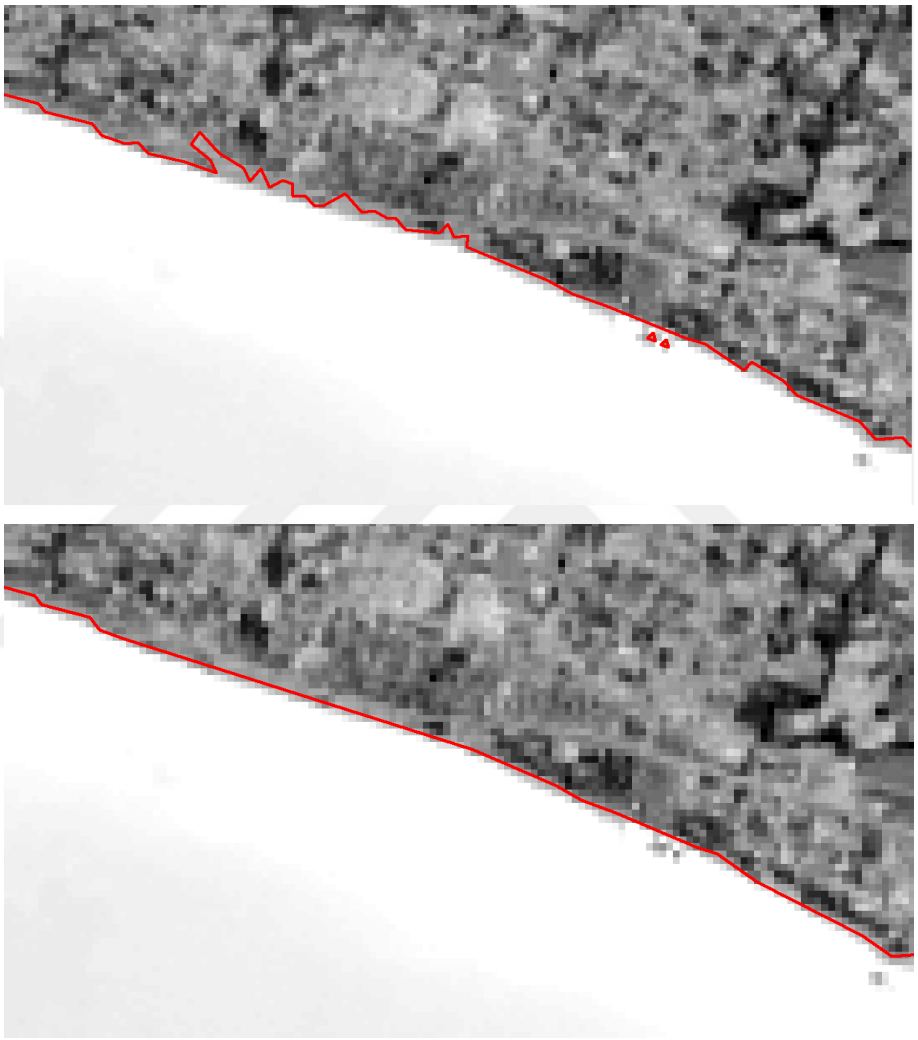

Figure 4.6. Manual Edition of Extracted Shoreline

4.2.1 Normalized Difference Water Index (NDWI)

Normalized Difference Water Index (NWDI) is an index that is used to classify the water and land bodies separately on a satellite image. In other words, the measure of water bodies is obtained by NDWI. Typical Landsat-8 data consists of nine bands, and NDWI is the ratio of differences between near-infrared (NIR) and short-wave-infrared (SWIR) bands. Also, the NDWI can be obtained from green and near-infrared bands. It is first proposed by Gao (1996) as a different application of the Normalized Difference Vegetation Index (NDVI). Gao (1996) concluded that from the laboratory tests and different applications of NDWI, the index uses two narrow channels centered near 0.86 μm and 1.24 μm.

After applying NDWI to the satellite imagery values in a range of minus one and plus one obtained for each pixel, typically, values greater than 0.5, which is the mean value, are classified as water bodies.

Further, each satellite imagery consists of different sensors and bands in different band numbers. Landsat-8 has two sensors: an Operational Land Imager (OLI) and a Thermal Infrared Sensor (TIRS). Landsat-7 employs an Enhanced Thematic Mapper (ETM+) as its sensor. Landsat-4 and Landsat-5 has Multi Spectral Scanner (MSS) and Thematic Mapper (TM). Lastly, the first three Landsat Satellites (Landsat1-3) have only MSS as their sensor. Users must be aware of the difference between different satellite images to obtain a true NDWI. The band designations of Landsat images with the names of the sensors on the corresponding satellites are tabulated in Table 4.1.

Two possible equations are available to calculate the NDWI. McFeeters (1996) suggested the division of the subtraction of the shortwave infrared (SWIR) band from the green band to the summation of these bands to calculate NDWI represented in Equation 4.1.

$$NDWI = \frac{X_{Green} - X_{SWIR}}{X_{Green} + X_{SWIR}} \tag{4.1}$$

The second option to calculate the NDWI is the division of the subtraction of the shortwave infrared (SWIR) band from the near-infrared (NIR) band to the summation of these bands, which is the first equation of NDWI represented in Equation 4.2.

$$NDWI = \frac{X_{NIR} - X_{SWIR}}{X_{NIR} + X_{SWIR}} \tag{4.2}$$

Throughout this study, the first equation of NWDI is used due to the availability of the bands in the images. Therefore, the Equation 4.1. can be derived for Landsat-8 images in the form of Equation 4.3. The raster calculator tool of ArcGIS software is used to execute this equation to the raster images. An example NDWI image corresponding to Landsat-8 data from the 8th of August, 2023, is represented in Figure 4.7.

$$NDWI = \frac{Band\ 3 - Band\ 5}{Band\ 3 + Band\ 5} \tag{4.3}$$

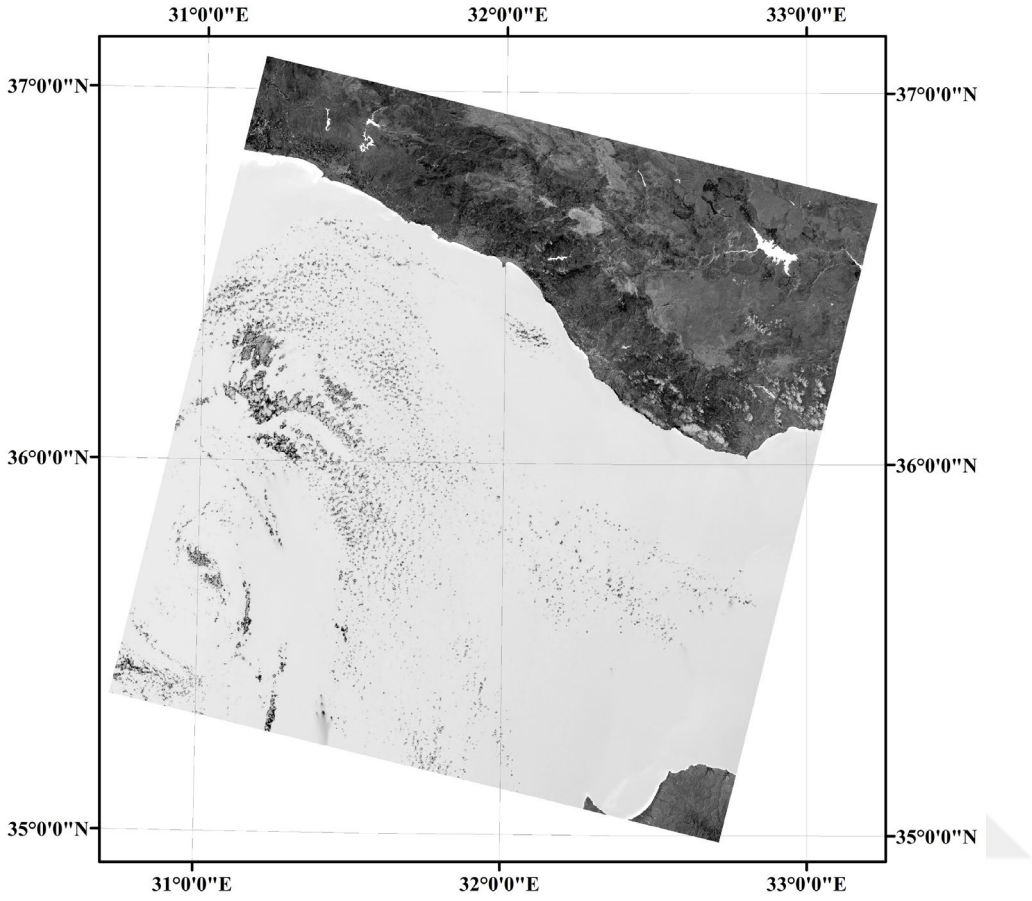

Figure 4.7. NDWI Image of 8th of August, 2023

4.2.2 Attributes of Shorelines

Digital Shoreline Analysis System (DSAS) needs certain types of attributes to execute the model. The GIS software automatically generates some of the required attributes, some of which are user-created. An identifier attribute (ID), shape, and shape length calculated by GIS are autogenerated attributes. DSAS Date and DSAS uncertainty are user-created.

Additionally, some attributes are provided to the shorelines for clarification. These are Image date, Cloudy, Year, and Source attributes.

The Image Date attribute is like the DSAS date, but the DSAS date has a text data format. On the other hand, the Image Date is in date data format as MM/DD/YYYY. The cloudy attribute includes information about the cloudiness of the shoreline. Three possible inputs are added to the Cloudy attribute. These are: “yes,” “no,” and “a bit.” Moreover, the Year attribute is added to sort the data in terms of Year, and the Source attribute is provided to record further information about the source of the shoreline. In Table 4.5, the designated characteristics of attributes are provided.

Table 4.4 Shoreline Attributes

Attribute Name	*Data Type*	*Attribute Addition*	*DSAS Requirement*
FID	Object Identifier	Autogenerated	Required
Shape	Geometry	Autogenerated	Required
Shape_Leng	Double	Autogenerated	Required
DSAS_date	Text	User-created	Required
DSAS_uncy	Any Numeric Field	User-created	Required
image_date	Date	User-created	Optional
cloudy	Text	User-created	Optional
year	Long	User-created	Optional
source	Text	User-created	Optional

4.3 Digital Shoreline Analysis System (DSAS)

Digital Shoreline Analysis System (DSAS) is a tool used as an add-in to ArcGIS. DSAS is provided open source by the United States Geological Survey (USGS). The software provides calculations for the determination of changes in shorelines. DSAS

provides an automated method for establishing measurement locations and making rate and statistical calculations. While the terminology of this software tool is designed for coastal applications, the DSAS application has the versatility to calculate rates of change for any scenario involving boundary changes. This includes instances where a distinct feature position can be identified at specific time intervals, such as glacier limits, riverbanks, or land use/cover boundaries (Himmelstoss et al., 2021).

DSAS generates transects that intersect shorelines by extending perpendicular lines to the reference baseline. The software has two different consecutive execution steps. In the first execution, DSAS software generates transect and intersect layers using the baseline and shoreline layers as inputs. These layers are created carefully because they are the core of the models. The reliability of the DSAS tool depends heavily on the accuracy of the inputs created by users. Rates and statistics are computed in the second execution using layers generated in the first execution. At the end of the second execution, DSAS provides results for Net Shoreline Movement (NSE), Shoreline Change Envelope (SCE) as distance measurements, End Point Rate (EPR), Linear Regression Rate (LRR), and Weighted Linear Regression Rate (WLR) as statistics, further, supplemental statistic for linear (L) and weighted (W) regressions. The supplemental statistics are Confidence Interval (LCI/WCI), Standard Error (LSE/WSE), and R-squared values (LR2/WR2).

The overall flowchart of DSAS software and execution inputs and outputs are presented in Figure 4.8. A more detailed workflow of DSAS with necessary steps, software icons, and explanations is given in Figure B.1. in Appendix B.

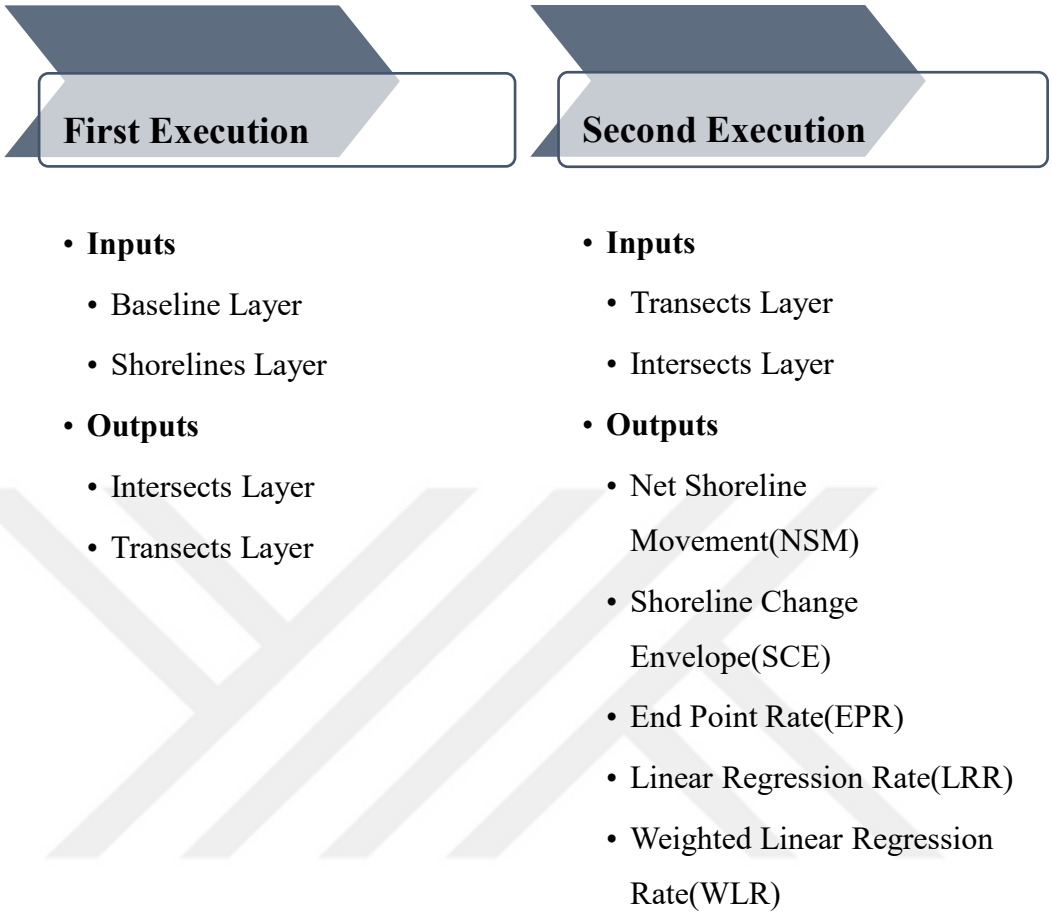

Figure 4.8. Digital Shoreline Analysis System (DSAS) Flowchart

4.3.1 Baseline Layer

The baseline is a line that represents the overall behavior of all shorelines and serves as the starting point for all transects cast by the DSAS application. The baseline can either consist of many segments or become a single line that characterizes the overall behavior of historical shorelines. It can be positioned onshore, offshore, or in the mid-shore, as shown in Figure 4.9. DSAS software can catch the type changes in baseline positions and generate required transects according to the positions of the baseline layer.

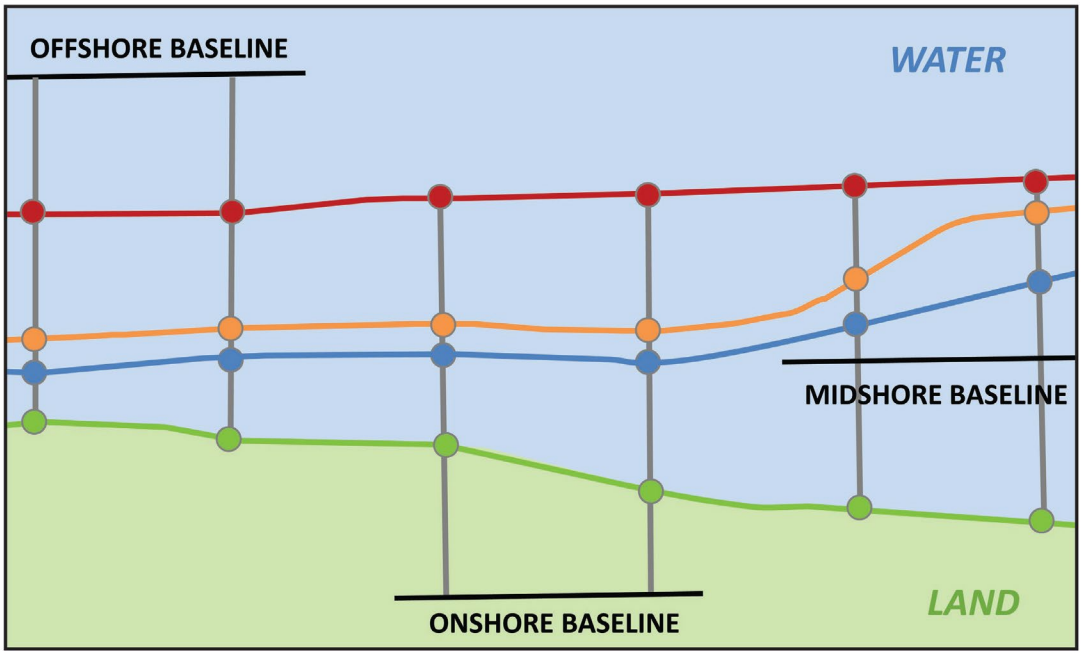

Figure 4.9. Types of Baseline Positioning (Himmelstoss et al., 2021)

Two approaches are suggested by DSAS developers to create a baseline layer. The first approach is creating a new feature class and manually generating the baseline layer. The second approach is using the buffer function of ArcGIS.

The oldest image in this study belongs to the year 1987, an image from the Landsat satellite. The shoreline of 1987 is used to generate a reference baseline throughout the study. Two hundred meters buffer is applied to the shoreline of the year 1987, and manual smoothing is applied to necessary sections. The partial view of the reference baseline of the study is presented in Figure 4.10.

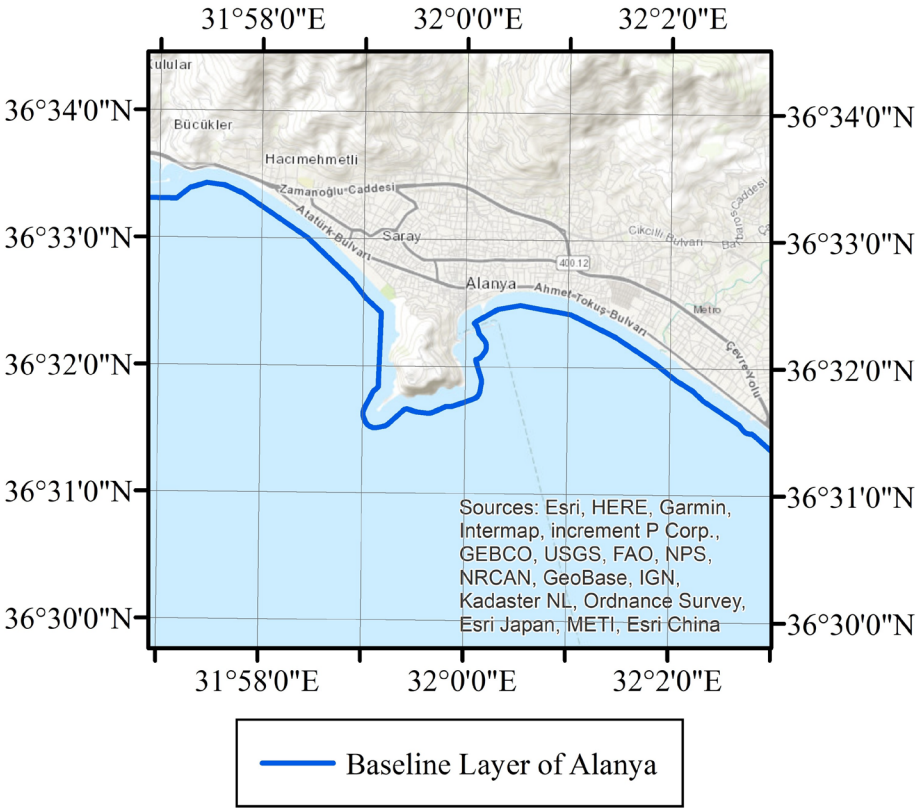

Figure 4.10. Partial View of the Baseline Layer of Alanya

The baseline layer requires specific attributes that DSAS needs to generate transect and intersect layers. As in the shorelines layer, some of these required attributes are user-generated, and some are generated automatically by ArcGIS. An object identifier attribute, a shape attribute, and a shape length attribute are generated by ArcGIS. One optional attribute named “DSAS_Search” is also created in “double” data format. “DSAS_Search” attribute refers to the search distance of the algorithm to intersect the shorelines layer in meters. The baseline layer attribute requirements are represented in Table 4.6.

Table 4.5 Baseline Layer Attributes

Attribute Name	*Data Type*	*Attribute Addition*	*DSAS Requirement*
FID	Object Identifier	Autogenerated	Required
Shape	Geometry	Autogenerated	Required
Shape_Leng	Double	Autogenerated	Required
DSAS_searc	Double	User-created	Required

4.3.2 Shoreline Layer

Shorelines can be digitized from many sources, such as digital orthophotos, global positioning systems (GPS), aerial photographs, or physical maps. Each shoreline vector represents a specific position in time, and it must be assigned a date in the shorelines feature class in the attribute table. It should be noted that the calculated rates of change in shorelines are only as correct as the reliability of the input data (Himmelstoss et al., 2021).

The semi-automatic shoreline extraction procedure that is discussed in detail in Section 4.2. is applied to each image collected from the Landsat database. Then, all the shorelines are merged to form a shoreline layer. Sixty-six Landsat images were used to construct the shoreline layer for shoreline change detection models. In the monthly changes study, the year 2023 is selected, and 12 images from each month of the year 2023 are used to obtain the monthly change in the region. Additionally, a Planet satellite image and a Landsat image that both have close generation dates are used to conduct a sensitivity study.

4.3.3 Intersections and Transections Layer

In the first execution of the Digital Shoreline Analysis System (DSAS), the baseline and shoreline layers are used as inputs. The measurements that are formed by DSAS from the baseline intersect with the shorelines. The points of intersection include location and time information that are used to calculate rates of change. The distances from the baseline to each intersection point along a transect are used to calculate the desired statistics. The inputs and outputs of the first execution of the DSAS are represented in Figure 4.11.

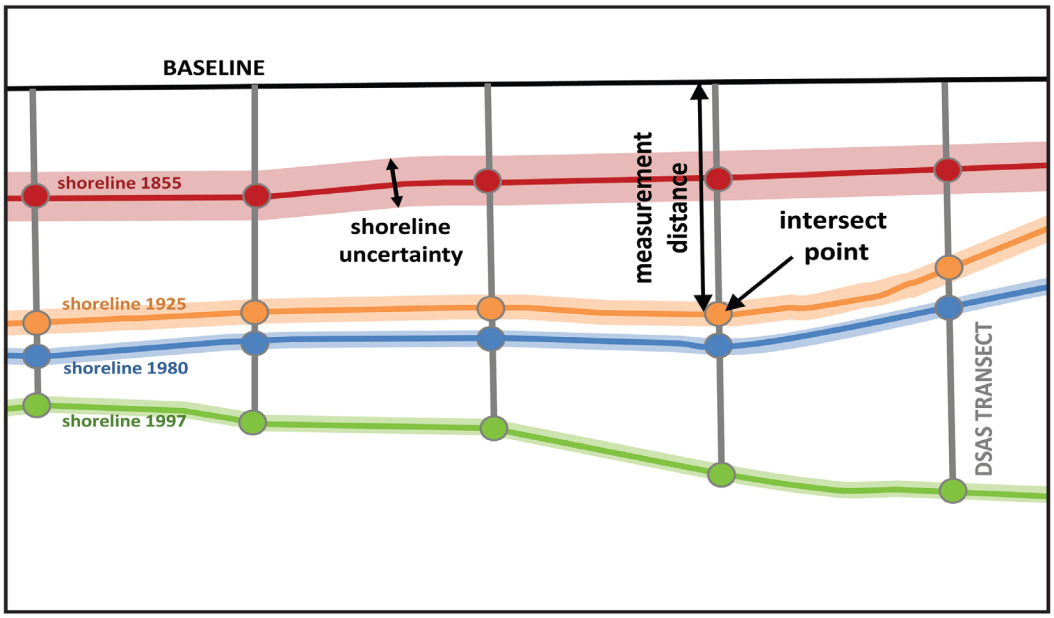

Figure 4.11. Baseline, Shoreline, Transect, and Intersection Layers Representation (Himmelstoss et al., 2021)

4.3.4 Rate Calculation

In the second execution of the Digital Shoreline Analysis System (DSAS), the tool is capable of a set of statistical calculations based on the selection of the desired parameters. Shoreline rate assessments rely on measuring differences in shoreline positions over time along designated transects. These rates, expressed in meters per year, are determined using different calculation methods. Once the user-defined calculations are done in DSAS, the software produces a new feature class for transect rates and a point intersect feature class. Table 4.7. presents standardized field headings for rate-change statistics, accompanied by detailed explanations in the subsequent section.

Table 4.6 DSAS Rates and Descriptions

DSAS Statistics	*Description*
NSM	Net Shoreline Movement
SCE	Shoreline Change Envelope
EPR	End Point Rate
EPRunc	Uncertainty of End Point Rate
LRR	Linear Regression Rate
LSE	Standard Error of Linear Regression
LCI	Confidence Interval of Linear Regression
LR2	R-squared of Linear Regression
WLR	Weighted Linear Regression Rate
WSE	Standard Error of Weighted Linear Regression
WCI	Confidence Interval of Weighted Linear Regression
WR2	R-squared of Weighted Linear Regression

Net Shoreline Movement (NSM)

The net shoreline movement (NSM) is the distance between the oldest and the newest shorelines in meters.

Shoreline Change Envelope (SCE)

The shoreline change envelope (SCE) represents the highest distance among all the shorelines that intersect in the given transect. SCE is a distance in meters, not a rate. It always has a positive sign.

End Point Rate (EPR)

The division of the distance between the newest and oldest shorelines measured in the selected transection into the elapsed time is defined as the end point rate (EPR). The unit of EPR is a meter per year. Its advantages are the ease of computation and the minimum requirement of two shoreline dates. However, it is a disadvantage when there is more data. The additional information obtained from more data is ignored while calculating EPR. Furthermore, the changes in the sign, in other words, the accretion or erosion of the shoreline, may be missed by only looking at EPR. Also, the seasonal changes might not be observed due to the nature of the EPR calculation.

The differences and calculation processes are illustrated in Figure 4.12.

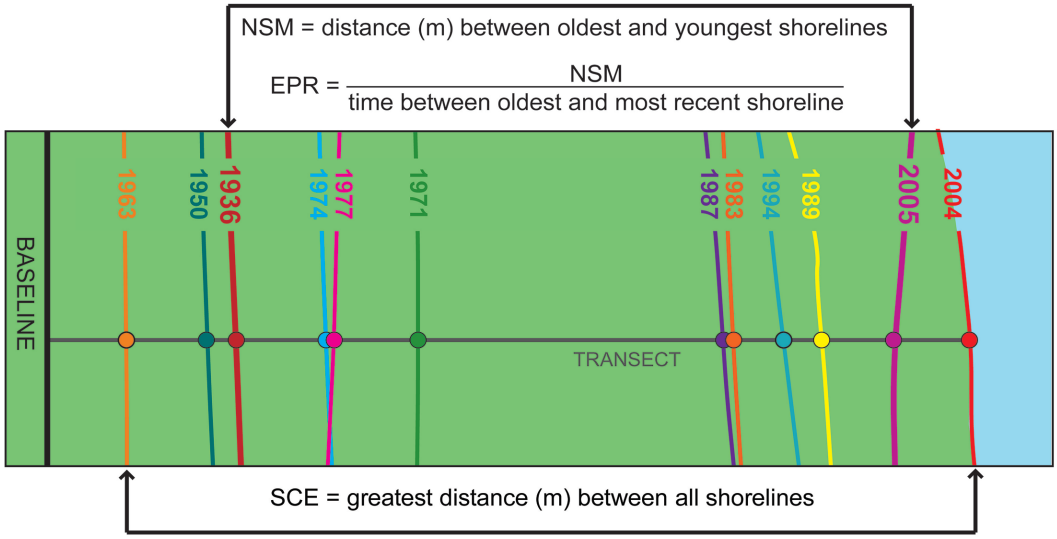

Figure 4.12. Visualization of NSM, SCE, and EPR Calculations (Himmelstoss et al., 2021)

Linear Regression Rate (LRR)

By fitting a least-squares regression line to all shoreline points for a transect, a linear regression rate of change in statistics can be calculated. To minimize the sum of the squared residuals, the regression line is placed. The slope of this line is the linear regression rate. The method of linear regression uses all the data without considering the changes in trend or accuracy. The method is essentially computational and needs further interpretation to make the calculation meaningful for the desired models. The calculation is based on accepted statistical concepts. Yet, the linear regression technique is vulnerable to outlier influence and tends to underestimate the rate of change compared to alternative statistics like EPR. The graphical representation of LRR calculation in DSAS is given in Figure 4.13.

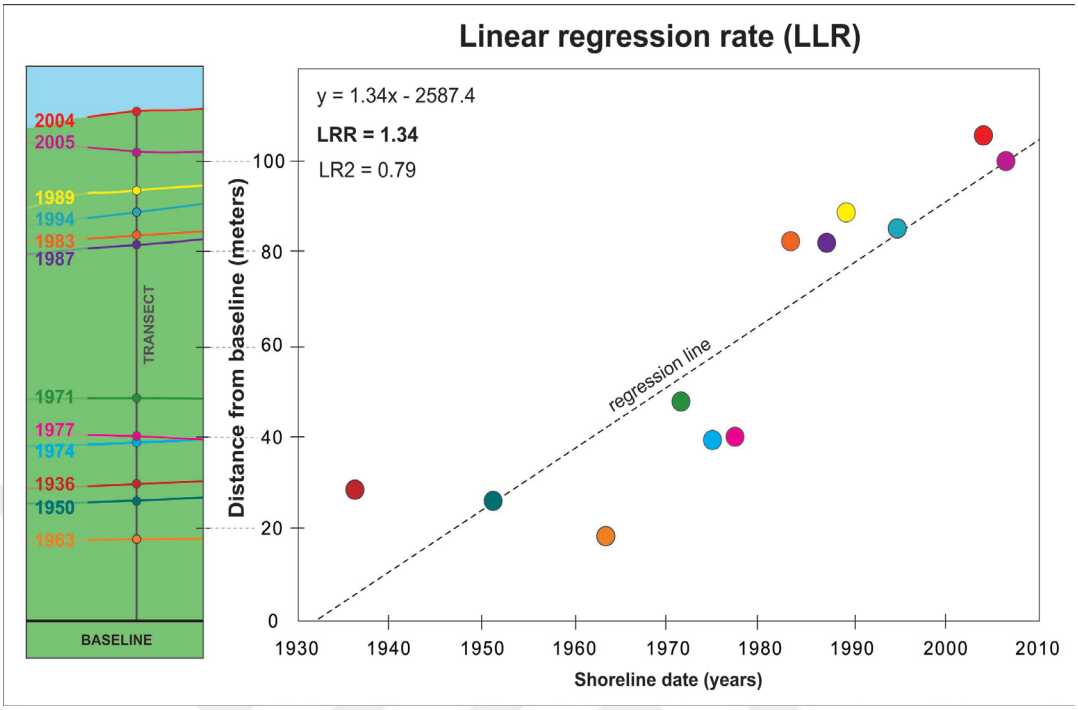

Figure 4.13. Graphical Procedural Representation of LRR Calculation by DSAS (Himmelstoss et al., 2021)

Weighted Linear Regression (WLR)

Weighted linear regression assigns higher importance or weight to more reliable data when determining a best-fit line. When computing rate-of-change statistics for shorelines, greater weight is given to data points with smaller position uncertainties. This weight (w) is determined by the variance in the measurement uncertainty (e), as defined by Genz et al. (2007) with the Equation 4.4:

$$w = \frac{1}{e^2} \tag{4.4}$$

where “e” represents the shoreline uncertainty value.

The uncertainty field within the shoreline feature class is utilized to compute this weight. The graphical representation of WLR calculation in DSAS is given in Figure 4.14.

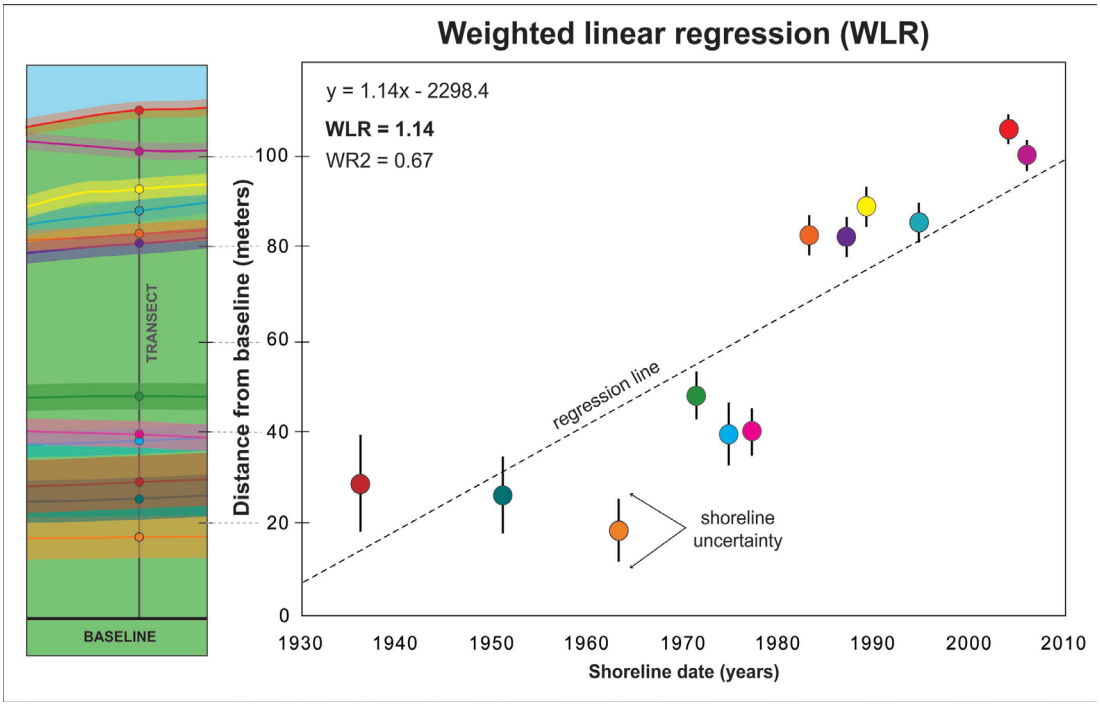

Figure 4.14. Graphical Procedural Representation of WLR Calculation by DSAS (Himmelstoss et al., 2021)

CHAPTER 5

ANALYSIS AND RESULTS

As described in Chapter 3, the study area is narrowed by starting from the swath width of the Landsat satellite to the Dim River mouth. Shorelines are formed for the entire area, then they are clipped to the desired lengths to execute more detailed models. In this chapter, the detailed description of each model and the results of the program are discussed and reported. Additionally, a sensitivity study and a monthly change investigation are made. At the end of this chapter, all model results are reported and compared with each other. Further, a comprehensive summary of the entire analysis and results of this thesis is provided.

There are three main models developed and executed. The first model covers the entire area that is equal to the swath width of the Landsat satellite. This analysis starts from the middle of Antalya City center, which corresponds to the west section of the picture, and ends at Tekmen Harbor in Mersin, which denotes the east section of the image. The total length of this shoreline is approximately 243 km. For this section, net shoreline movement (NSM), shoreline change envelope (SCE), end point rate (EPR), and linear regression rate (LRR) are calculated.

The second model is developed for Alanya County, which has a shoreline length of 135 km roughly. The same parameters are calculated for this section as in the initial model.

The third model is created for the Dim River mouth, which has almost 10 km shoreline length. This section of Alanya County is selected because it is free from human activities that directly lead to changing the shorelines. Additionally, Dim River is a dynamic section to observe shoreline changes and seasonal effects on the shoreline.

In these three models, Landsat images that belong to the years between 1987 and 2023 are used for the analysis. Only summer months are selected, which are June, July, and August. In total, sixty-six images are used to construct the shoreline layer. However, to check the sensitivity of the study, a planet satellite image was chosen that has a close date to the corresponding Landsat image. A sensitivity study is made by using these two shorelines to consider the relative correctness of the satellites. Further, the mean of the sensitivity study is used as the uncertainty value of the Dim River Mouth model, and a meta-analysis is made by using this value.

The Digital Shoreline Analysis System (DSAS) does not capture the relative differences between the provided shorelines; therefore, if there is a seasonal change that results in accretion and erosion throughout the year, DSAS misses it. This situation is discussed in detail in Chapter 6. But, to check the seasonal changes, Dim River Mouth is modeled for the year 2023 by providing an image from each month. The monthly change model is created by using these images.

5.1 Model for Initial Area of Interest

As expressed before, the initial area of interest corresponds to an approximately 243 km long shoreline that has a west border in the middle of the Antalya City Center and an east border at Tekmen Harbor, Mersin. The corresponding shoreline and baseline layers are expressed in Figure 5.1. In Figure 5.2. baseline and shoreline layers are represented in detail by zooming in. The red line on the figures represents the shoreline layer that involves sixty-six shorelines from different years extracted from Landsat images. The blue line represents the baseline that is created by buffering the oldest Landsat image 200 meters away from the shore. The oldest image is from 1987.

Landsat images have a 30-meter resolution. Therefore, it is hard to detect and catch changes in wavy zones of the costs. The wavy zones that cause anomalies in the rate

calculation are manually excluded from the analysis. This problem is discussed in detail in Chapter 6.

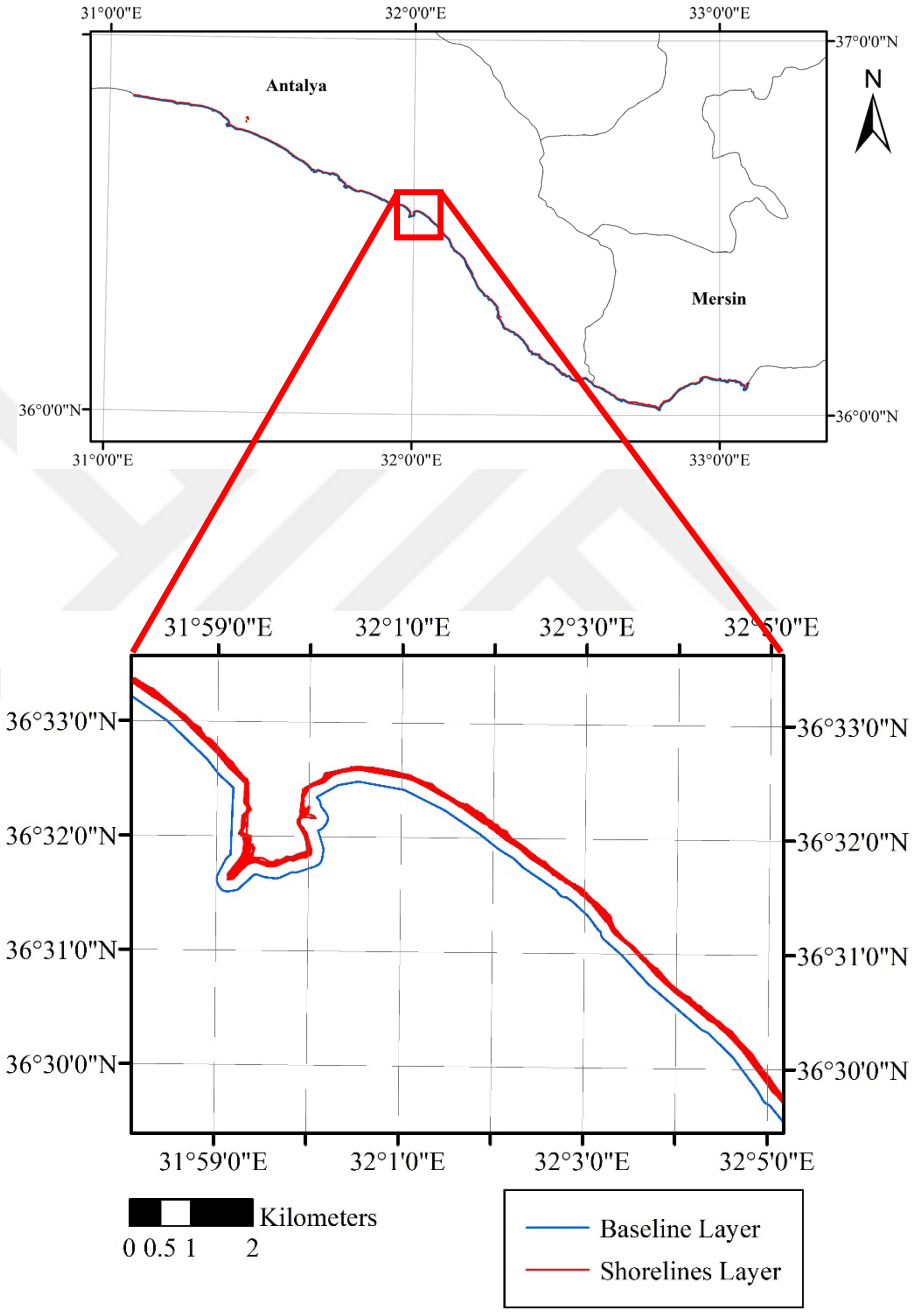

Figure 5.1. Baseline and Shoreline Layers for the Initial Area of Interest

By using the shoreline and baseline layers, a set of rates is calculated by employing DSAS. The net shoreline movement (NSM), shoreline change envelope (SCE), end point rate (EPR), and linear regression rate (LRR) are calculated and presented in Appendix C. Based on the NSM results shoreline of the initial area of interest is classified based on erosion and accretion zones which is represented in Figure 5.2.

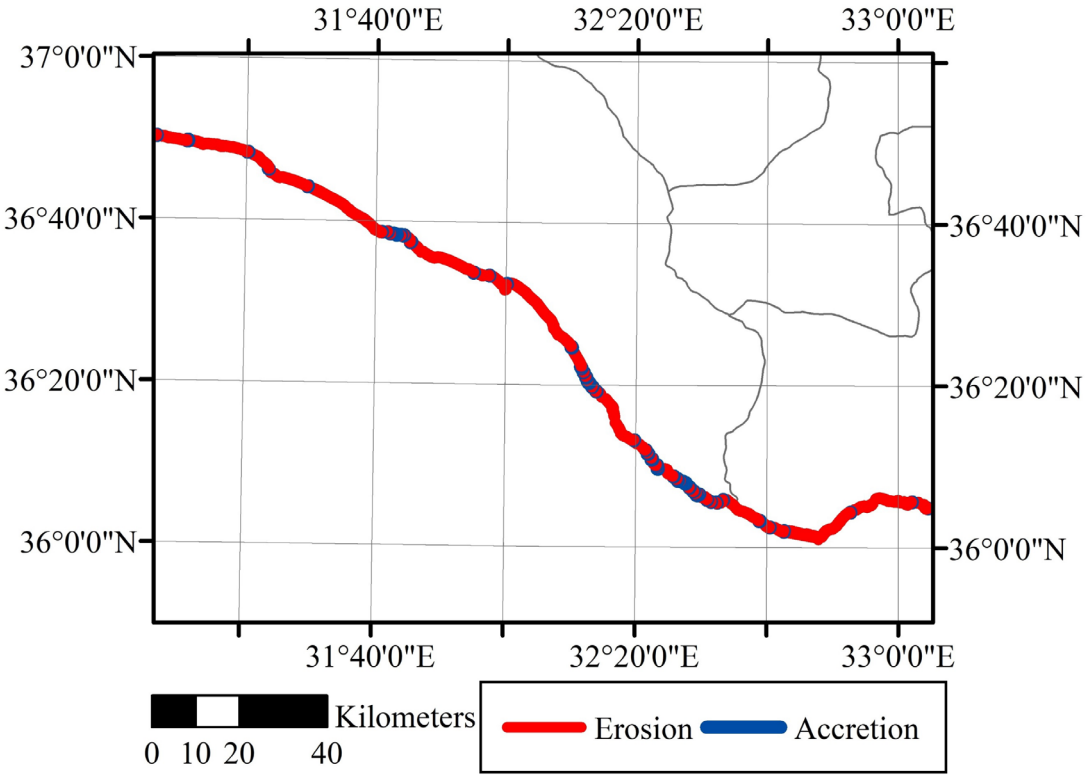

Figure 5.2. Erosion and Accretion Classification of Initial Area of Interest

5.2 Model for Alanya

The second model is created by narrowing the areas up to the borders of Alanya County. The same shorelines and baseline areas are used to develop the model, and similarly, the same rates are calculated for the Alanya County model. The shoreline

distance of the second model is about 135 km, which is nearly half of the initial area of interest. The corresponding baseline and shorelines are represented in Figure 5.3.

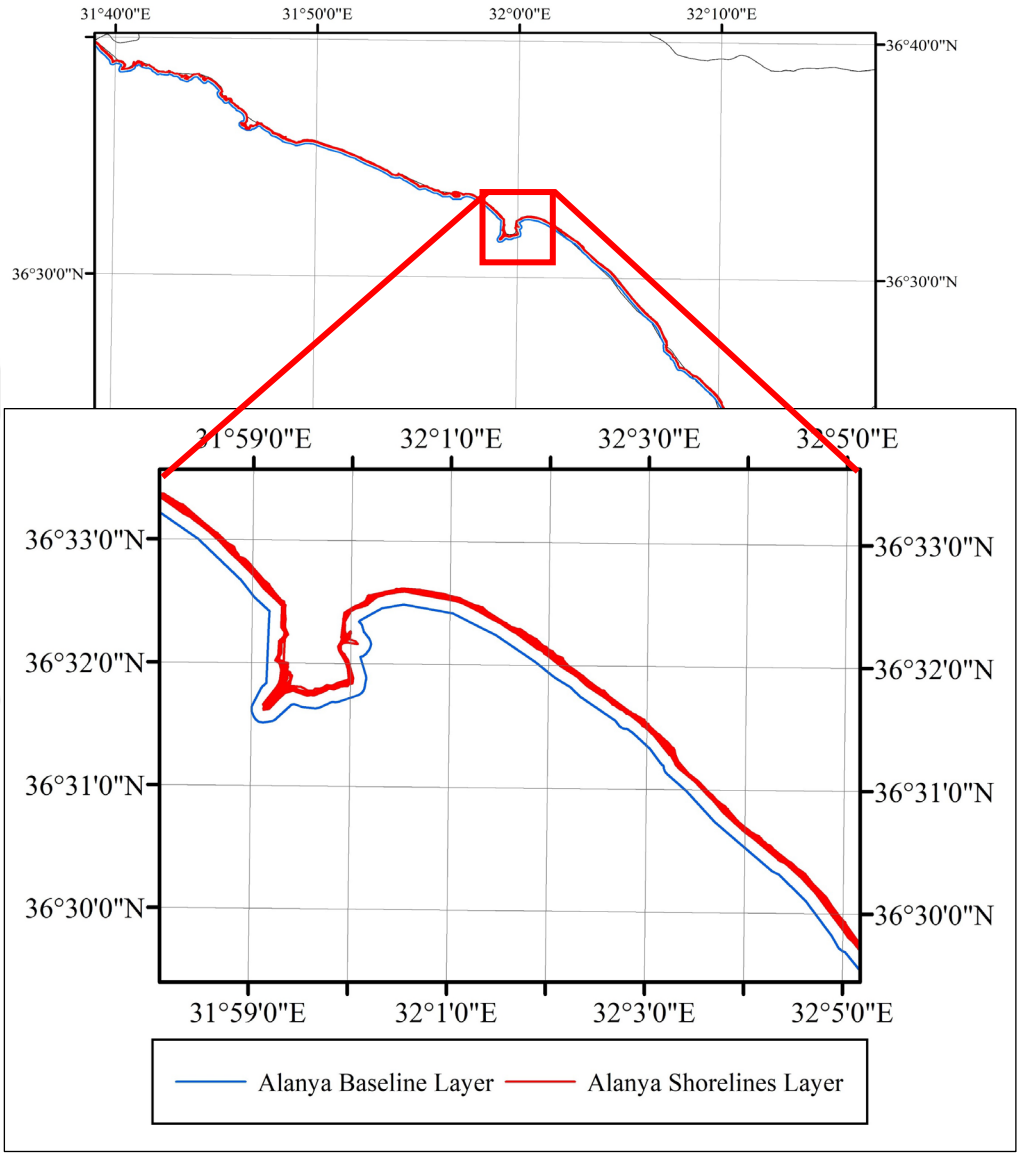

Figure 5.3. Baseline and Shoreline Layers of Alanya County

The net shoreline movement (NSM), shoreline change envelope (SCE), end point rate (EPR), and linear regression rate (LRR) of Alanya County are also calculated

and represented in Appendix C. Furthermore, the Alanya County shoreline is classified as an accretion and erosion zone by using NSM values, which are represented in Figure 5.4.

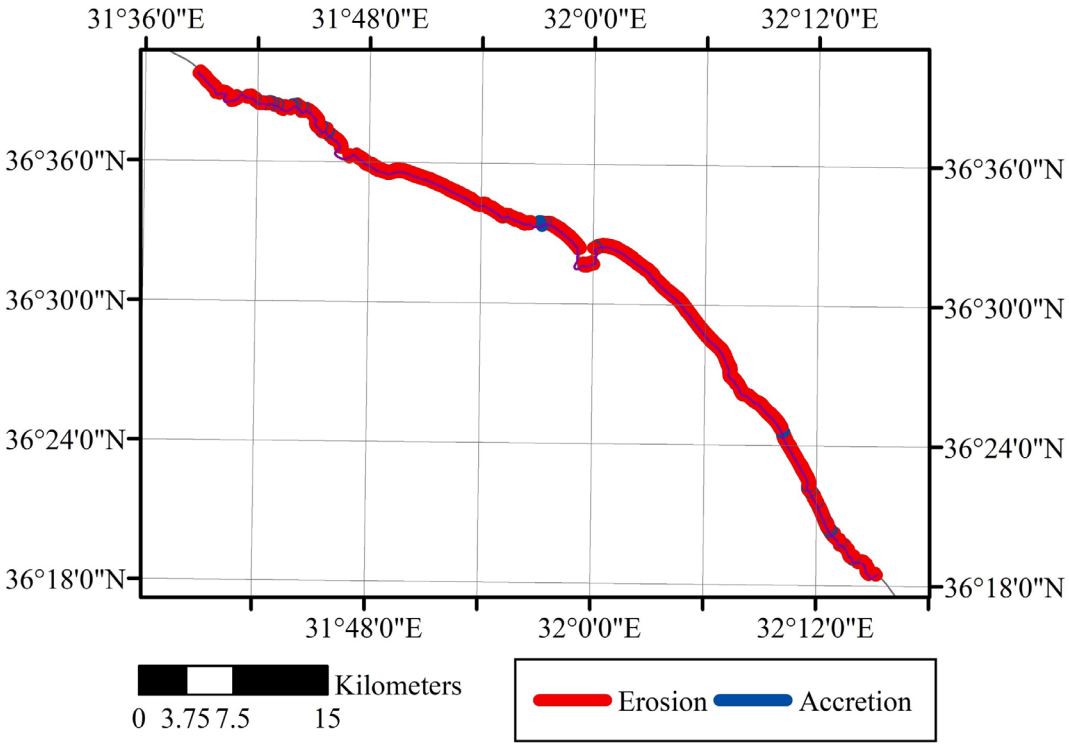

Figure 5.4. Erosion and Accretion Classification of Alanya County

5.3 Model for Dim River

The last model is narrowed up to the borders of Dim River Mouth. The shoreline distance of the Dim River Model is about 10 km. As expressed before, the zone is mostly free from human activities that can directly change the shoreline and dynamic due to sediment transportation. As before, the same baseline and shoreline layers are used to analyze the changes in Dim River Mouth, and the rates of the previous models are calculated. Further, to check the accuracy of the results, temporal change

based on the years and accumulation is constructed by employing Excel. The baseline and shoreline layers for the Dim River Mouth Model are represented in Figure 5.5. The Net Shoreline Movement (NSM), Shoreline Change Envelope (SCE), End Point Rate (EPR), and Linear Regression Rate (LRR) are presented in Figures 5-9.

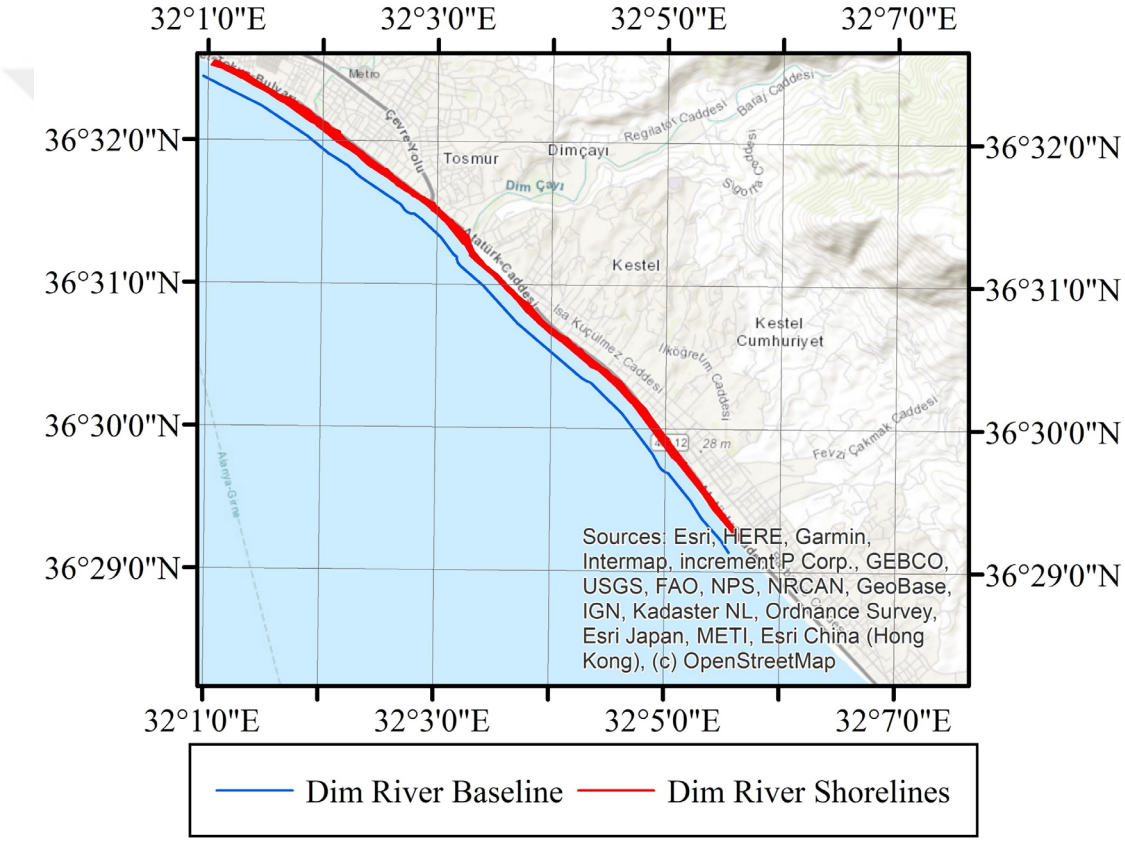

Figure 5.5. Baseline and Shoreline Layers for Dim River Model

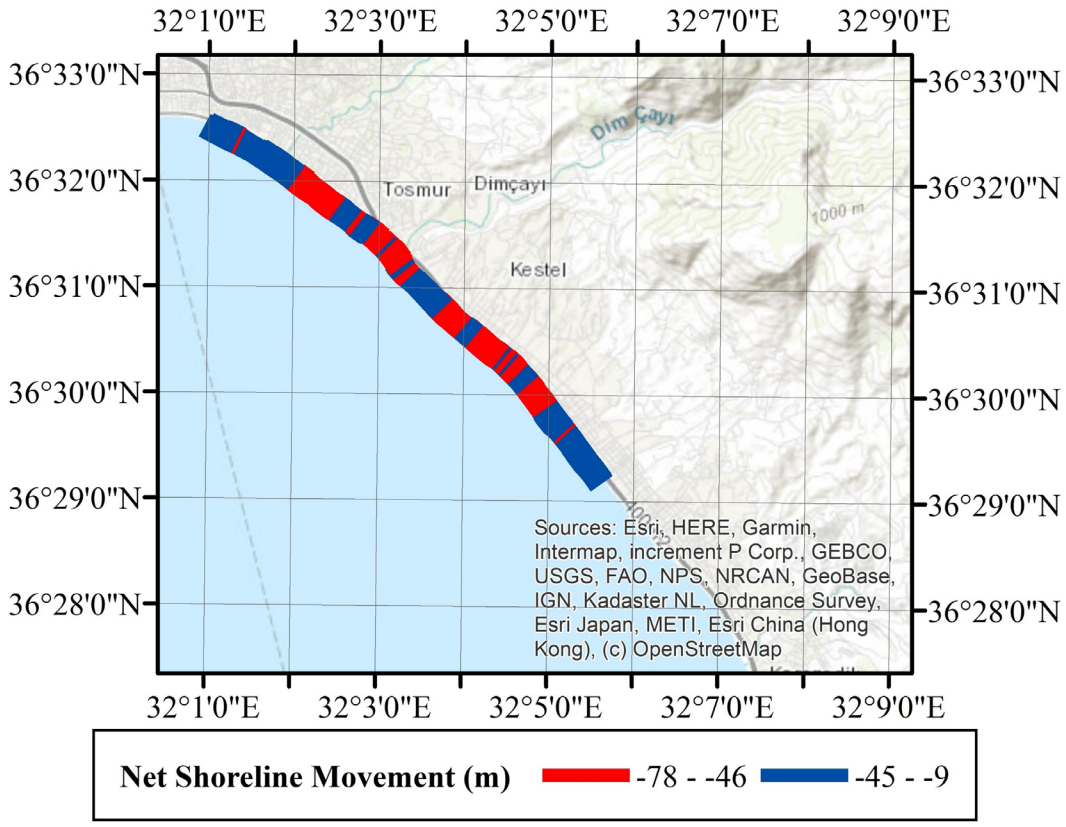

Figure 5.6. Net Shoreline Movement (NSM) in Dim River Model

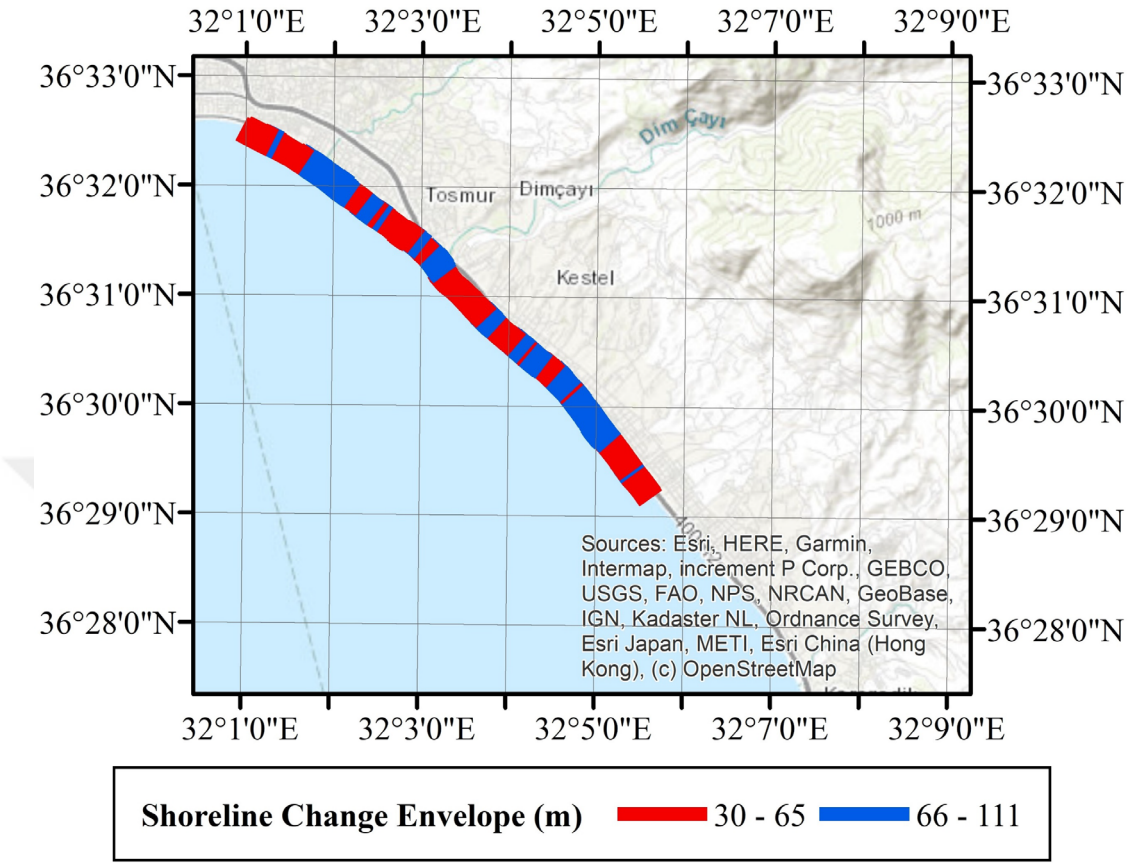

Figure 5.7. Shoreline Change Envelope (SCE) for Dim River Model

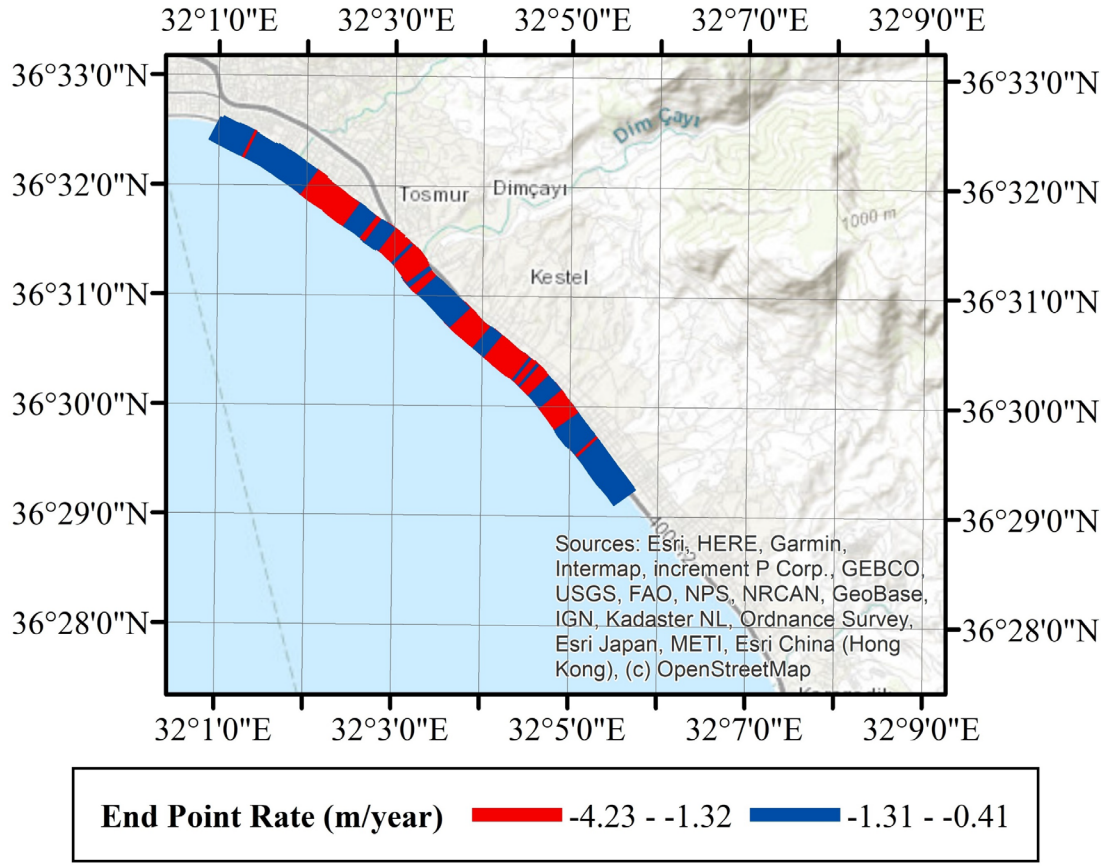

Figure 5.8. End Point Rate (EPR) for Dim River Model

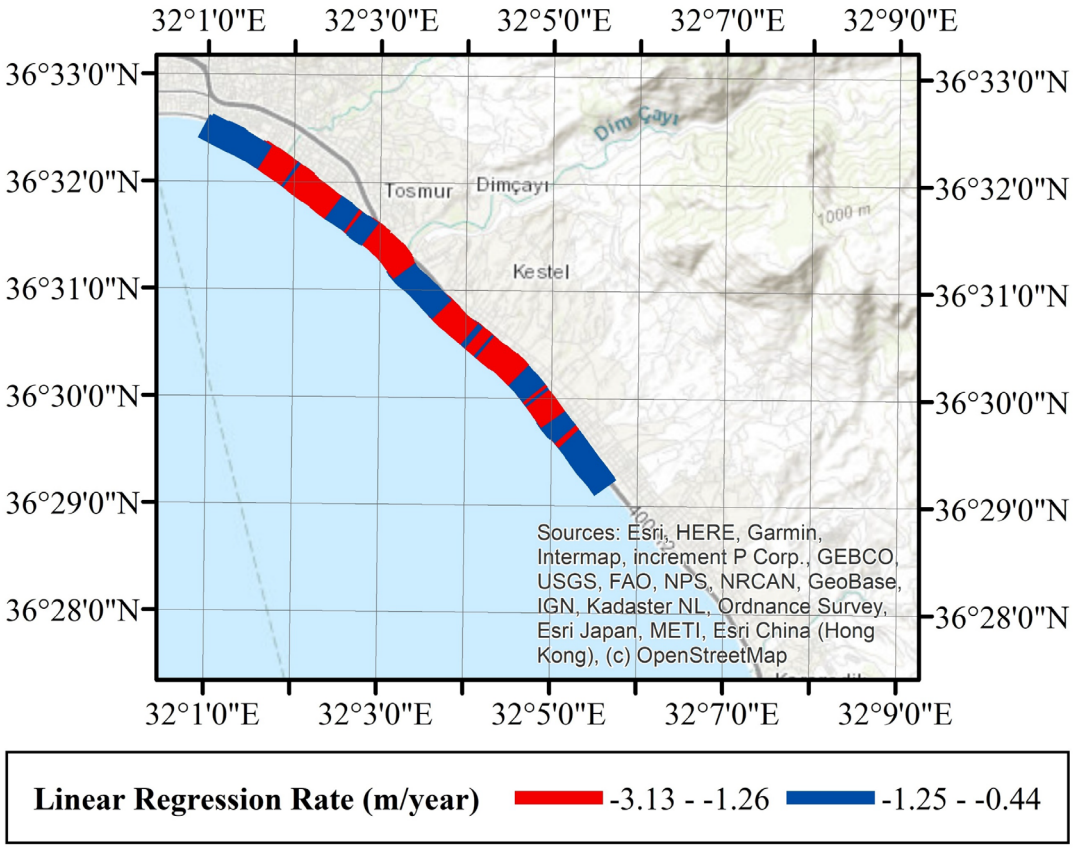

Figure 5.9. Linear Regression Rate (LRR) for Dim River Model

Up to this model, accretion is observed in the study area. However, only erosion is observed in the Dim River model. Therefore, to check the accuracy of the results, a change in the time graph is manually constructed to determine whether there is a cyclical situation in-between years. To do that, the oldest image is considered a starting point, and yearly changes are reported. At the end of this analysis, a cyclical behavior in the area is observed. The cyclical behavior is represented in Figure 5.10.

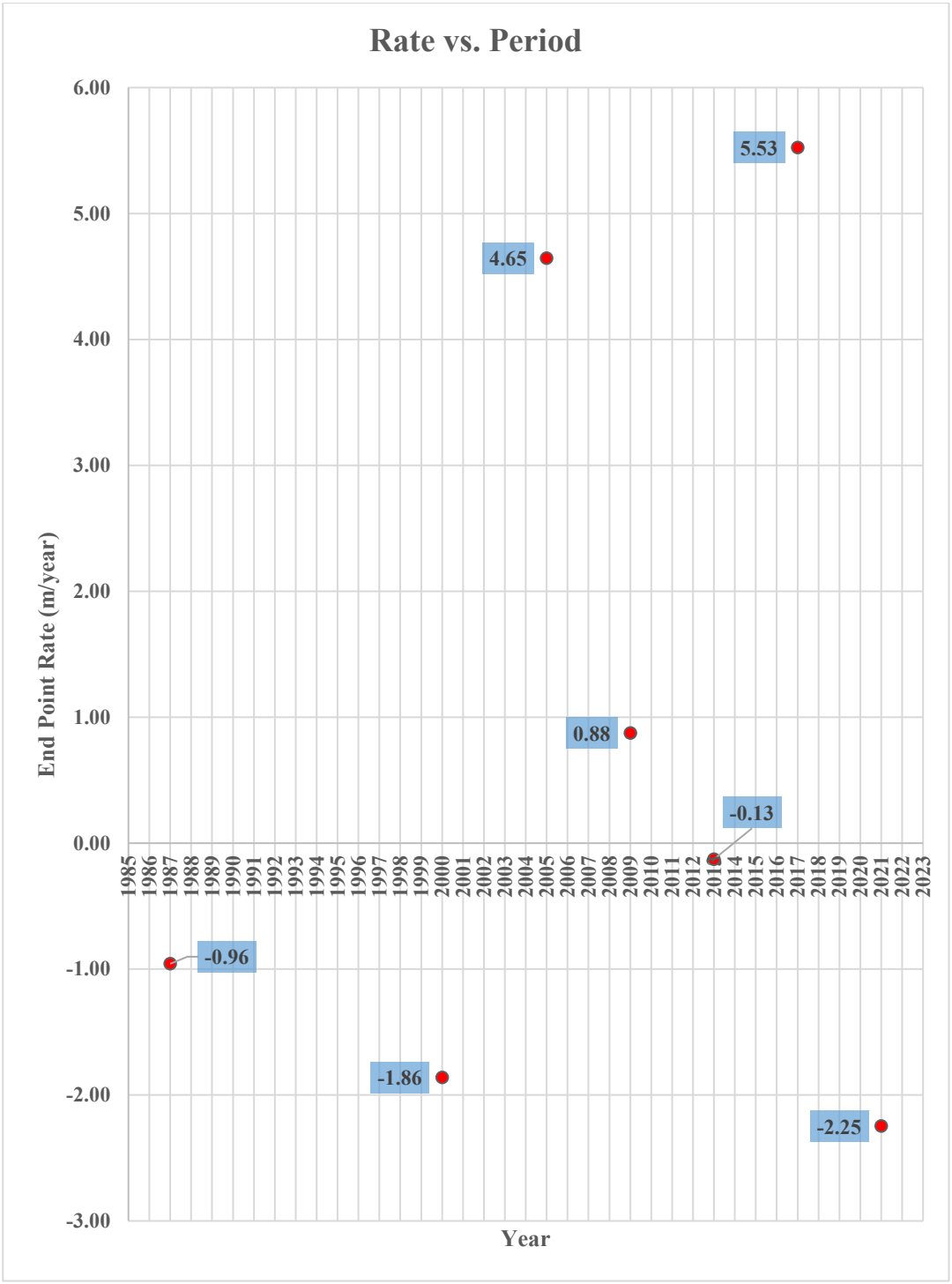

Figure 5.10. Yearly Change Graph for Dim River Model for Summer Months between 2013-2022 from Landsat-8 Imagery

The cyclical behavior is studied by considering different time intervals based on the endpoint rate calculation. A cyclical behavior that lasts for more than one year is observed. In almost every four years, the shoreline is exposed to accretion and erosion consecutively, as expressed in Table 5.1. and Figure 5.11.

Table 5.1 Cyclical Behavior Data of Dim Model

	Year #1	Year #2	Duration (yr)	Rate (m/yr)	Type
Period #1	1987	2000	13	-0.96	Erosion
Period #2	2000	2005	5	-1.86	Erosion
Period #3	2005	2009	4	4.65	Accretion
Period #4	2009	2013	4	0.88	Accretion
Period #5	2013	2017	4	-0.13	Erosion
Period #6	2017	2021	4	5.53	Accretion
Period #7	2021	2023	3	-2.25	Erosion

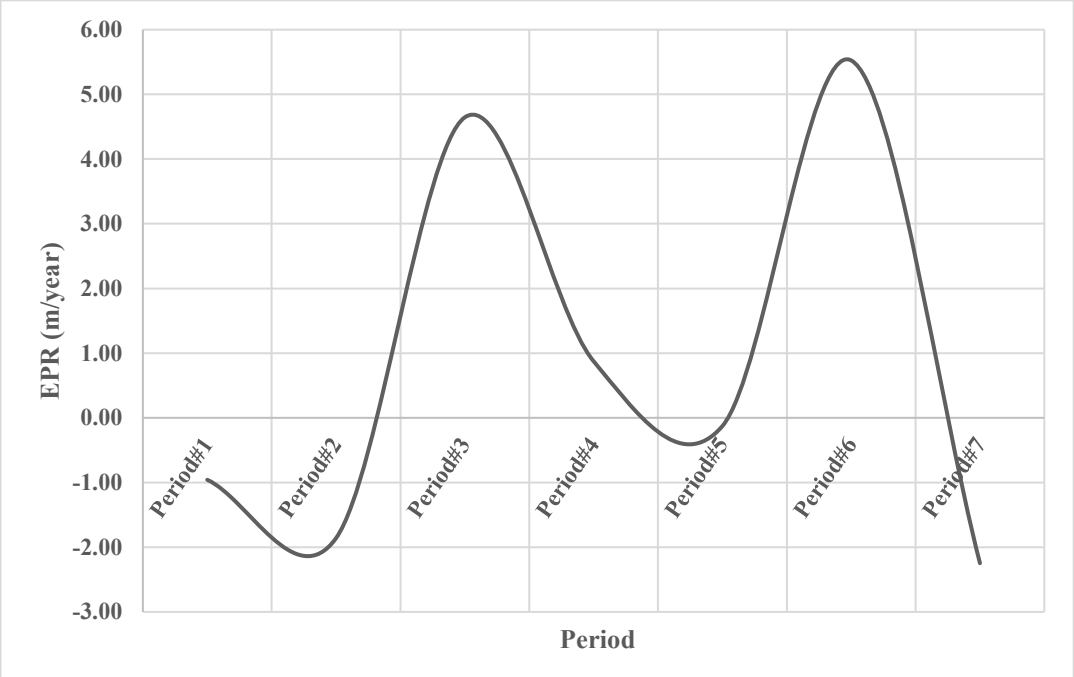

Figure 5.11. End Point Rate vs. Period Graph for Dim River Mouth from Landsat-8 Imagery

5.4 Monthly Change Investigation Study

The behavior of the shoreline in the study area is not linear. In the beginning, only summer months are used to develop the model to abstain from intense cloud cover in the area. Because of having a cyclical behavior even in the summer months, a monthly change study is done to check the seasonal changes in the shoreline in Dim River Mouth. The year 2023 is selected to create the monthly change study with Landsat-8 and Planet Satellite imagery separately, and a single image from each month is used to construct the shoreline layer. The shoreline and baseline layers of Landsat-8 images are represented in Figure 5.12.

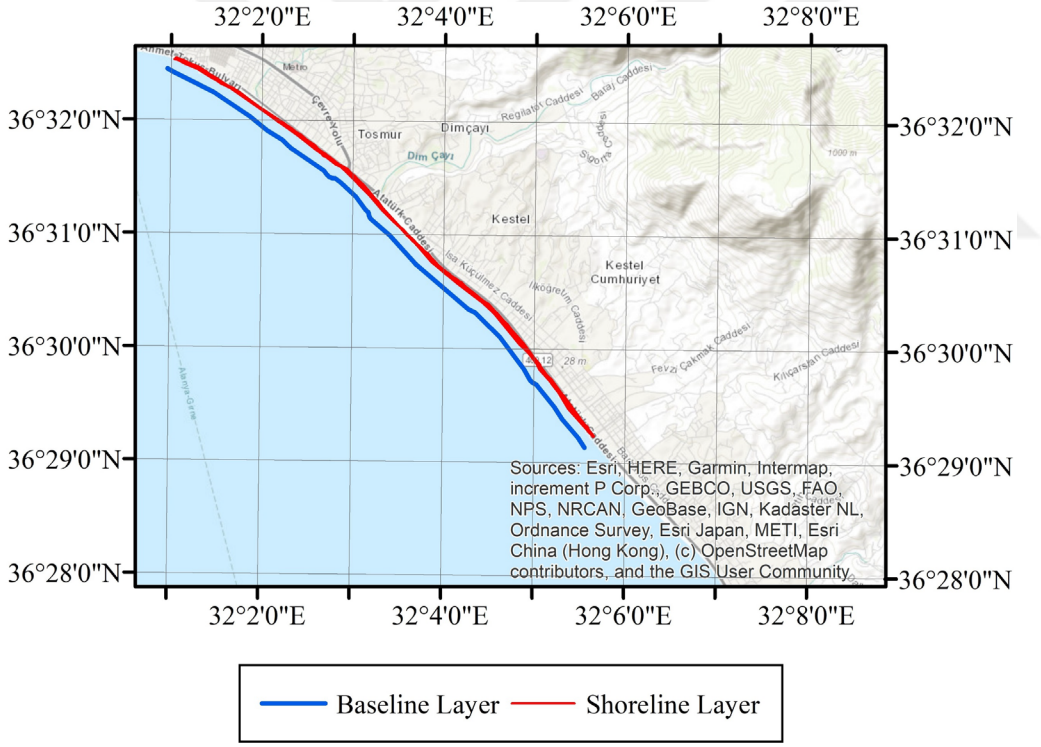

Figure 5.12. Baseline and Shoreline Layers for Landsat-8 Monthly Change Study

The same statistics are calculated as in the previous models in the monthly change study. The net shoreline movement (NSM), shoreline change envelope (SCE), and linear regression rate (LRR) results for the monthly change study are represented in Appendix C. The end point rate (EPR) results are represented in Figure 5.13.

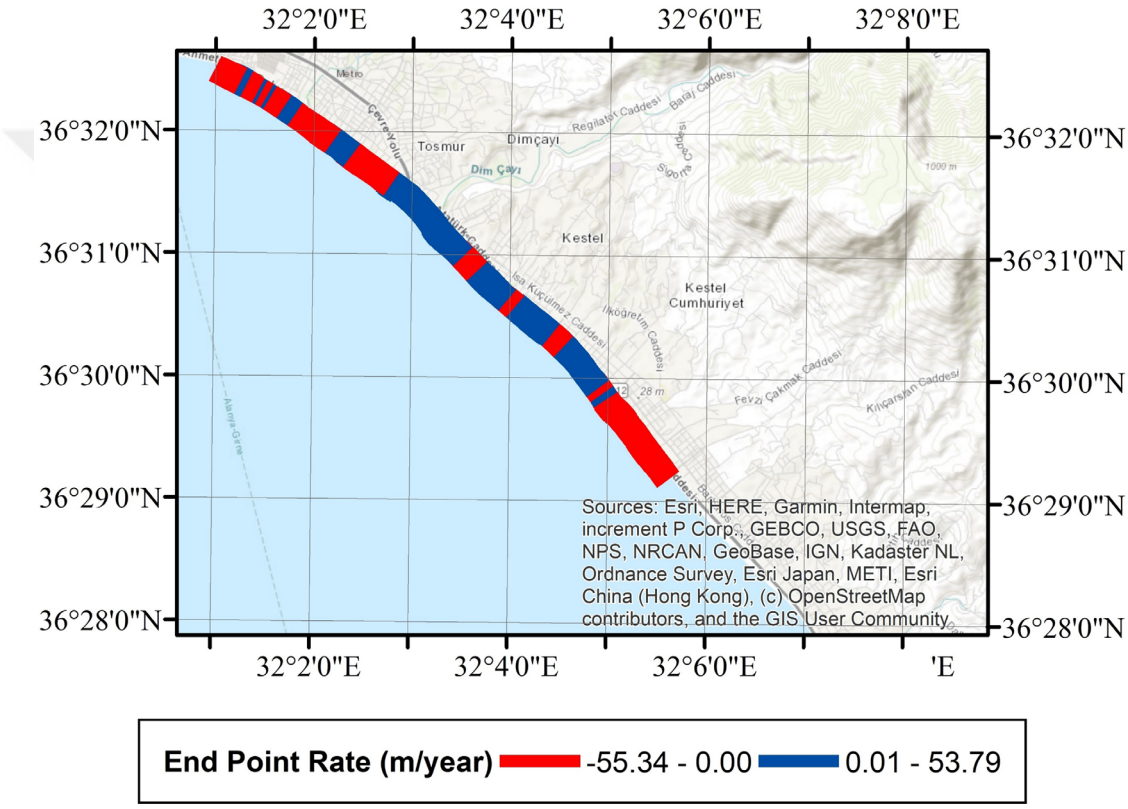

Figure 5.13. End Point Rate (EPR) Results of Landsat-8 Monthly Change Study

The same methodology for the detection of cyclical behavior in the Dim River Model is applied here to determine monthly changes in a year. To do that, a single transect is selected, and changes in order between months are reported. The selected transect is presented in Figure 5.14. Based on the obtained data, a change in time graph is

created by ordering monthly changes. The change is represented in Figure 5.15. The Digital Shoreline Analysis System (DSAS) is not capable of detecting monthly and/or cyclical changes. Therefore, further interpretation of data is needed. This is discussed in Chapter 6.

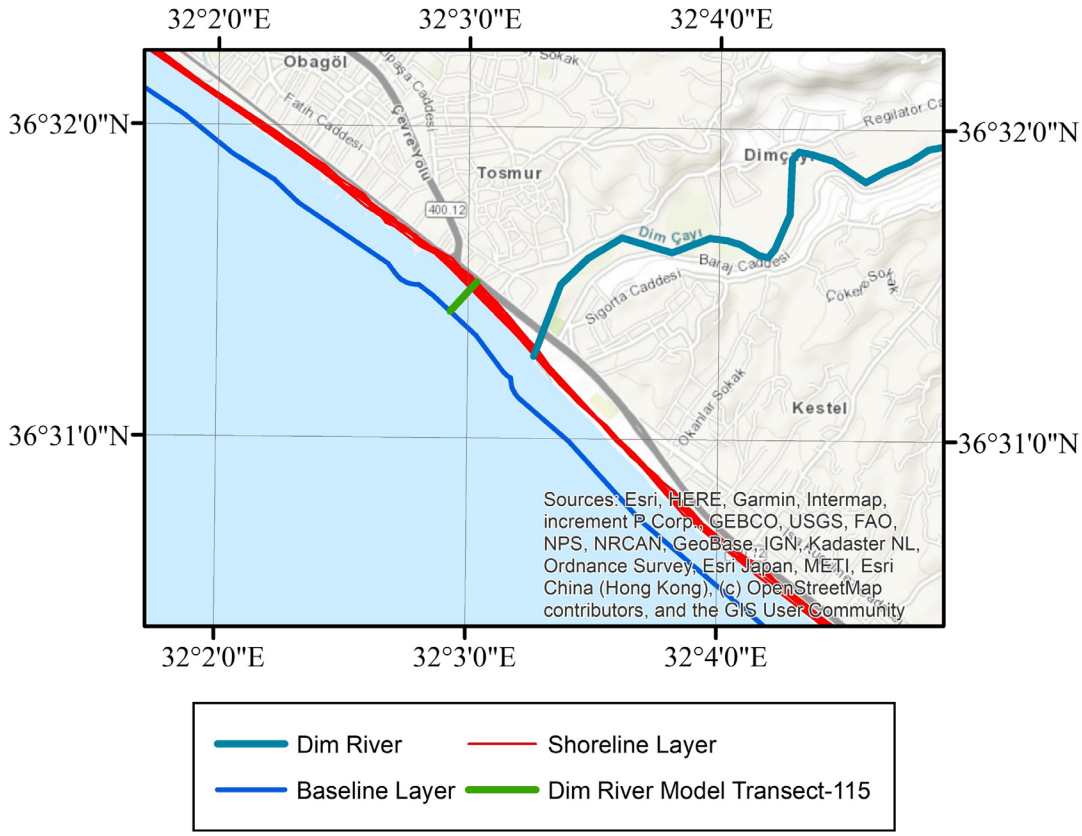

Figure 5.14. Closer Representation Selected Transect for Monthly Change Study for 2023 using Landsat-8 Data

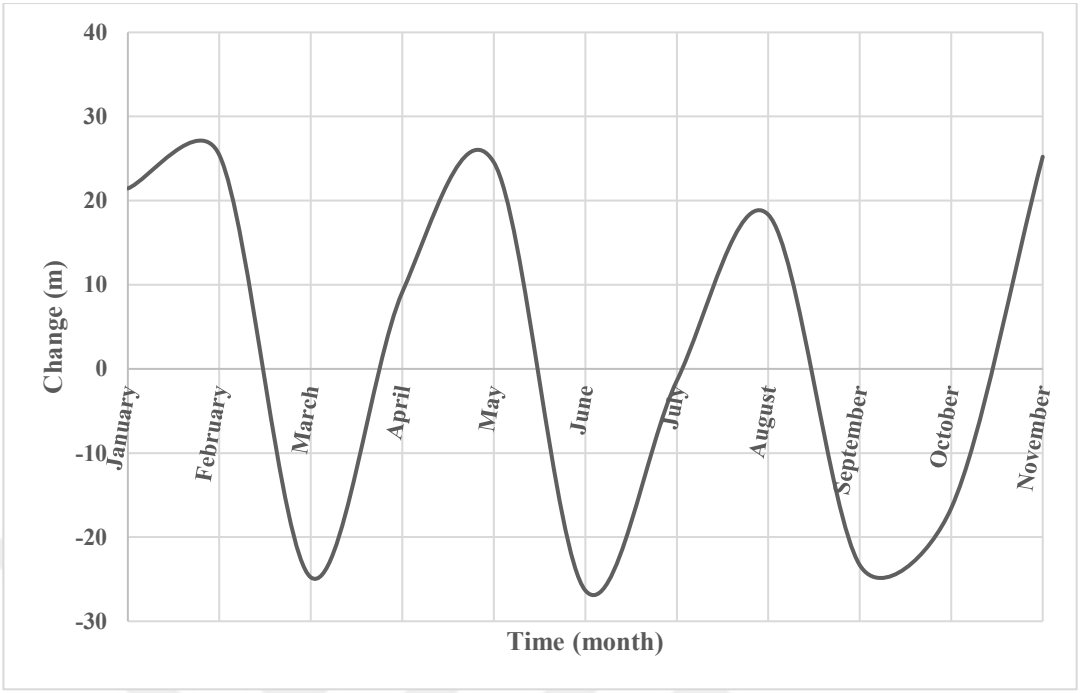

Figure 5.15. Monthly Shoreline Change Obtained from Landsat-8 for 2023

The same procedure and calculations are applied to the Planet imagery. Shorelines from each month of 2023 are extracted from Planet imagery, and a closer transect is selected to obtain the seasonal behavior of the Dim River Mouth. The shorelines and baseline of the Planet imagery monthly change model are represented in Figure 5.16.

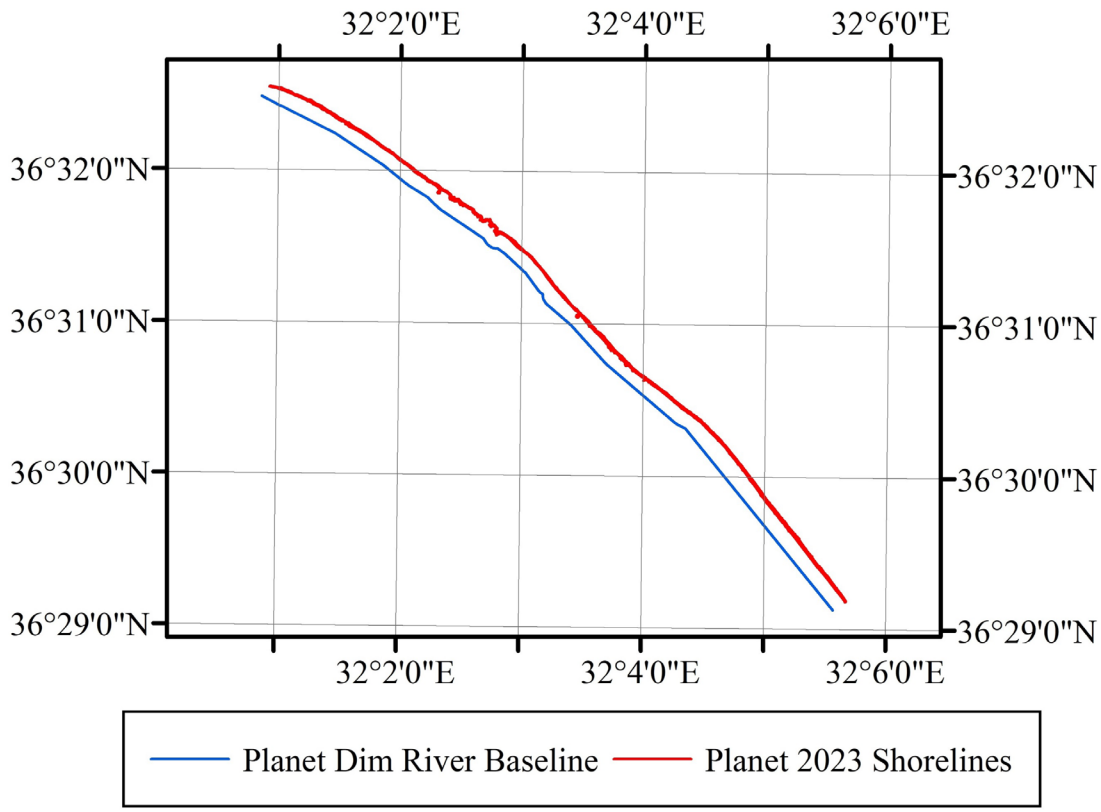

Figure 5.16. Shoreline and Baseline Layers of Planet Monthly Change Study

Based on the Net Shoreline Movement (NSM) results, the shoreline is classified as erosion and accretion, which is represented in Figure 5.17. Further, similar to the previous model that is formed with Landsat-8 imagery, a single transect that is close to the north of the Dim River mouth is selected, and temporal changes are examined by considering the relative distances between shorelines. The temporal change that is obtained from Planet imagery is represented in Figure 5.18. The corresponding dates of Planet Satellite imagery that are used in the monthly change study are tabulated in Table A.2. in Appendix A.

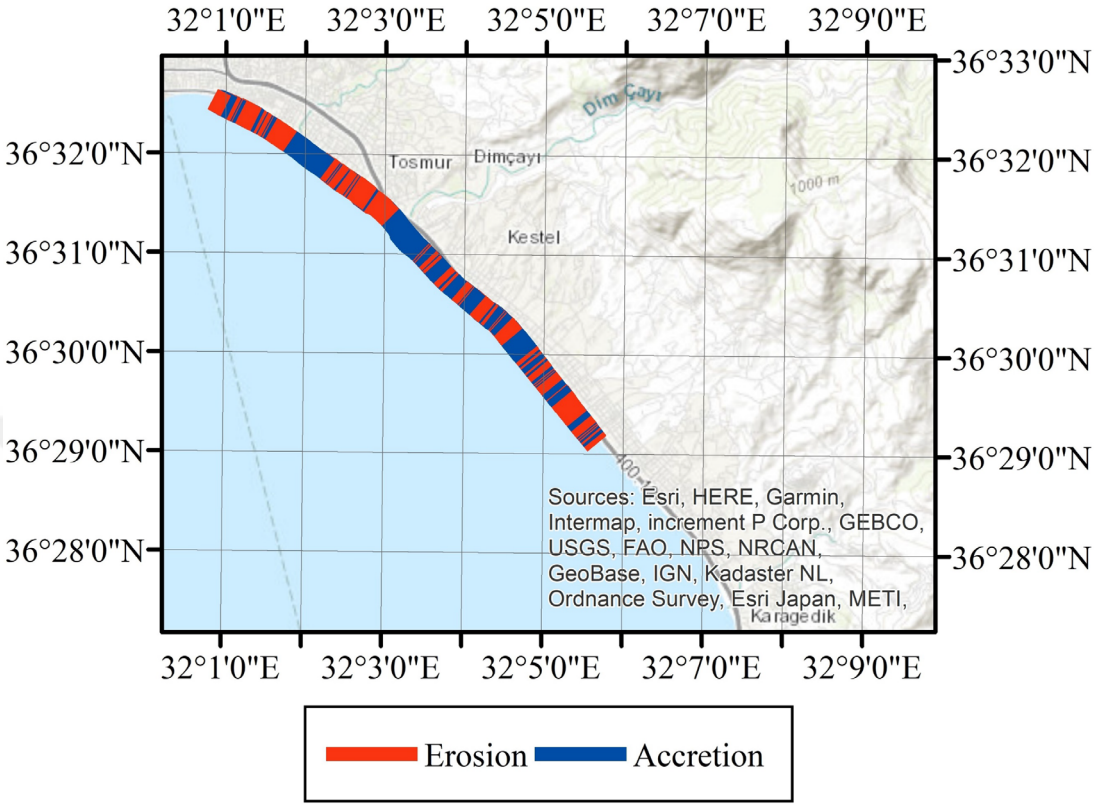

Figure 5.17. Erosion and Accretion Zones of Dim River Mouth Obtained from Planet Data for 2023

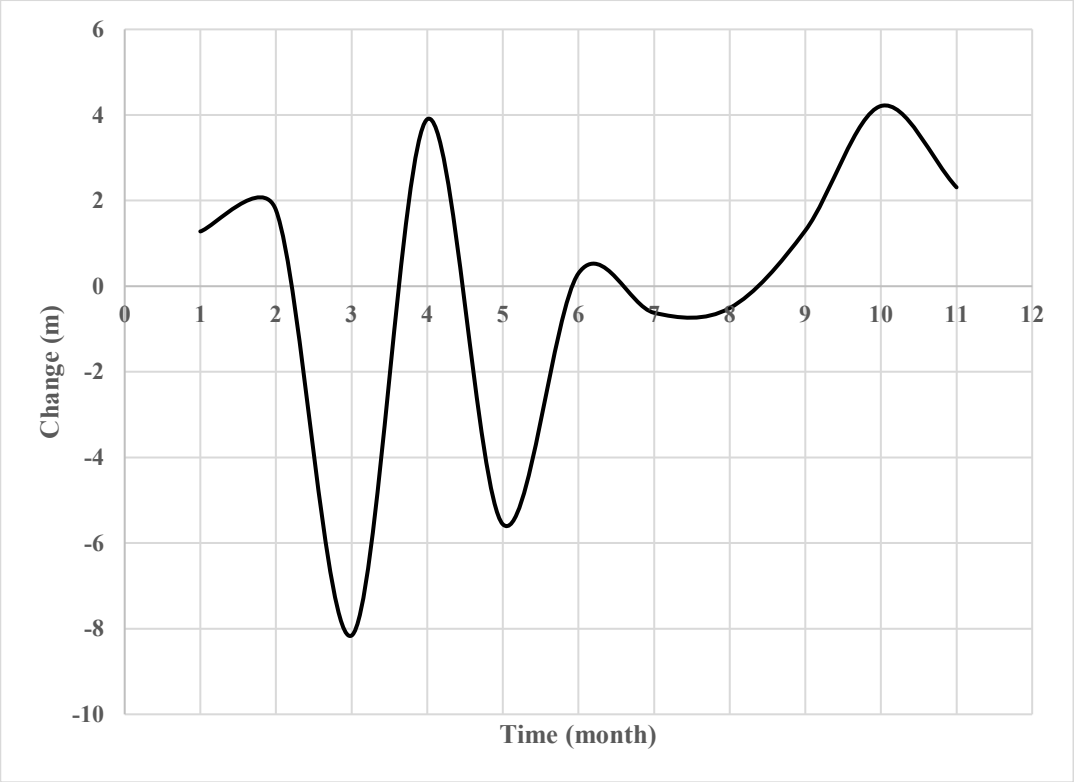

Figure 5.18. Monthly Shoreline Change Obtained from Planet for 2023

The monthly change in Landsat-8 images is in a range of roughly -25 and +25 meters. As expressed before, Landsat-8 images have a resolution of 30 by 30 meters. On the other hand, Planet has a three-by-three-meter resolution with a monthly change range between roughly -8 and +4 meters. The value difference between these satellites proves there is a monthly change in the area, and the methodology used to obtain this is correct. However, as the resolution of the imagery used increases, the reliability of the results will also increase. As expressed before, data characteristics for the monthly change studies from two different satellite data are expressed in Table A.2. in Appendix A. As can be seen from the data dates, the Landsat-8 data do not directly coincide with the Planet data by considering their dates. There are two-to-three-day differences between the instant times at which the images are captured. Therefore, during these differentiated times of events, storm surges are observed in the Dim River Mouth. The storm surge event resulted in having different monthly change

results between Planet and Landsat-8 data. Further, it is essential to express that the Dim River Mouth zone is naturally dynamic, and the values reported in the seasonal change graphs can change transect by transect. The intention of this study is to see whether there is a cyclical/seasonal behavior in the area or not. Based on the provided result, it is clear that there is a differentiated monthly change behavior in Dim River Mouth, and the DSAS tool lacks capturing the temporal differences. This situation is discussed in Chapter 6.

5.5 Sensitivity Study

Landsat data has a 30-meter resolution, while Planet Satellite has a 3-meter. The accuracy and sensitivity of the study are checked by using two images from Landsat-8 and Planet Satellite that have close dates. The dates of these images are tabulated in Table 5.2.

Table 5.2 Sensitivity Data Dates

Year	*Image Date (MM.DD.YYYY)*	*Source*
2023	07.27.2023	Planet
2023	07.29.2023	Landsat-8

The Digital Shoreline Analysis System (DSAS) is employed to determine the relative distances between two shorelines. The two shorelines and baseline are represented in Figure 5.19.

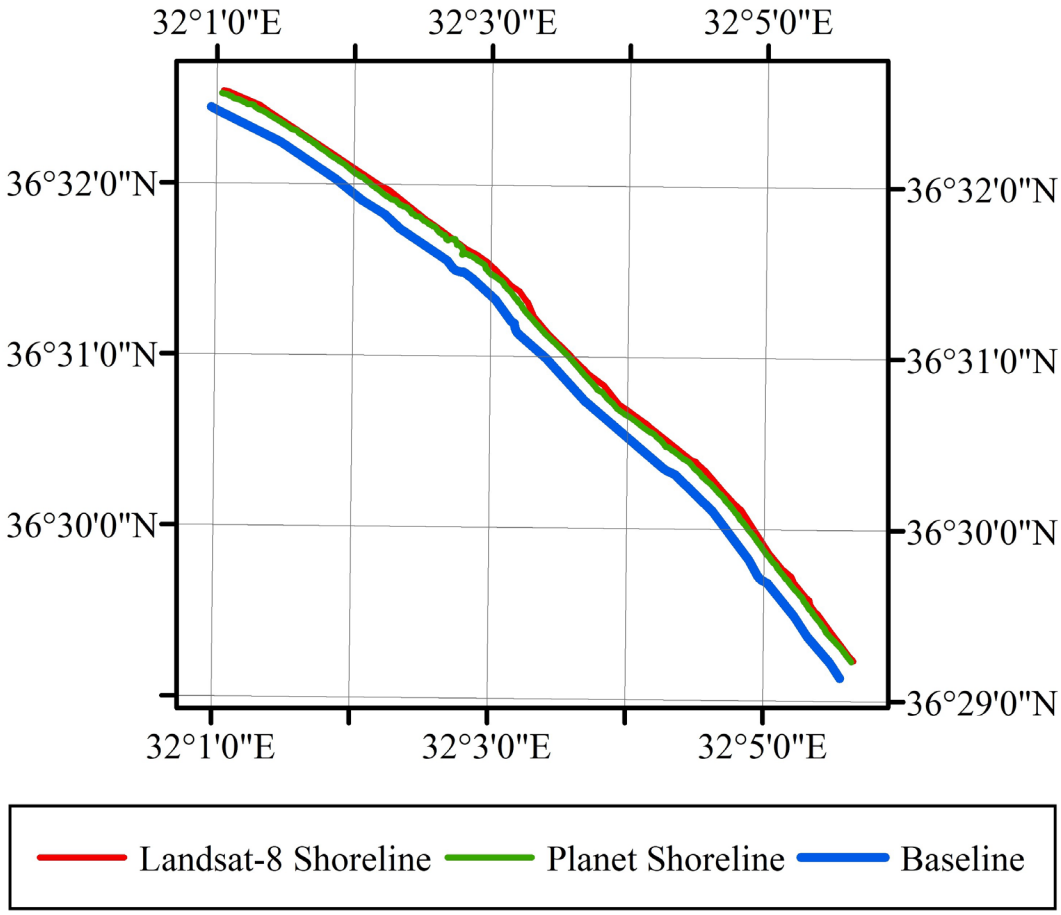

Figure 5.19. Shoreline and Baseline Layers of Sensitivity Study

As previously explained in Chapter 4, the net shoreline movement (NSM) measures the distances between the oldest and the youngest boundaries. In this case, two shorelines are provided. Therefore, the NSM value represents the distances between these two boundaries. The statistical distribution of NSM values of the sensitivity study is presented in Figure 5.27. and the mean value of this distribution is used as the uncertainty value of the Dim River Model. The same results are obtained after executing the Dim River Model with an uncertainty value that is obtained as the

mean of the sensitivity analysis result. This match is interpreted as the error of this study. In other words, the error of the study is equal to the mean value of NSM results in sensitivity analysis.

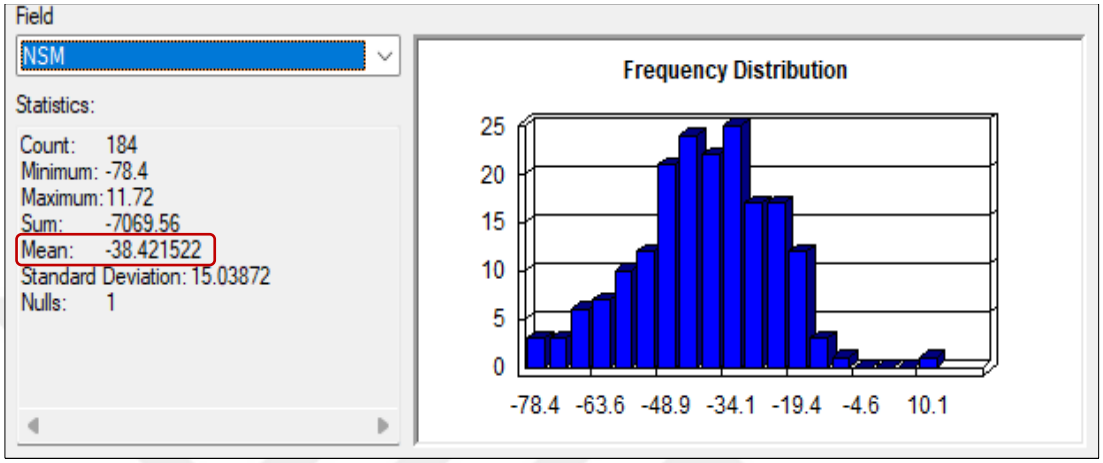

Figure 5.20. Frequency Distribution of Sensitivity Study

5.6 Results

The results of this study reveal significant insights into shoreline monitoring through the Alanya shoreline. The Net Shoreline Movement (NSM), Shoreline Change Envelope (SCE), End Point Rate (EPR), and Linear Regression Rate (LRR) are calculated for each model and compared. Further, cyclical behavior and seasonal behavior are checked by interpreting the results in a timely order.

Results provided insights based on the vulnerability of the sections of the shoreline. Since the resolution of the Landsat images is 30 meters, in this scale, the acceptable error should be equal to about a pixel. This error range is satisfied throughout the studies.

The maximum and minimum values of the calculations for the initial area of interest with the units are tabulated in Table 5.1.

Table 5.3 Calculation Results for Models

Model of Initial Area of Interest			
Rate	*Maximum*	*Minimum*	*Unit*
NSM	39.98	-210.81	meter
SCE	197.73	0.33	meter
EPR	1.23	-6.51	meter/year
LRR	0.89	-10.28	meter/year
Model of Alanya County			
NSM	49.24	-104.22	meter
SCE	108.31	2.31	meter
EPR	1.37	-8.03	meter/year
LRR	0.73	-4.22	meter/year
Model of Dim River Mouth			
NSM	-18.65	-77.61	meter
SCE	97.42	30.48	meter
EPR	-0.50	-4.23	meter/year
LRR	-0.44	-3.13	meter/year

5.7 Comprehensive Summary of the Chapter

The study focuses on analyzing shoreline changes in the area shrinking from the swath width of Landsat satellite imagery to the Dim River mouth zone. Three main models are developed and executed to assess shoreline dynamics and seasonal effects. The first model covers the entire area, approximately 243 km long, from Antalya City center to Tekmen Harbor in Mersin. The second model focuses on Alanya County, with a shoreline length of about 135 km, while the third model concentrates on the Dim River mouth, with a shoreline length of approximately 10 km.

Using Landsat satellite images from 1987 to 2023, shorelines are extracted for summer months (June, July, and August) to account for variations. The analysis employs parameters such as net shoreline movement (NSM), shoreline change envelope (SCE), end point rate (EPR), and linear regression rate (LRR) to quantify shoreline changes. A sensitivity study using Planet satellite imagery is conducted to assess the accuracy and reliability of the results.

The study reveals significant shoreline changes over the years, with both accretion and erosion observed in different sections. Detailed analyses, including graphical representations and statistical summaries, are provided for each model. Additionally, a monthly change study is conducted to examine the variations in shoreline behavior throughout the year, particularly focusing on the Dim River mouth area.

Furthermore, the study identifies cyclical patterns in shoreline changes, with alternating periods of accretion and erosion observed over several years. These cyclical behaviors are analyzed and graphically represented to understand long-term trends. Sensitivity analysis helps determine the uncertainty associated with the study results, providing insights into the reliability of the findings.

Overall, the study provides a comprehensive understanding of shoreline dynamics in the study area, highlighting the influence of both natural processes and human activities. It emphasizes the importance of considering monthly variations and conducting sensitivity analyses to ensure the accuracy of shoreline change assessments.

CHAPTER 6

DISCUSSION OF THE RESULTS

The discussion encompasses various aspects of this study. Three main discussions are developed to evaluate the results and models. As described in the methodology and analysis chapters, shorelines are extracted with a semi-automatic process and evaluated by employing a Digital Shoreline Analysis System (DSAS). DSAS makes several statistical calculations after the generation of intersections and transects.

The shoreline extraction process is discussed by focusing on both semi-automatic and fully automated approaches. In semi-automatic processes, meticulous steps such as coregistration, NDWI calculation, reclassification, and manual editing ensure accuracy. However, challenges like cloud cover and building interference can lead to errors. Fully automated methods like DDWI offer efficiency but may still require manual correction. Additionally, raster-to-vector conversion introduces uncertainties that result from data type changes. Geographic Information Systems (GIS) software aids in automation but has limitations.

Digital Shoreline Analysis System (DSAS) aids in analyzing shoreline changes but faces challenges in curvy zones and in capturing cyclical behaviors. The accuracy of DSAS results depends on the accuracy of shoreline extraction. Statistical measures like Net Shoreline Movement (NSM), Shoreline Change Envelope (SCE), End Point Rate (EPR), and Linear Regression Rate (LRR) provide insights into coastal dynamics but have limitations in capturing nuances and seasonal variations. Understanding these statistical measures is crucial for accurate interpretation of shoreline changes. Overall, the discussion emphasizes the need for further interpretation and integration of various data sources and technologies to enhance shoreline analysis methodologies.

6.1 Shoreline Extraction Discussion

The semi-automatic process in this study defines a meticulous approach required for shoreline extraction. Coregistration, normalized difference water index (NDWI) calculation, reclassification, and manual editing collectively form a robust framework aimed at ensuring the accuracy and reliability of extracted shoreline data. Each step of the extraction process should be addressed systematically to define and discuss potential errors. Coregistration is done by selecting previously known places in the area, such as a lighthouse, football pitch, architectural monument, etc. In 30-meter resolution, it is hard to define places in Landsat images. NDWI emerges as a powerful tool for differentiating between water bodies and land surfaces in satellite imagery. By leveraging specific spectral bands, such as green and near-infrared, NDWI calculations enable the precise delineation of shorelines. However, NDWI may generate a certain level of inconsistency due to some factors, such as cloud cover, light-colored landmarks, or buildings across the desired area that might cause deviations in the division of water and land boundaries. Reclassification is done based on the NDWI results with natural breaks, and the potential errors in NDWI calculation may lead to false division in reclassification. At the end of the semi-automatic process, manual editing is needed to correct fluctuations throughout the shorelines that may bring human-made mistakes with them.

On the other hand, fully automated approaches are being researched in shoreline extraction studies by different disciplines. Abdelhady et al. (2022) suggested a fully automated shoreline extraction algorithm by using different multispectral images in their study of the Lake Michigan shoreline. The algorithm is based on the Direct Difference Water Index (DDWI). The results of the algorithm are classified based on the extracted shoreline as accurate, good, and failed, as represented in Figure 6.1.

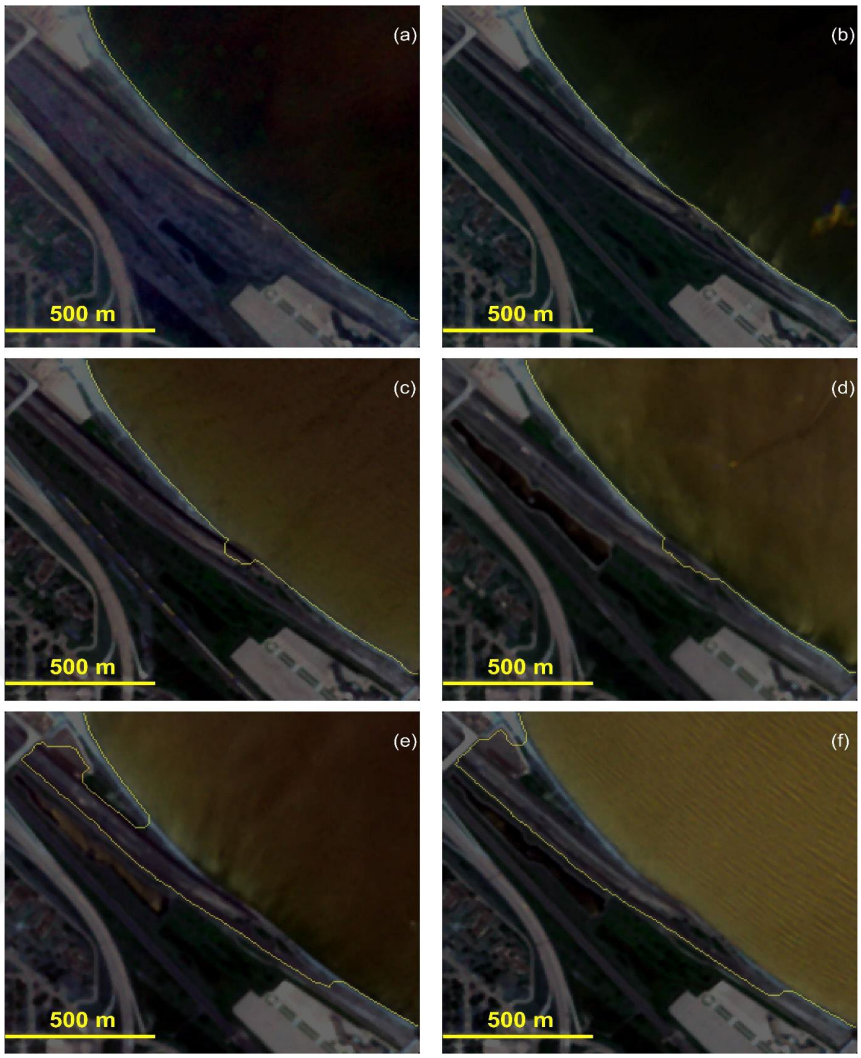

Figure 6.1. Sample of the detected shoreline from the images, shorelines are shown in yellow. (a,b) were classified as accurate; (c,d) were classified as good; (e,f) were classified as failed.(Abdelhady et al., 2022)

Similarly, as a result of the semi-automated shoreline extraction process suggested in this study, some "failed" results are edited manually. Therefore, the automation processes do not guarantee accurate results.

Due to the resolution of data and pixel-based nature of satellite images, conversion of raster data into vector data may lead to some uncertainties in the position of shorelines. The conversion of raster files to vector formats facilitates the extraction

of detailed spatial information, particularly in delineating polygons representing water bodies. This conversion enhances the granularity of shoreline data, enabling more nuanced analyses and insights into coastal dynamics. However, the potential data loss and/or distortion during the conversion process should be considered as another factor for the resulting errors. Therefore, a certain level of uncertainty is provided in the studies for each shoreline, and the calculated result should not be evaluated by neglecting this fact.

The pivotal role of Geographic Information Systems (GIS) software, particularly ArcGIS, in automating tasks and facilitating data management cannot be overstated. However, it is crucial to consider the limitations of GIS software, such as algorithmic biases and computational constraints, which may impact the accuracy of extracted shoreline data.

The extracted shoreline data can be seamlessly integrated with diverse studies and applications, ranging from coastal erosion modeling to habitat mapping and land-use planning. By leveraging interdisciplinary approaches and multi-source data integration, it is possible to enhance the holistic understanding of coastal dynamics and inform evidence-based decision-making in environmental management and conservation efforts. For instance, satellite data only provides an instant image at the time of data collection. At that time, the shore might be under the effect of some biological, tidal, or other environmental changes that might not directly change the shoreline. However, it is not possible to discriminate against these effects by just looking at satellite imagery.

6.2 Digital Shoreline Analysis System (DSAS) Procedure Discussion

The Digital Shoreline Analysis System (DSAS) is used to analyze the changes in distances and calculate some statistics based on these measurements. DSAS uses a shoreline layer and a baseline layer to automatically generate transects and intersection points starting from the baseline and crossing to the shorelines.

However, in the curvy zones of the study area, DSAS misses the ending shorelines and crosses the land to reach the last shoreline. This problem is presented in Figure 6.2. In Figure 6.2. light blue transects are ill-conditioned transects automatically generated by DSAS. It is observed that the ill-conditioned transects are the transects that intersect to each other. Also, ill-conditioned transects are longer than the regular transects. To automatically detect the ill-conditioned transects two filters can be implemented to the transects layers. These two filters are based on the length of the transect and intersection of the transects. To overcome this problem, the peninsula can be divided into two in a perpendicular direction to the cape. Nevertheless, DSAS cannot overcome this issue automatically. On the other hand, to understand the overall trend of desired location, all transects are needed for statistical calculations. Eliminating some transects due to the ill-conditioned generation of DSAS eventually changes the statistical results. This inconsistency might lead to a misunderstanding of the overall behavior of the desired study location. In this study, the effects of curvatures are observed in the models of Initial Area of Interest and Alanya. The Dim River Mouth model does not have curvy zones that are exposed to the elimination of ill-conditioned transects.

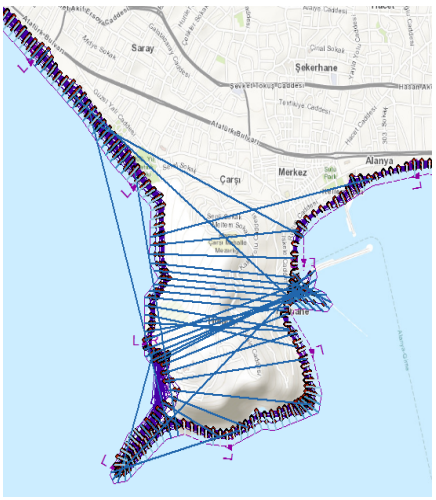

Figure 6.2. DSAS Transect Generation Anomaly Representation

An additional concern is that DSAS uses the primary and ending shorelines while making calculations based on the generated transects. This DSAS calculation procedure eliminates the effects of providing more data to increase the accuracy of results. In other words, DSAS gives the same results if the primary and ending shorelines are provided to the program as input. Shorelines that are in the middle of primary and ending ones do not have any effect in the calculations NSM and EPR in DSAS. This was the motivation for temporal change studies in this research.

DSAS only captures the distance changes between the provided shoreline without considering these changes in a timely order. Therefore, this leads to missing the cyclical and/or seasonal behaviors in the area. To overcome this, relative distances are calculated as it is done in Chapter 5 in the monthly change study. Ordering measurements in a timely manner leads to an exploration of monthly change and cyclical behavior in the study area. In this study, no direct upward or downward trend was observed in the shoreline changes, but even if there is, DSAS is not capable of capturing the trends. Therefore, DSAS should be used as an automatic transect and intersect generation tool in shoreline monitoring studies, and the results need further interpretation.

Furthermore, the accuracy of the results is in the range that is provided to the DSAS tool as the shorelines layer. In other words, the more accurate shorelines lead to more accurate calculations by DSAS (Himmelstoss et al., 2021). The accuracy of the shoreline extraction procedure directly affects the accuracy of DSAS results. Even if a certain level of uncertainty is provided before the calculations for each shoreline, the uncertainty value only refers to the probability of having a mistake for each data source. In this study, Landsat-8 images are used to analyze shoreline changes. The United States Geological Survey (USGS) suggests that using a 10-meter uncertainty value in both a positive and negative direction is acceptable. Therefore, a 10-meter uncertainty value is used in all of the shorelines. However, as a result of the sensitivity study using a 3-meter resolution Planet Satellite image, the accuracy is obtained at 38 meters, which is close to a pixel size. In the literature, Bayram et al. (2013) conducted a study using Landsat images, which resulted in a 37-meter

accuracy. This similarity explains that the procedure and calculations in this thesis are conducted accordingly and matched with the examples in the literature. However, shoreline changes observed in the Planet data may be linked with the existence of coastal structures in the area that can not be identified in Landsat-8 imagery, which has a 30-meter resolution. These human-made coastal structures are not regulated in the area. The existence and visibility of these coastal structures might be a reason for observing accretion in the Dim Model that is generated by using Planet Imagery. A similar procedure can be followed to obtain more accurate results by using higher spatial resolution images. In that case, researchers should consider different uncertainty values if they use different data sources at the same time in the shoreline layer.

6.3 Statistical Results Discussion

In shoreline analysis, understanding the statistical calculations employed by software like DSAS is crucial for accurate assessment and interpretation of coastal changes. DSAS offers a range of statistical measures, each providing unique insights into shoreline dynamics.

Net Shoreline Movement (NSM) measures the overall change in shoreline position over time. It provides a straightforward metric of coastal erosion or accretion, quantifying the net distance between the oldest and newest shorelines. NSM serves as a foundational metric, offering a broad overview of shoreline change. It misses the monthly change and/or cyclical changes in the provided data. An increase in the accuracy of results is expected as the amount of data used in the studies increases. However, NSM only measures the distance between a starting point and an ending point, which are shorelines in this study. Thus, it is possible to expect the same or close result by also reducing the amount of data. This is another reason for the need for further interpretation of results.

The Shoreline Change Envelope (SCE) represents the maximum extent of shoreline variability within a transect. Unlike rates, SCE is a distance measure, offering insight into the range of shoreline fluctuations. Its positive sign indicates the magnitude of change, irrespective of direction. SCE provides valuable context for understanding the variability and dynamic nature of coastal zones. Hence, the envelope value can only be used to classify shoreline zones in terms of their vulnerability. Further examination is needed after this kind of classification.

End Point Rate (EPR) calculates the average rate of shoreline change between two endpoints over a specified time period. While EPR is straightforward to compute and interpret, it has limitations, particularly with extensive datasets. EPR may overlook nuances in shoreline dynamics and fail to capture seasonal variations or changes in trend direction. Nevertheless, it remains a useful metric for basic trend analysis. Also, it gives the most logical results in this study by providing data that has units of meters per year. However, in the monthly change study, only the year 2023 is selected for analysis. Therefore, DSAS misses the changes in months by only focusing on years in the calculation of EPR. To overcome this issue, imaginary years can be assigned to each shoreline for better EPR results. Even in this case, DSAS is capable of missing the seasonal behavior in the provided data, and further clarification is needed.

Linear Regression Rate (LRR) employs a least-squares regression approach to quantify the rate of shoreline change. By fitting a regression line to all shoreline points, LRR captures the overall trend while minimizing residual errors. However, LRR may underestimate rates compared to EPR, particularly in the presence of outliers. Despite this, it offers a robust statistical framework based on established concepts. The DSAS tool uses a linear regression rate by using statistical concepts rather than considering coastal studies. Therefore, the LRR can give more accurate results based on the effect of coastal dynamics such as tides, tornados, currents, etc. In this study, the Alanya shoreline is exposed to a nearly 0.9-meter tidal effect, which may not be logical to discuss in a 30-meter resolution.

In conclusion, DSAS offers a comprehensive suite of statistical measures for shoreline analysis, each with its strengths and limitations. Understanding these statistical points is essential to effectively interpret shoreline change dynamics.

CHAPTER 7

CONCLUSION AND RECOMMENDATIONS

In conclusion, this study delved into the assessment of shoreline changes in the Mediterranean region of Turkey, with a particular focus on the Alanya area, utilizing a combination of remote sensing data, Geographic Information Systems (GIS) tools, and Digital Shoreline Analysis System (DSAS). Throughout the comprehensive analysis conducted, several significant findings and implications emerged.

Firstly, the study successfully demonstrated the feasibility and practicality of utilizing Landsat-8 imagery for shoreline monitoring purposes. Leveraging Landsat-8 data with its 30-meter pixel resolution and its accessibility through the United States Geological Survey (USGS) provided valuable insights into the dynamics of shoreline changes over time. Additionally, the study underscored the importance of accuracy and reliability in shoreline extraction processes. Employing a semi-automatic approach involving coregistration, Normalized Difference Water Index (NDWI) calculation, reclassification, and manual editing proved effective but also highlighted the need for systematic error handling, especially in areas with complex topography or ambiguous land-water boundaries. Moreover, the utilization of the Digital Shoreline Analysis System (DSAS) facilitated the statistical analysis of shoreline changes, offering metrics such as Net Shoreline Movement (NSM), Shoreline Change Envelope (SCE), End Point Rate (EPR), and Linear Regression Rate (LRR). These metrics provided valuable insights into the overall trends and variability of shoreline dynamics despite certain limitations in capturing seasonal variations and nuanced changes. The study identified areas for future research, emphasizing the integration of emerging technologies such as machine learning and unmanned aerial systems (UAS) to enhance shoreline monitoring accuracy and scalability. Furthermore, there is a need for further exploration of seasonal and cyclical shoreline changes, as well as improving the interoperability of data sources

for more comprehensive analyses. As it is discussed and represented in detail throughout the study, the study area is narrowed step by step by starting roughly 240 km extent to 10 km extent. The Digital Shoreline Analysis System (DSAS) evaluates the calculation as a whole and calculates statistical results based on the overall area of study. Therefore, to reduce the potential error, the study area is narrowed. This narrowing process resulted in more accurate results in obtaining the erosion and accretion zones in the area in detail and classifying the parameters. Additionally, as the resolution of the input data increases, the accuracy of the results also increases. By comparing the results from Landsat-8 and Planet Satellite data, it is acceptable to say that the procedure followed in this study is promising and gives better results with higher resolution values. On the other hand, a combination of Landsat and Planet data together to get more accurate results by considering their uncertainty values can be recommended for further studies in shoreline change determination.

Moreover, throughout the model generation, only geospatial data is used, and no sediment transportation data is included in the analysis. However, by considering the situation from a coastal engineering perspective, there is a need to include sediment transportation data to result in more accurate calculations and understand the behavior of the location. In the Dim River Mouth Model, there might be some human effects on the Dim River, such as sand collection from the river bed upstream, which prevents sediment transport from the river to the shore.

The implications of this study extend beyond academia, with significant relevance to coastal management and conservation efforts. By enhancing our understanding of shoreline dynamics and vulnerabilities, informed decisions can be made to mitigate risks, plan for sustainable land use, and address environmental challenges in coastal areas. Ultimately, this study contributes to the existing body of literature by providing insights into the feasibility, accuracy, and implications of utilizing remote sensing and GIS tools for shoreline monitoring in coastal regions. It underscores the importance of interdisciplinary approaches and ongoing research efforts to advance our understanding of coastal dynamics and inform evidence-based decision-making for coastal management and conservation.

Based on the results and the effort throughout the study, some recommendations for future researchers can be expressed. Future research endeavors should focus on advancing shoreline extraction techniques through the integration of emerging technologies, such as machine learning, deep learning, and unmanned aerial systems (UAS). Additionally, efforts to improve spatial resolution, temporal coverage, and data interoperability hold promise for enhancing the accuracy, scalability, and applicability of shoreline extraction methodologies in diverse geospatial contexts.

REFERENCES

Abdelhady, H. U., Troy, C. D., Habib, A., & Manish, R. (2022). A Simple, Fully Automated Shoreline Detection Algorithm for High-Resolution Multi-Spectral Imagery. *Remote Sensing*, *14*(3), 557. https://doi.org/10.3390/rs14030557

Acar, U., Bayram, B., Sanli, F. B., Abdikan, S., Sunar, F., & Cetin, H. I. (2012). An Algorithm for Coastline Detection Using SAR Images. *The International Archives of the Photogrammetry, Remote Sensing and Spatial Information Sciences*, *XXXIX-B3*, 457–460. https://doi.org/10.5194/isprsarchives-XXXIX-B3-457-2012

Al Ruheili, A. M., & Boluwade, A. (2021). Quantifying Coastal Shoreline Erosion Due to Climatic Extremes Using Remote-Sensed Estimates from Sentinel-2A Data. *Environmental Processes*, *8*(3), 1121–1140. https://doi.org/10.1007/s40710-021-00522-2

Ari, H. A., Yüksel, Y., Özkan Çevik, E., Güler, I., Cevdet Yalçiner, A., & Bayram, B. (2007). Determination and control of longshore sediment transport: A case study. *Ocean Engineering*, *34*(2), 219–233. https://doi.org/10.1016/j.oceaneng.2006.01.009

Arjasakusuma, S., Kusuma, S. S., Saringatin, S., Wicaksono, P., Mutaqin, B. W., & Rafif, R. (2021). Shoreline Dynamics in East Java Province, Indonesia, from 2000 to 2019 Using Multi-Sensor Remote Sensing Data. *Land*, *10*(2), 100. https://doi.org/10.3390/land10020100

Bamdadinejad, M., Ketabdari, M. J., & Chavooshi, S. M. H. (2021). Shoreline Extraction Using Image Processing of Satellite Imageries. *Journal of the Indian Society of Remote Sensing*, *49*(10), 2365–2375. https://doi.org/10.1007/s12524-021-01398-3

Bayram, B., Erdem, F., Akpinar, B., Ince, A. K., Bozkurt, S., Catal Reis, H., & Seker, D. Z. (2017). The Efficiency of Random Forest Method for Shoreline Extraction from LANDSAT-8 and GOKTURK-2 Imageries. *ISPRS Annals of the Photogrammetry, Remote Sensing and Spatial Information Sciences*, *IV-4/W4*, 141–145. https://doi.org/10.5194/isprs-annals-IV-4-W4-141-2017

Bayram, B., & Ince, A. (2019). Integration of Self-Organizing Map and Machine Learning Methods to Extract Shorelines from LANDSAT-8 Images. *The 40th Asian Conference on Remote Sensing(ACRS 2019)*.

Bayram, B., Seker, D. Z., Acar, U., Yuksel, Y., Guner, H. A. A., & Cetin, I. (2013). An Integrated Approach to Temporal Monitoring of the Shoreline and Basin of Terkos Lake. *Journal of Coastal Research*, *29*(6), 1427. https://doi.org/10.2112/JCOASTRES-D-12-00084.1

Bayram, B., Seker, D. Z., & Akpinar, B. (2019). Efficiency of Different Machine Learning Methods for Shoreline Extraction from UAV Images. *The 40th Asian Conference on Remote Sensing(ACRS 2019)*.

Bengoufa, S., Niculescu, S., Mihoubi, M. K., Belkessa, R., Rami, A., Rabehi, W., & Abbad, K. (2021). Machine learning and shoreline monitoring using optical satellite images: case study of the Mostaganem shoreline, Algeria. *Journal of Applied Remote Sensing*, *15*(02). https://doi.org/10.1117/1.JRS.15.026509

Demir, N., Bayram, B., Şeker, D. Z., Oy, S., & Erdem, F. (2019). A nonparametric fuzzy shoreline extraction approach from Sentinel-1A by integration of RASAT pan-sharpened imagery. *Geo-Marine Letters*, *39*(5), 401–415. https://doi.org/10.1007/s00367-019-00608-9

Demir, N., Bayram, B., Şeker, D. Z., Oy, S., İnce, A., & Bozkurt, S. (2019). Advanced Lake Shoreline Extraction Approach by Integration of SAR Image and LIDAR Data. *Marine Geodesy*, *42*(2), 166–185. https://doi.org/10.1080/01490419.2019.1581861

Demir, N., Oy, S., Erdem, F., Şeker, D. Z., & Bayram, B. (2017). Integrated Shoreline Extraction Approach with Use of RASAT MS and SENTINEL-1A SAR Images. *ISPRS Annals of the Photogrammetry, Remote Sensing and Spatial Information Sciences*, *IV-2/W4*, 445–449. https://doi.org/10.5194/isprs-annals-IV-2-W4-445-2017

Ding, Y., Yang, X., Jin, H., Wang, Z., Liu, Y., Liu, B., Zhang, J., Liu, X., Gao, K., & Meng, D. (2021). Monitoring Coastline Changes of the Malay Islands Based on Google Earth Engine and Dense Time-Series Remote Sensing Images. *Remote Sensing*, *13*(19), 3842. https://doi.org/10.3390/rs13193842

Elkafrawy, S. B., Basheer, M. A., Mohamed, H. M., & Naguib, D. M. (2021). Applications of remote sensing and GIS techniques to evaluate the effectiveness of coastal structures along Burullus headland-Eastern Nile Delta, Egypt. *The Egyptian Journal of Remote Sensing and Space Science*, *24*(2), 247–254. https://doi.org/10.1016/j.ejrs.2020.01.002

Ergin, A., Güler, I., Yalciner, A., Baykal, C., Artagan, S., & Şafak, I. (2006). A One-Line Numerical Model for Wind Wave Induced Shoreline Changes. *Seventh International Congress on Advances in Civil Engineering*.

Gao, B. (1996). NDWI—A normalized difference water index for remote sensing of vegetation liquid water from space. *Remote Sensing of Environment*, *58*(3), 257–266. https://doi.org/10.1016/S0034-4257(96)00067-3

Genz, A., Fletcher, C., Dunn, R., Frazer, N., Rooney, J., Fletcher, A., Dunn, C., & Frazer, R. (2007). The Predictive Accuracy Of Shoreline Change Rate Methods And Alongshore Beach Variation On Maui, Hawai'i. *Journal of Coastal Research*, *23*. https://doi.org/10.2112/05-0521.1

Gokceoglu, C., Nefeslioglu, H. A., Turer, D., Akgun, A., Ayas, Z., & Temimhan, M. (2015). Determination of coastal border line: an integrated approach for a part of Antalya coast (Turkey). *Arabian Journal of Geosciences*, *8*(2), 1145–1154. https://doi.org/10.1007/s12517-014-1287-0

Güler, I., Ergin, A., & Yalçiner, A. C. (1998). The Effect of the Use of Wave Data for the Numerical Simulation of Shoreline Evaluation. *Journal of Coastal Research*, 195–200. http://www.jstor.org/stable/25736136

Gutman, G., Huang, C., Chander, G., Noojipady, P., & Masek, J. G. (2013). Assessment of the NASA–USGS Global Land Survey (GLS) datasets. *Remote Sensing of Environment*, *134*, 249–265. https://doi.org/10.1016/j.rse.2013.02.026

Hallermeier, R. J. (1978). "Uses for a Calculated Limit Depth to Beach Erosion." *Proceedings of the 16th Coastal Engineering Conference, American Society of Civil Engineers*, 1493–1512.

Himmelstoss, E. A., Henderson, R. E., Kratzmann, M. G., & Farris, A. S. (2021). *Digital Shoreline Analysis System (DSAS) version 5.1 user guide: U.S. Geological Survey Open-File Report 2021–1091*.

Hoffmann, G., & Lampe, R. (2007). A sediment budget calculation is needed to estimate Holocene coastal changes on the southwest Baltic Sea (Germany). *Marine Geology*, *243*(1–4), 143–156. https://doi.org/10.1016/j.margeo.2007.04.014

Hossain, M. S., Yasir, M., Wang, P., Ullah, S., Jahan, M., Hui, S., & Zhao, Z. (2021). Automatic shoreline extraction and change detection: A study on the southeast coast of Bangladesh. *Marine Geology*, *441*, 106628. https://doi.org/10.1016/j.margeo.2021.106628

Incekara, A. H., Seker, D. Z., & Bayram, B. (2018). Qualifying the LIDAR-Derived Intensity Image as an Infrared Band in NDWI-Based Shoreline Extraction. *IEEE Journal of Selected Topics in Applied Earth Observations and Remote Sensing*, *11*(12), 5053–5062. https://doi.org/10.1109/JSTARS.2018.2875792

Kamphuis, J. W. (1991). Alongshore Sediment Transport Rate. *Journal of Waterway, Port, Coastal, and Ocean Engineering*, *117*(6), 624–640. https://doi.org/10.1061/(ASCE)0733-950X(1991)117:6(624)

Kamphuis, J. W. (2000). *Introduction to Coastal Engineering and Management*. World Scientific. https://doi.org/10.1142/7021

Karaman, M. (2021). Comparison of thresholding methods for shoreline extraction from Sentinel-2 and Landsat-8 imagery: Extreme Lake Salda, track of Mars on Earth. *Journal of Environmental Management*, *298*, 113481. https://doi.org/10.1016/j.jenvman.2021.113481

Kennedy, R. E., Townsend, P. A., Gross, J. E., Cohen, W. B., Bolstad, P., Wang, Y. Q., & Adams, P. (2009). Remote sensing change detection tools for natural resource managers: Understanding concepts and tradeoffs in the design of landscape monitoring projects. *Remote Sensing of Environment*, *113*(7), 1382–1396. https://doi.org/10.1016/j.rse.2008.07.018

Koulibaly, C. T., & Ayoade, J. O. (2021). The Application of GIS and Remote Sensing in a Spatiotemporal Analysis of Coastline Retreat in Rufisque, Senegal. *Geomatics and Environmental Engineering*, *15*(3), 55–80. https://doi.org/10.7494/geom.2021.15.3.55

Kumar Das, S., Sajan, B., Ojha, C., & Soren, S. (2021). Shoreline change behavior study of Jambudwip island of Indian Sundarban using DSAS model. *The Egyptian Journal of Remote Sensing and Space Science*, *24*(3), 961–970. https://doi.org/10.1016/j.ejrs.2021.09.004

Kumar, L., Afzal, M. S., & Afzal, M. M. (2020). Mapping shoreline change using machine learning: a case study from the eastern Indian coast. *Acta Geophysica*, *68*(4), 1127–1143. https://doi.org/10.1007/s11600-020-00454-9

Matin, N., & Hasan, G. M. J. (2021). A quantitative analysis of shoreline changes along the coast of Bangladesh using remote sensing and GIS techniques. *CATENA*, *201*, 105185. https://doi.org/10.1016/j.catena.2021.105185

McAllister, E., Payo, A., Novellino, A., Dolphin, T., & Medina-Lopez, E. (2022). Multispectral satellite imagery and machine learning for the extraction of shoreline indicators. *Coastal Engineering*, *174*, 104102. https://doi.org/10.1016/j.coastaleng.2022.104102

McFeeters, S. K. (1996). The use of the Normalized Difference Water Index (NDWI) in the delineation of open water features. *International Journal of Remote Sensing*, *17*(7), 1425–1432. https://doi.org/10.1080/01431169608948714

Natarajan, L., Sivagnanam, N., Usha, T., Chokkalingam, L., Sundar, S., Gowrappan, M., & Roy, P. D. (2021). Shoreline changes over last five decades and predictions for 2030 and 2040: a case study from Cuddalore, southeast coast of India. *Earth Science Informatics*, *14*(3), 1315–1325. https://doi.org/10.1007/s12145-021-00668-5

Ozturk, D., Beyazit, I., & Kilic, F. (2015). Spatiotemporal Analysis of Shoreline Changes of the Kizilirmak Delta. *Journal of Coastal Research*, *316*, 1389–1402. https://doi.org/10.2112/JCOASTRES-D-14-00159.1

Parthasarathy, K. S. S., & Deka, P. C. (2021). Remote sensing and GIS application in assessment of coastal vulnerability and shoreline changes: a review. *ISH Journal of Hydraulic Engineering*, *27*(sup1), 588–600. https://doi.org/10.1080/09715010.2019.1603086

Planet Scope. (2023). https://developers.planet.com/docs/data/planetscope/#planetscope-imagery-collection-versus-publication

Quang, D. N., Ngan, V. H., Tam, H. S., Viet, N. T., Tinh, N. X., & Tanaka, H. (2021). Long-Term Shoreline Evolution Using DSAS Technique: A Case Study of Quang Nam Province, Vietnam. *Journal of Marine Science and Engineering*, *9*(10), 1124. https://doi.org/10.3390/jmse9101124

Reclass by ranges of values. (n.d.). ArcGIS Pro 3.2. https://pro.arcgis.com/en/pro-app/latest/tool-reference/spatial-analyst/reclass-by-ranges-of-values.htm

Shenbagaraj, N., Senthil kumar, K., Rasheed, A. M., Leostalin, J., & Kumar, M. N. (2021). Mapping and Electronic Publishing of Shoreline Changes using UAV Remote Sensing and GIS. *Journal of the Indian Society of Remote Sensing*, *49*(8), 1769–1777. https://doi.org/10.1007/s12524-020-01287-1

Süzen, M., & Özhan, E. (2003). Monitoring shoreline changes at Yesilirmak Delta by remote sensing and GIS. *MEDCOAST 03:Proceeding of the Sixth International Conference on the Mediterranean Coastal Environment*, 2311–2322.

Süzen, M., & Rojay, B. (2005). Active shoreline changes of Büyük Menderes River Delta in the last 50 years. *MEDCOAST 05:Proceeding of the Seventh International Conference on the Mediterranean Coastal Environment*, *2*, 1309–1316.

Wulder, M. A., White, J. C., Loveland, T. R., Woodcock, C. E., Belward, A. S., Cohen, W. B., Fosnight, E. A., Shaw, J., Masek, J. G., & Roy, D. P. (2016). The global Landsat archive: Status, consolidation, and direction. *Remote Sensing of Environment*, *185*, 271–283. https://doi.org/10.1016/j.rse.2015.11.032

Xu, N., Wang, Y., Huang, C., Jiang, S., Jia, M., & Ma, Y. (2022). Monitoring coastal reclamation changes across Jiangsu Province during 1984–2019 using landsat data. *Marine Policy*, *136*, 104887. https://doi.org/10.1016/j.marpol.2021.104887

Yiğit, A. Y., Kaya, Y., & Şenol, H. İ. (2022). Monitoring the change of Turkey's tourism city Antalya's Konyaaltı shoreline with multi-source satellite and meteorological data. *Applied Geomatics*, *14*(2), 223–236. https://doi.org/10.1007/s12518-022-00431-5

Online Sources

URL-1: T. C. Antalya Valiliği. (n.d.). *Alanya*. http://www.antalya.gov.tr/alanya

URL-2: Diler Enerji. (n.d.). *URL-2: Diler Enerji*. https://www.dilerhld.com/grup.asp?anagrup_no=4&grup_no=19

URL-3: Emodnet. (n.d.). *URL-3: Emodnet*. https://emodnet.ec.europa.eu/geoviewer/

APPENDICES

A. Details of Study Data

Table A.1 Data Details

No.	Year	Image Date (YYYY-MM-DD)	Cloudy (yes/A bit/no)	Landsat No.
1	1987	1987-08-19	no	Landsat-5
2	2000	2000-07-13	no	Landsat-7
3	2005	2005-08-12	yes	Landsat-7
4	2009	2009-08-15	no	Landsat-5
5	2013	2013-06-23	no	Landsat-8
6	2013	2013-07-09	yes	Landsat-8
7	2013	2013-07-25	no	Landsat-8
8	2013	2013-08-10	no	Landsat-8
9	2013	2013-08-26	no	Landsat-8
10	2014	2014-06-10	A bit	Landsat-8
11	2014	2014-06-26	no	Landsat-8
12	2014	2014-07-12	yes	Landsat-8
13	2014	2014-08-13	yes	Landsat-8
14	2014	2014-08-29	yes	Landsat-8
15	2015	2015-06-13	yes	Landsat-8
16	2015	2015-07-15	no	Landsat-8
17	2015	2015-08-16	yes	Landsat-8
18	2016	2016-06-15	yes	Landsat-8
19	2016	2016-07-16	yes	Landsat-8
20	2016	2016-08-02	A bit	Landsat-8
21	2016	2016-08-18	yes	Landsat-8
22	2017	2017-06-02	no	Landsat-8
23	2017	2017-07-04	A bit	Landsat-8
24	2017	2017-07-20	no	Landsat-8
25	2017	2017-08-05	yes	Landsat-8
26	2017	2017-08-21	yes	Landsat-8
27	2018	2018-06-05	no	Landsat-8
28	2018	2018-07-07	A bit	Landsat-8
29	2018	2018-07-23	no	Landsat-8

Table A.1 Continued

30	2018	2018-08-08	no	Landsat-8
31	2018	2018-08-24	yes	Landsat-8
32	2018	2018-07-07	A bit	Landsat-8
33	2019	2019-06-08	no	Landsat-8
34	2019	2019-07-10	no	Landsat-8
35	2019	2019-07-26	yes	Landsat-8
36	2019	2019-08-11	no	Landsat-8
37	2019	2019-08-27	no	Landsat-8
38	2020	2020-06-10	A bit	Landsat-8
39	2020	2020-06-26	no	Landsat-8
40	2020	2020-07-12	A bit	Landsat-8
41	2020	2020-07-28	no	Landsat-8
42	2020	2020-08-13	no	Landsat-8
43	2020	2020-08-29	no	Landsat-8
44	2021	2021-06-29	no	Landsat-8
45	2021	2021-07-15	no	Landsat-8
46	2021	2021-07-31	yes	Landsat-8
47	2021	2021-08-16	no	Landsat-8
48	2022	2022-06-16	A bit	Landsat-8
49	2022	2022-06-24	no	Landsat-8
50	2022	2022-07-02	no	Landsat-8
51	2022	2022-07-10	yes	Landsat-8
52	2022	2022-07-18	no	Landsat-8
53	2022	2022-07-26	no	Landsat-8
54	2022	2022-08-11	yes	Landsat-8
55	2022	2022-08-19	A bit	Landsat-8
56	2022	2022-08-27	no	Landsat-8
57	2022	2022-06-16	A bit	Landsat-8
58	2023	2023-06-07	no	Landsat-8
59	2023	2023-07-05	yes	Landsat-8
60	2023	2023-07-13	no	Landsat-8
61	2023	2023-07-21	no	Landsat-8
62	2023	2023-07-29	no	Landsat-8
63	2023	2023-08-06	yes	Landsat-8
64	2023	2023-08-14	yes	Landsat-8
65	2023	2023-08-22	A bit	Landsat-8
66	2023	2023-08-30	no	Landsat-8

Table A.2 Data Details of Monthly Change Study

ID	image_date	cloudy	source	Shape_Leng (m)
1	2023-01-26	yes	Landsat-8	7212.73
2	2023-02-11	no	Landsat-8	9335.67
3	2023-03-15	no	Landsat-8	9304.59
4	2023-04-24	no	Landsat-8	9316.20
5	2023-05-02	no	Landsat-8	9308.46
6	2023-06-19	no	Landsat-8	9304.16
7	2023-07-21	no	Landsat-8	9310.15
8	2023-08-30	no	Landsat-8	9312.51
9	2023-09-23	no	Landsat-8	9330.57
10	2023-10-25	no	Landsat-8	9320.64
11	2023-11-02	abit	Landsat-8	9307.84
12	2023-12-23	no	Landsat-8	9300.04
13	2023-07-21	no	Landsat-8	9310.15
14	2023-04-24	no	Landsat-8	9316.20

ID	image_date	source	Shape_Leng (m)
1	1/24/2023	Planet PBC	9550.77
2	2/15/2023	Planet PBC	10244.49
3	3/15/2023	Planet PBC	10315.11
4	4/23/2023	Planet PBC	9928.21
5	5/1/2023	Planet PBC	10329.32
6	6/17/2023	Planet PBC	10738.35
7	7/22/2023	Planet PBC	10430.49
8	8/30/2023	Planet PBC	2324.82
9	9/23/2023	Planet PBC	10427.64
10	10/22/2023	Planet PBC	9999.56
11	11/23/2023	Planet PBC	10180.99

B. Digital Shoreline Analysis System (DSAS) Workflow

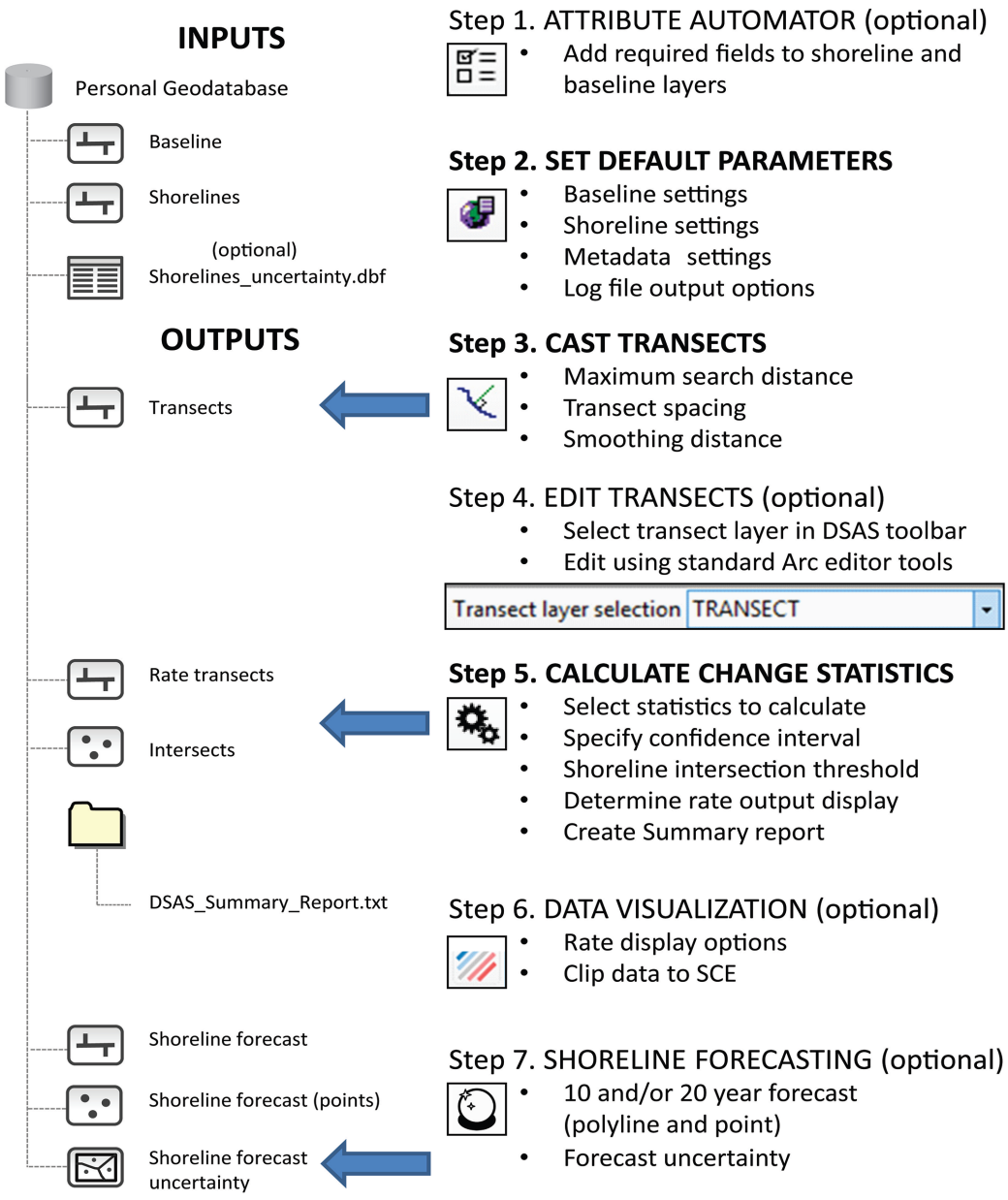

Figure B.1. Workflow of Digital Shoreline Analysis System (DSAS) (Himmelstoss et al., 2021)

C. Analysis Results and Charts

As explained in detail in Chapter 4, net shoreline movement represents the total change in between the youngest and the oldest shorelines in meters. In Figure C.2. blue zones represent the positive changes in shorelines, which denote an accretion, and red zones represent coastal erosion. Shoreline change envelope (SCE) is the maximum value in a change in meter by not considering the sign of the change as expressed in detail in Chapter 4. Therefore, in Figure C.3. All of the values represented in the charts are positive. The legend is divided by considering the mean of total values. Red zones represent the SCE values that are less than the mean, and blue zones represent values above the mean. The end point rate (EPR) is the rate at which the zones change per year in meters. It might have either positive or negative values. Positive EPR value represents the amount of accretion in meters per year. Similarly, negative values represent the amount of erosion per year. The calculation procedure is expressed in detail in Chapter 4.

In Figure C.4. red zones are erosion zones, and blue zones are accretion zones. Lastly, the linear regression rate (LRR) is calculated. In LRR calculation, DSAS uses all the data provided without considering whether there is a trend or accuracy mistake. The LRR calculation is made using statistical fundamentals and represents a rate that needs further interpretation. In Figure C.5. red zones represent negative LRR values, while blue zones represent positive LRR values.

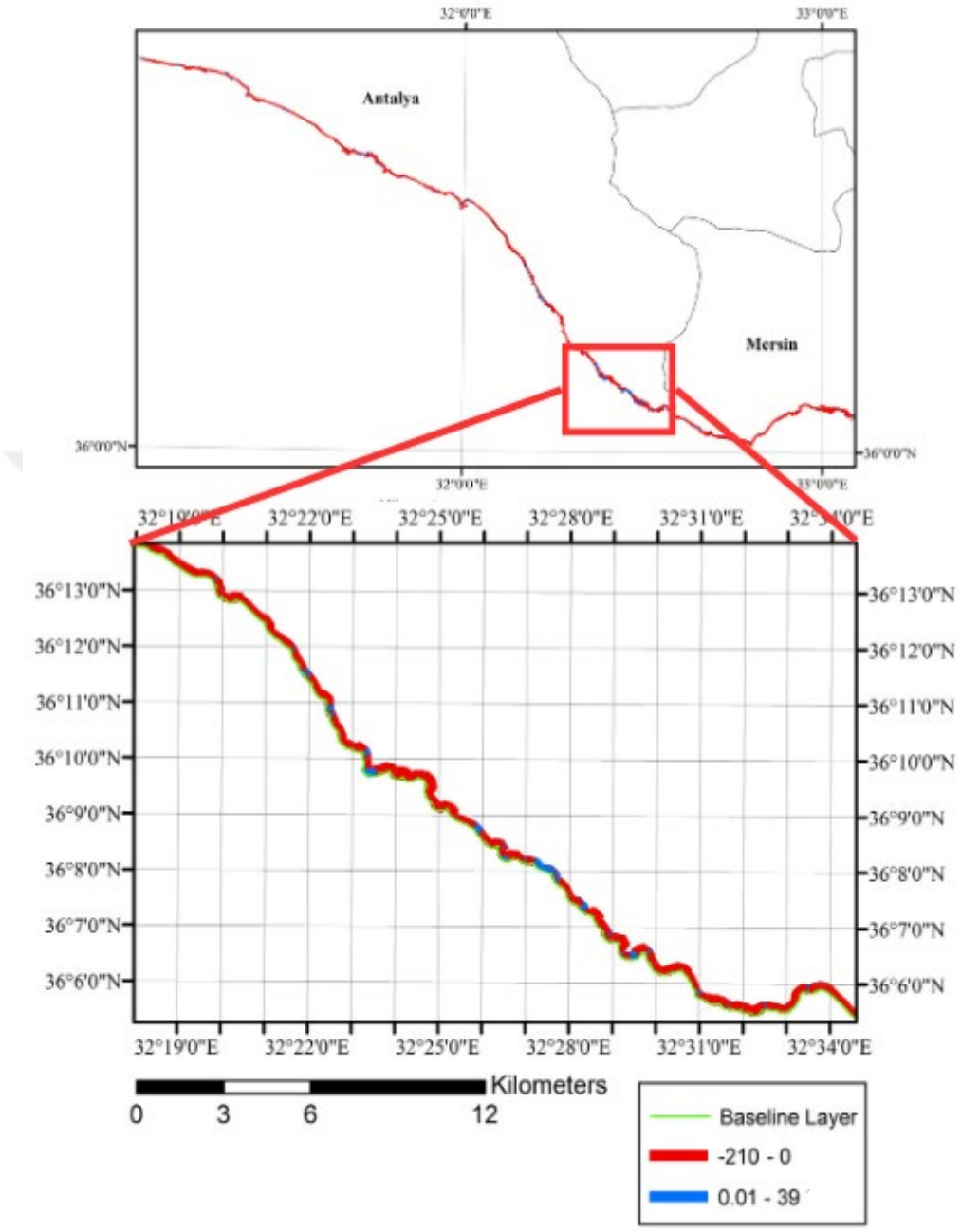

Figure C.2. Net Shoreline Movement (NSM) for the Initial Area of Interest

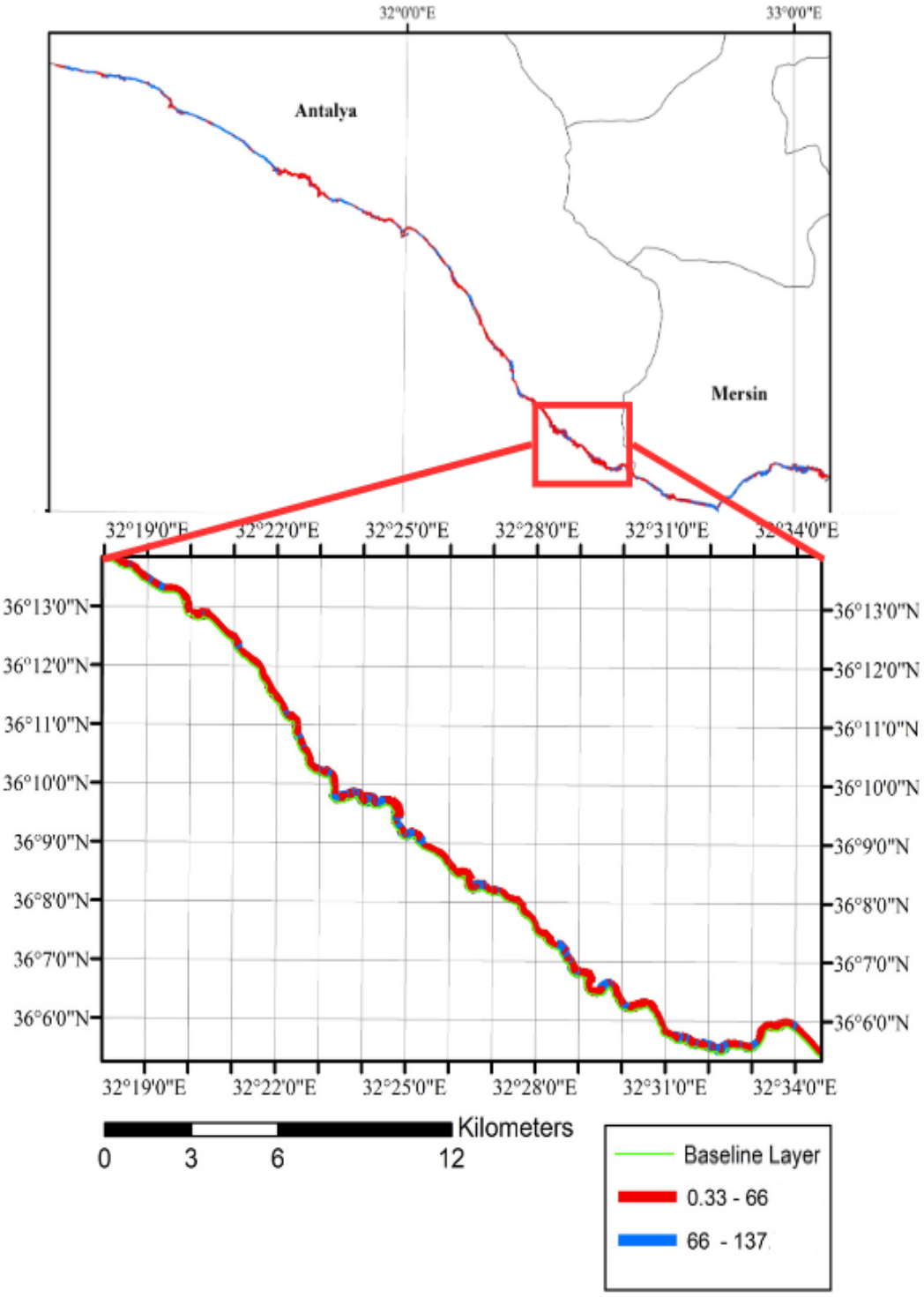

Figure C.3. Shoreline Chance Envelope (SCE) for the Initial Area of Interest

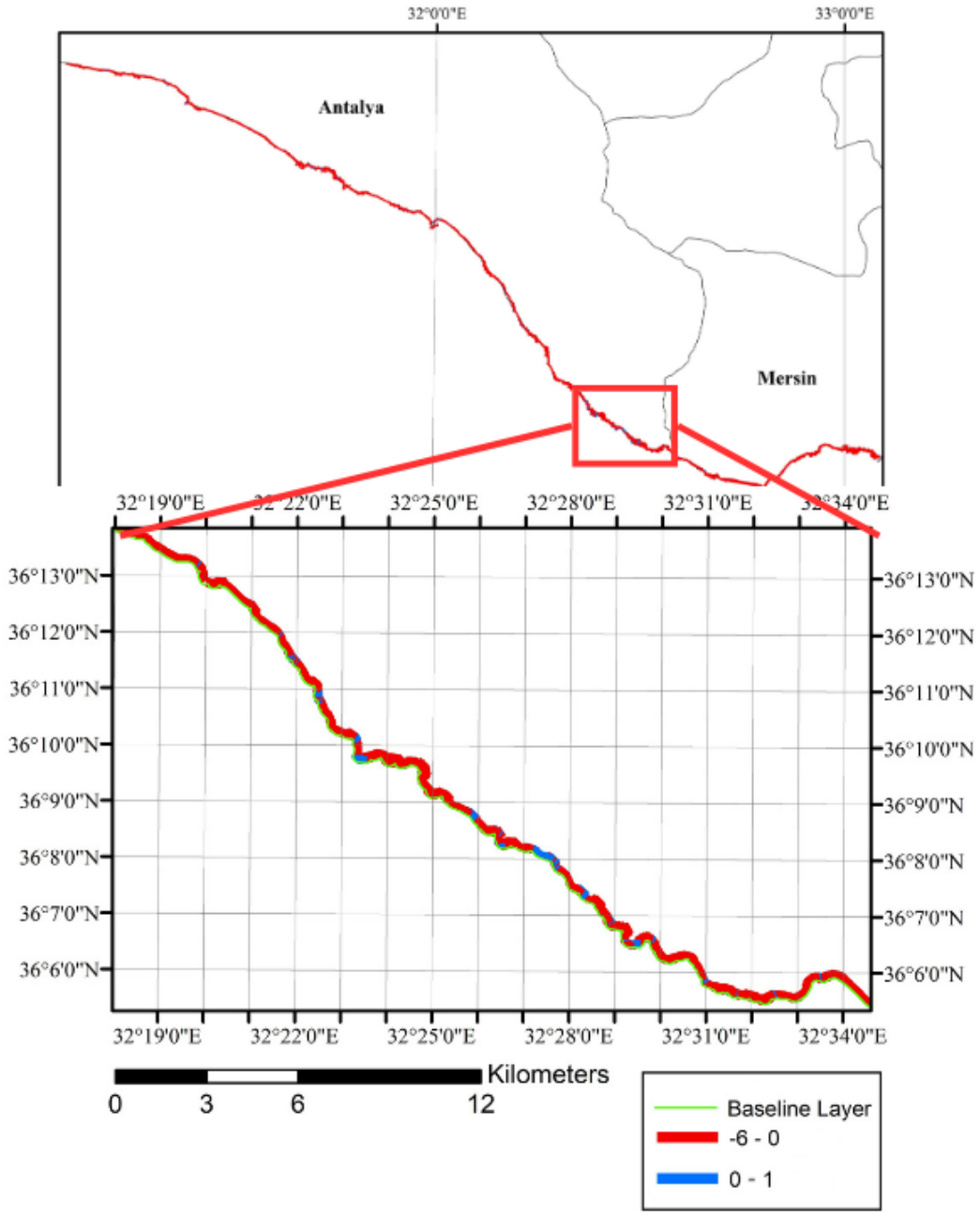

Figure C.4. End Point Rate (EPR) for the Initial Area of Interest

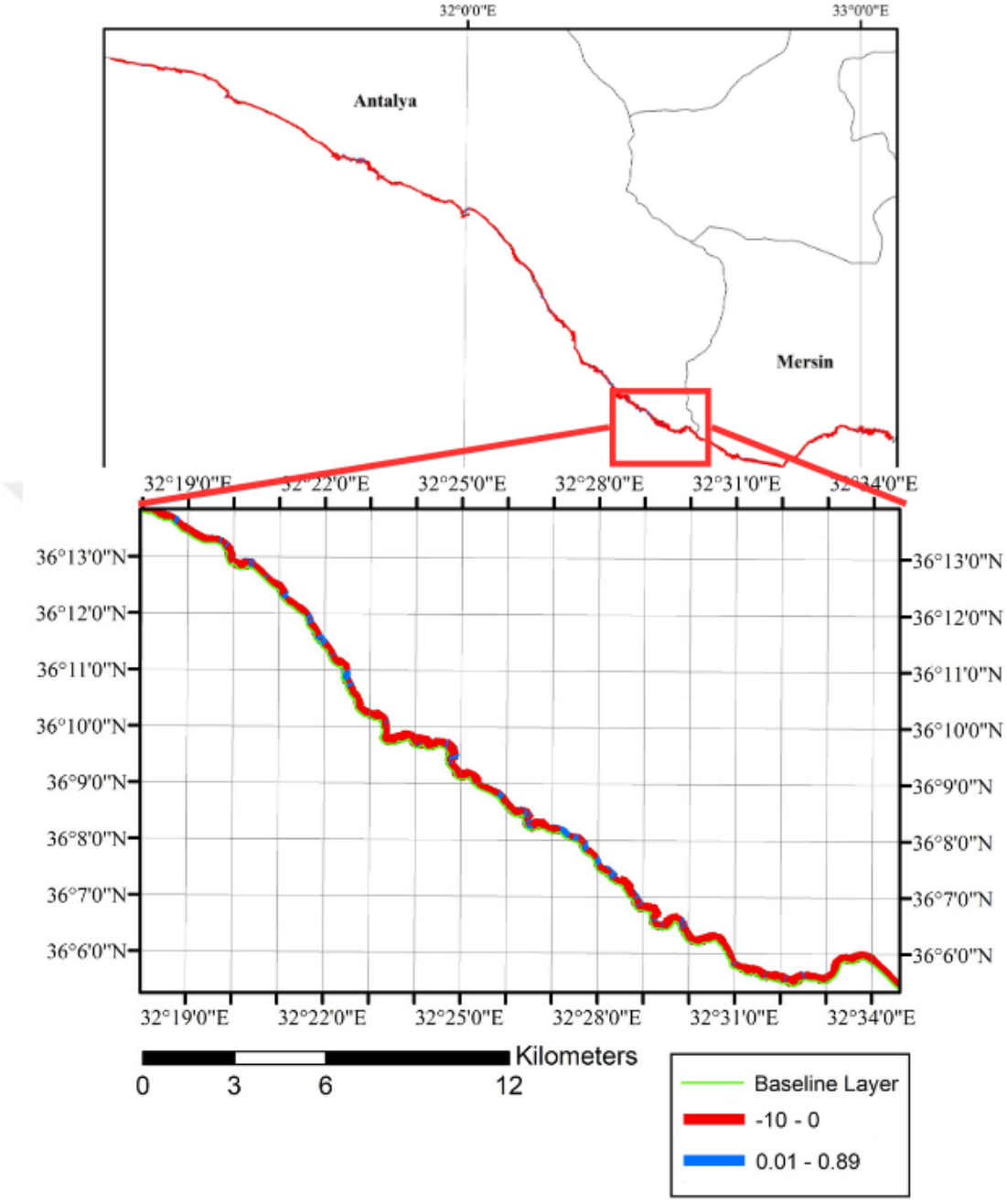

Figure C.5. Linear Regression Rate (LRR) for the Initial Area of Interest

Similar to the initial model, red zones represent the areas that are vulnerable to erosion, and blue zones represent accretion. The green line is the baseline used in the Alanya Model.

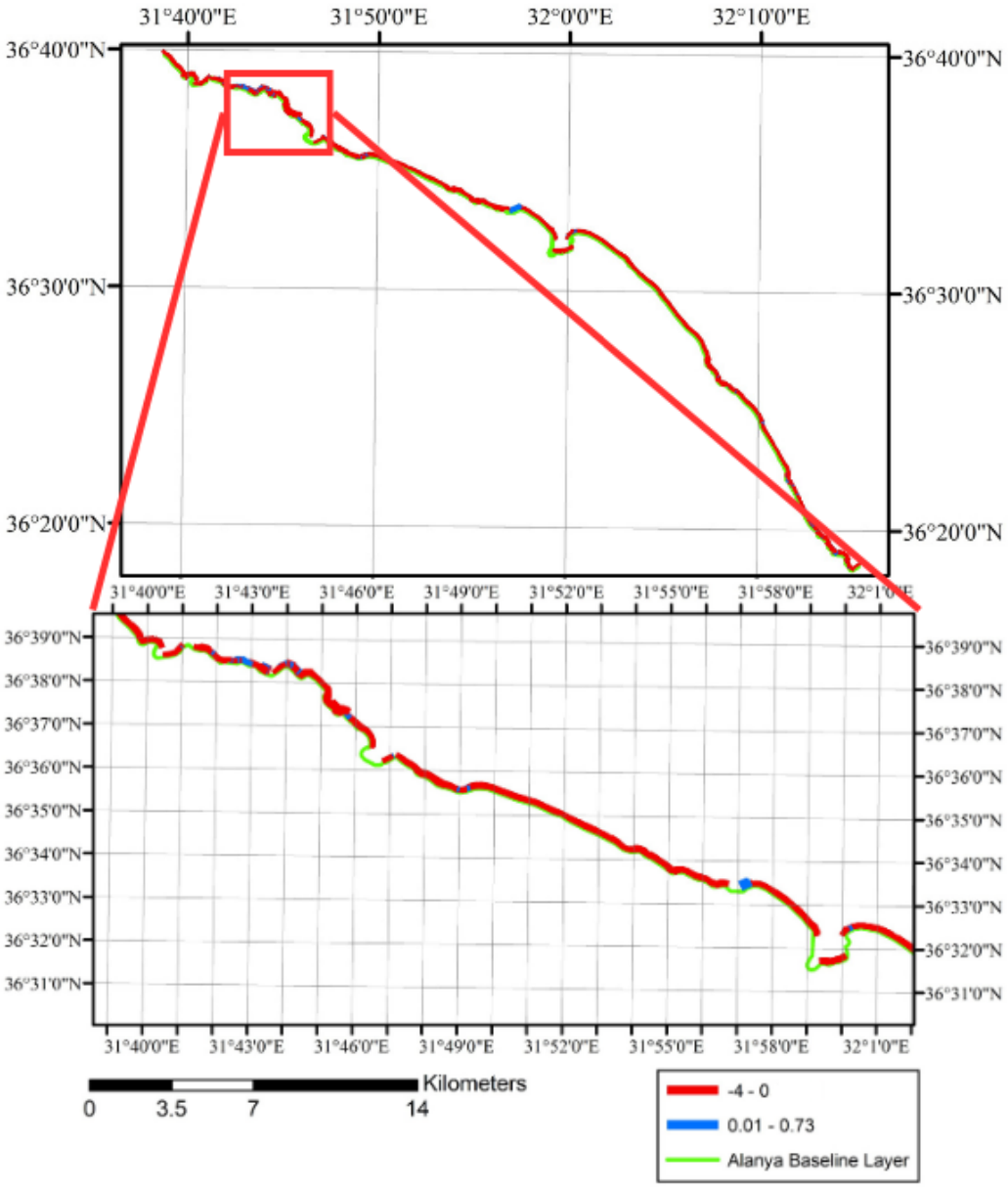

Figure C.6. Net Shoreline Movement (NSM) for Alanya Model

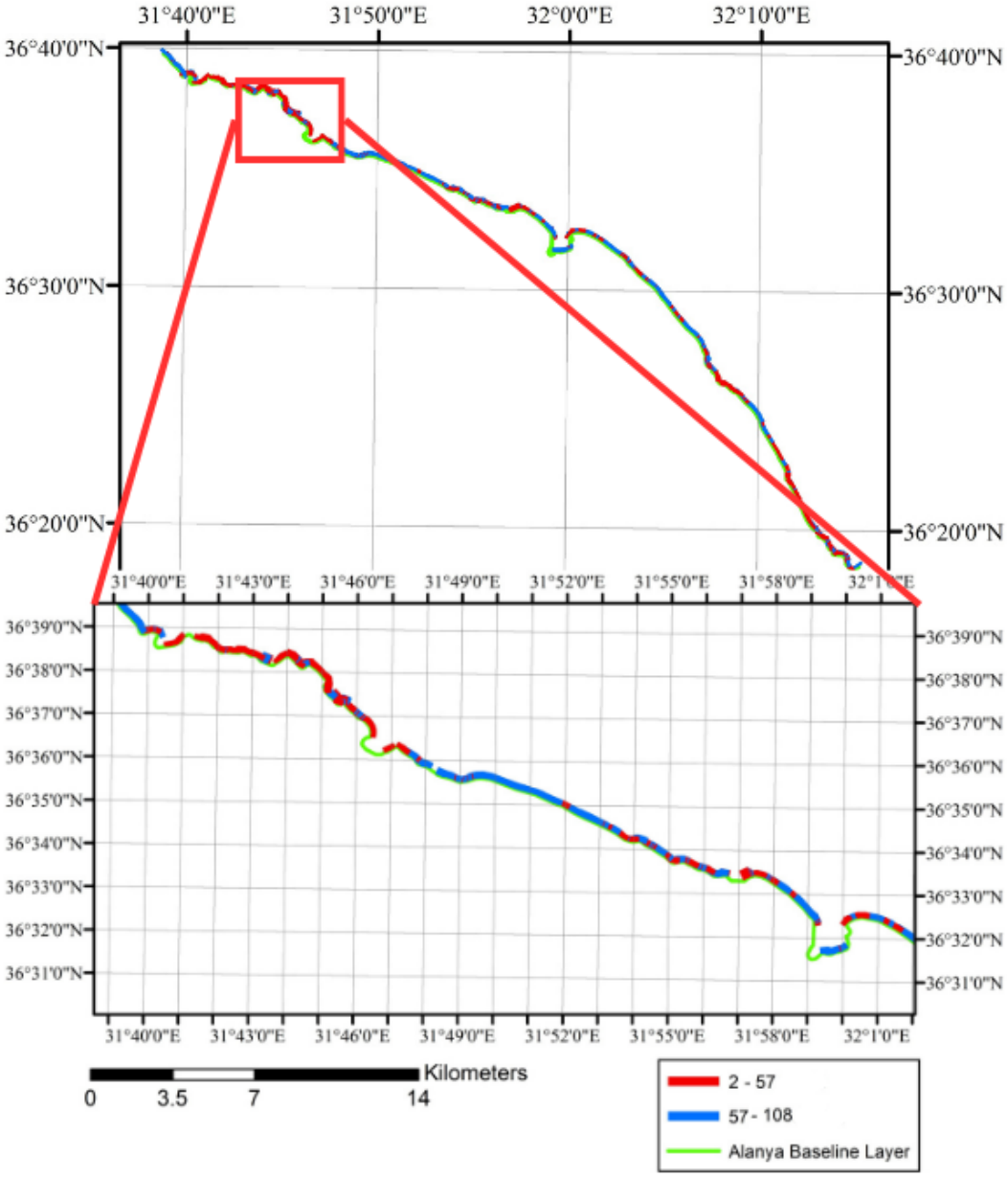

Figure C.7. Shoreline Change Envelope (SCE) for Alanya Model

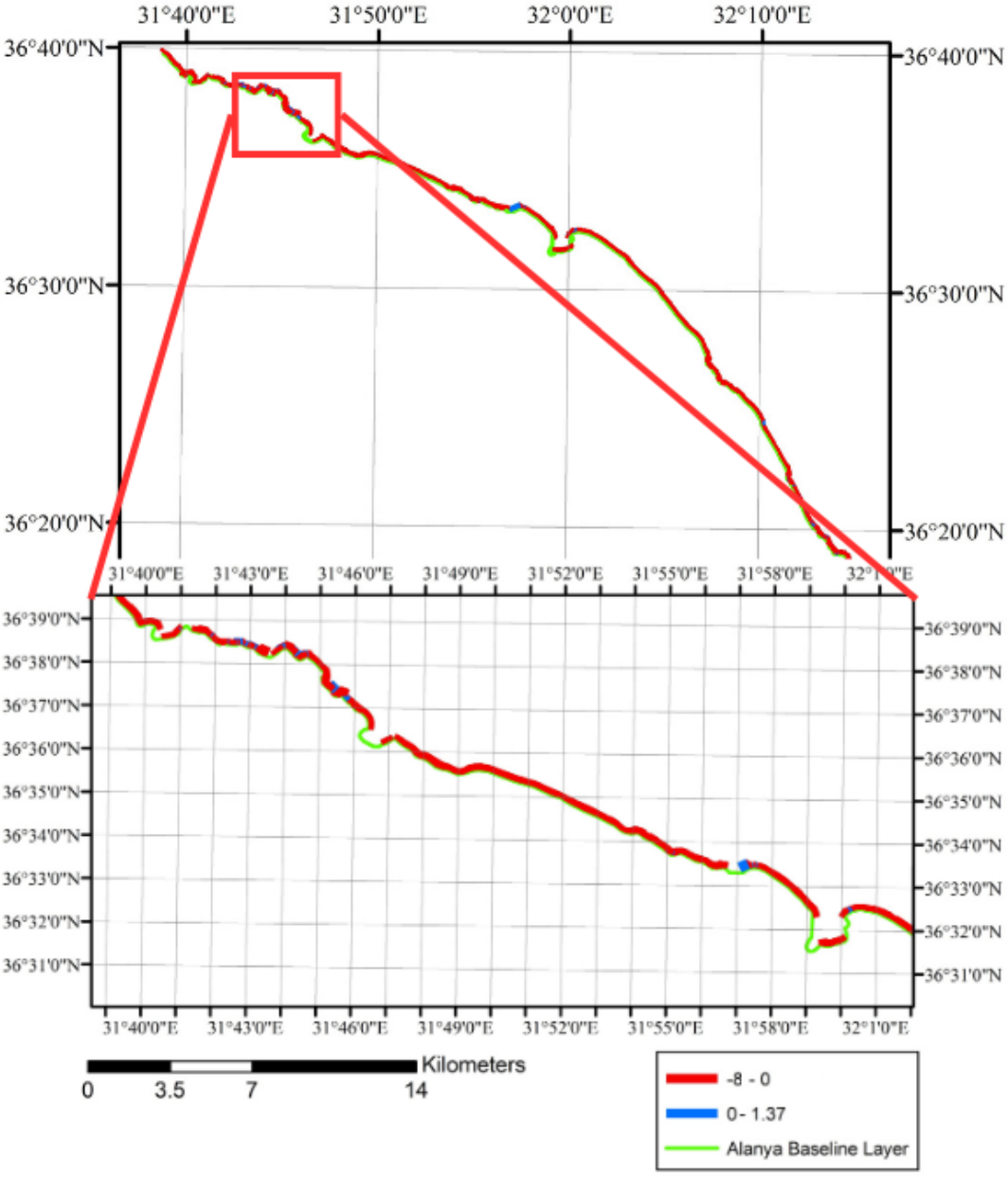

Figure C.8. End Point Rate (EPR) for Alanya Model

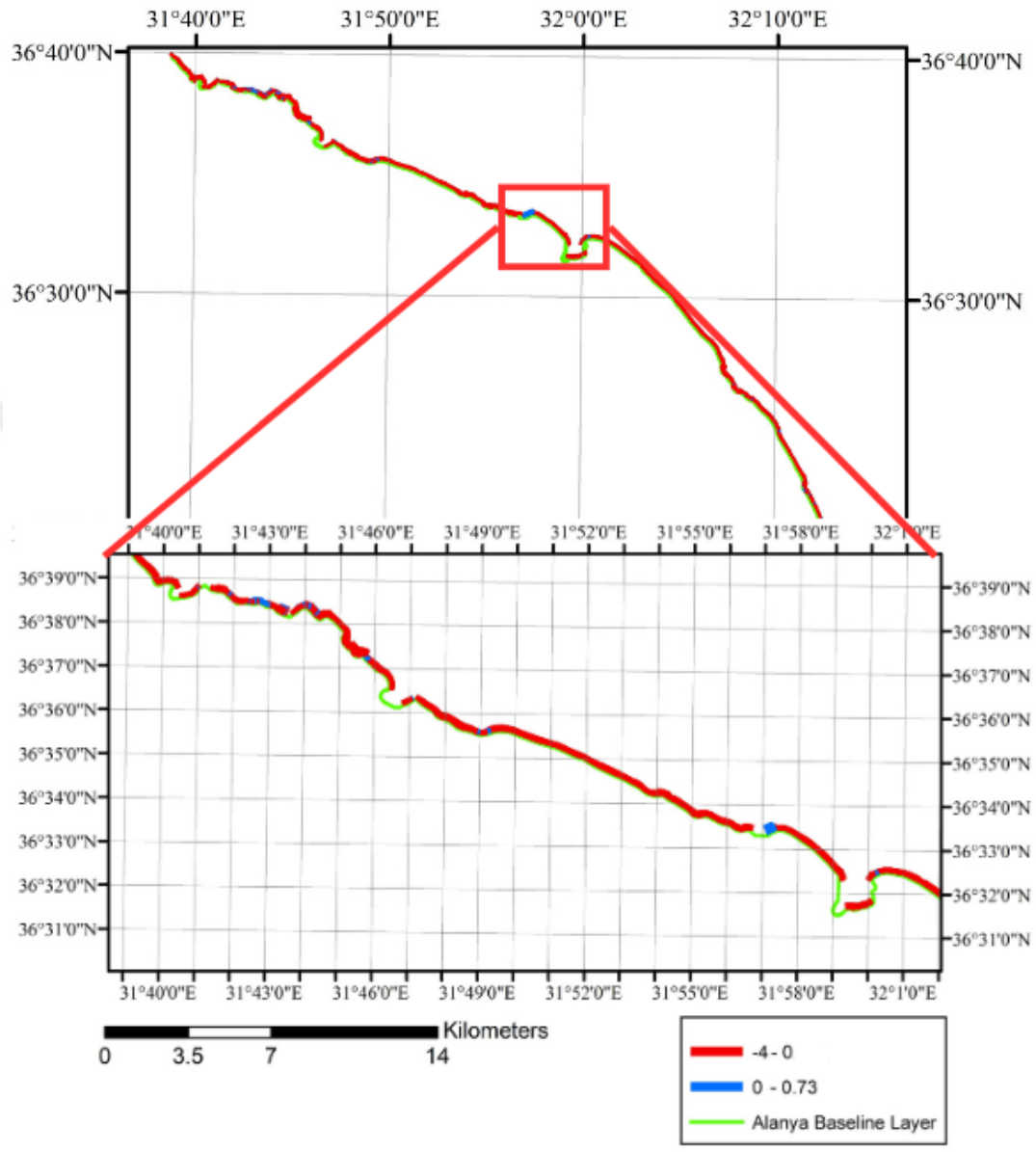

Figure C.9. Linear Regression Rate (LRR) for Alanya Model

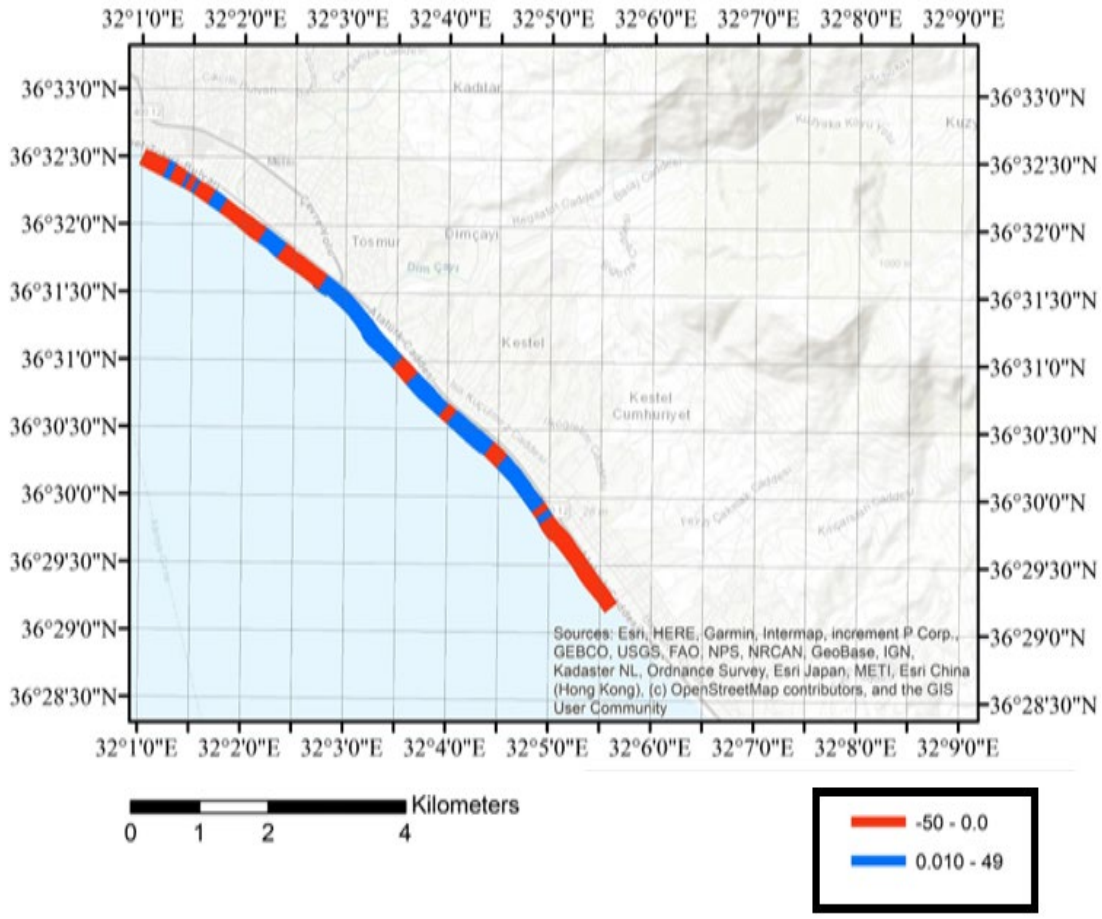

Figure C.10. Net Shoreline Movement (NSM) Results of Monthly Change Study

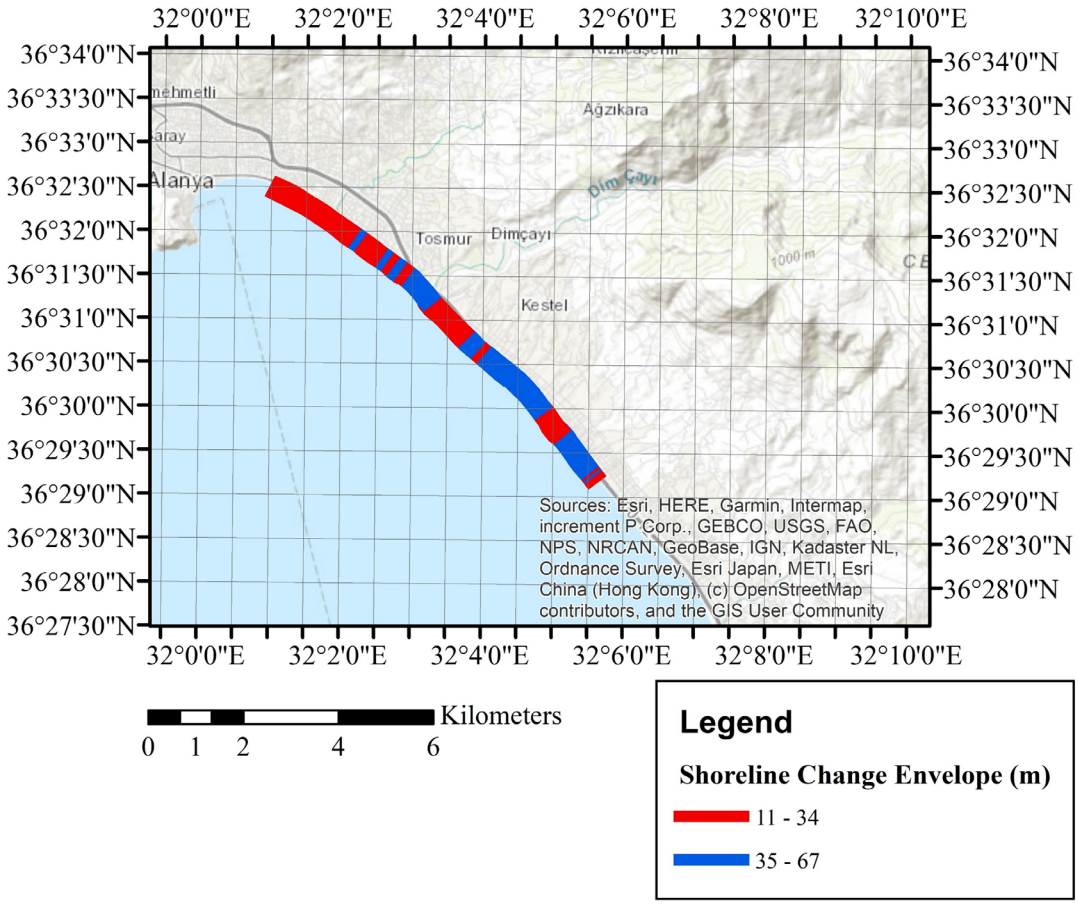

Figure C.11. Shoreline Change Envelope (SCE) Results of Monthly Change Study

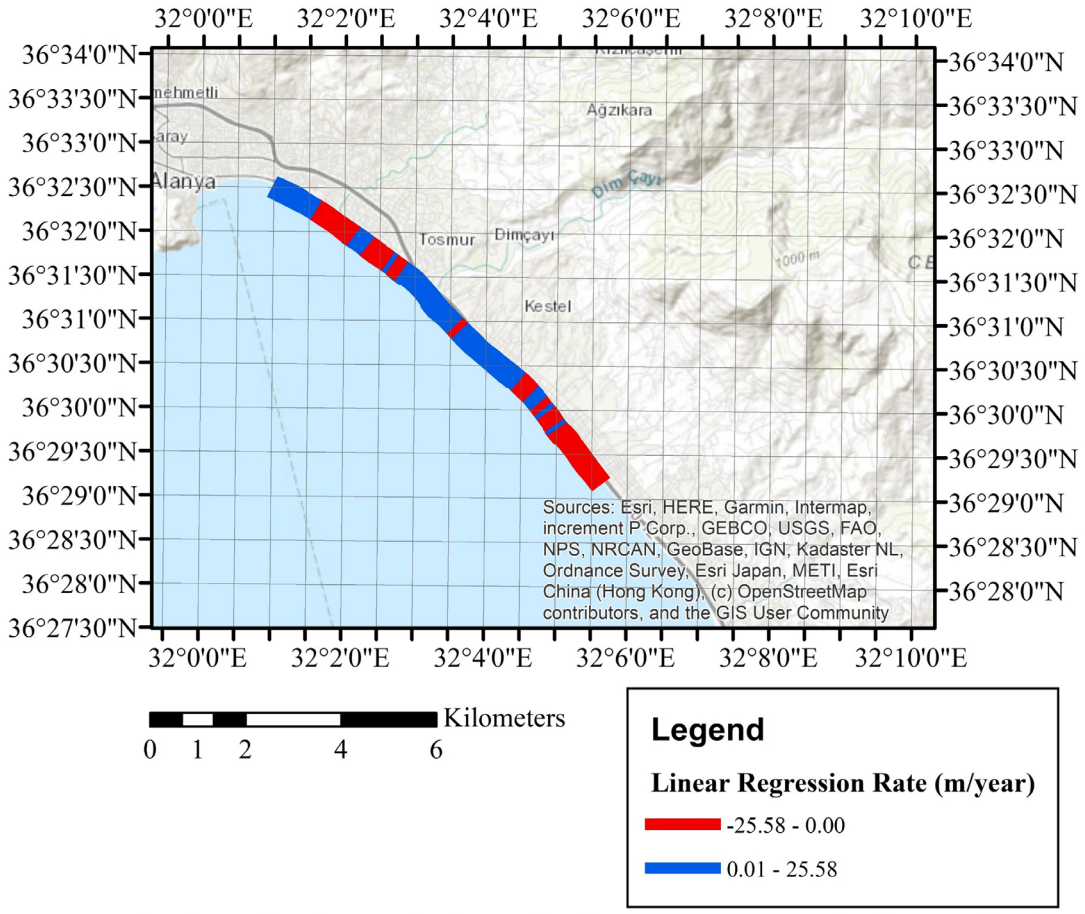

Figure C.12. Linear Regression Rate (LRR) Results of Monthly Change Study